Modeling the Endothelial Glycocalyx Post Pneumonectomy in a 3D Fluidic Chip

A Major Qualifying Project Report submitted to the faculty of

WORCESTER POLYTECHNIC INSTITUTE

in partial fulfillment of the requirements for the degree of Bachelor of Science

Submitted by:

_____

Eric Johnson

_____

Mia Long

_____

John Martel

_____

Megan Ouellette

_____

Sudish Vengat

April 27, 2023

_____

Professor Solomon Mensah, Ph.D., Advisor

Department of Biomedical Engineering, Department of Mechanical Engineering

Table of Contents

Table of Authorship

Section	Subsection	Primary Author(s)	Primary Editor(s)
Abstract		Johnson	Martel
1. Introduction		Martel, Long	Long, Martel
2. Literature Review	2.1 Physiology and Function of the Lungs	Ouellette	Martel
	2.2 The Pulmonary-Vascular System	Ouellette, Vengat	Martel
	2.3 Physiology of the Endothelial Glycocalyx	Johnson	Martel
	2.4 Pneumonectomy	Ouellette, Vengat	Martel
	2.5 Prior Art	Ouellette, Long	Ouellette, Long
3. Project Strategy	3.1 Initial Client Statement	Ouellette	Martel
	3.2 Technical Design Requirements and Standards	Ouellette, Vengat	Martel, Johnson
	3.3 Revised Client Statement	Ouellette	Ouellette
	3.4 Project Strategy Management	Vengat	Martel
4. Design Process	4.1 Needs Analysis	Johnson, Ouellette	Martel
	4.2 Alternative Designs	Martel	Ouellette, Johnson
	4.3 Design Concept Prototyping and Feasibility Studies	Ouellette, Vengat	Martel
	4.4 Final Design Modeling	Ouellette, Vengat	Johnson, Martel
5. Design Verification and Data Results	5.1 COMSOL Model Results	Long, Ouellette	Long, Ouellette
	5.2 Cell Culture Testing	Martel, Johnson, Vengat	Ouellette
	5.3 Device Assembly Testing	Vengat, Johnson	Ouellette
	5.4 Image Methods	Vengat	Ouellette

	5.5 Final In Vitro Assembly Trials	Johnson	Ouellette
6. Final Design and Validation	6.1 Project Goals	Johnson, Long	Ouellette
	6.2 COMSOL and MATLAB	Long	Ouellette
	6.3 General Ethical Concerns and Mitigation	Johnson	Vengat
	6.4 Economic Impacts	Ouellette	Johnson
	6.5 Environmental Impact	Vengat	Martel
	6.6 Societal Impact	Johnson	Vengat
	6.7 Global Impact	Vengat	Johnson
	6.8 Health and Safety Concerns	Martel	Johnson
	6.9 Manufacturability	Vengat	Martel
7. Discussion	7.1 SOLIDWORKS Model and COMSOL Flow Simulations	Ouellette, Long	Martel
	7.2 Staining and Imaging	Johnson	Martel
8. Conclusions and Recommendations		Vengat, Martel	Martel

Acknowledgments

Abstract

The endothelial glycocalyx lines the interior of blood vessels, regulating cell properties in response to changes in blood flow. Under high shear stresses, it has been found that the glycocalyx experiences lasting damage, resulting in unknown consequences. It has been theorized to play a role in post pneumonectomy complications which occur after the surgical removal of one lung. Research has examined the effects of general shear stress on the endothelial vasculature, but the magnitude and effects of post pneumonectomy shear stress are unknown. In this project, a SOLIDWORKS model of the lung vasculature before and after a pneumonectomy was created to assess the changes in shear stress, velocity, and pressure. Based on findings from simulations performed on these models in COMSOL, a fluidic chip was created and seeded with human lung microvascular endothelial cells (HLMVECs) to test the effects of elevated shear stress for elongated periods of time. Specific points of interest were selected to be modeled from regions with notably higher values of shear stress and pressure in the pneumonectomy models from the COMSOL simulations. After testing, the HLMVECs were fixed and stained to qualitatively assess the state of the glycocalyx layer under normal and increased stresses caused by a pneumonectomy.

List of Figures:

List of Tables:

1. Introduction

A pneumonectomy is an invasive, high-risk surgical procedure performed to remove the right or left lung, usually as a treatment for conditions such as lung cancer, traumatic lung injury, and pulmonary tuberculosis[1]. However, pneumonectomies have high morbidity rates, with complications ranging from arrhythmias to pulmonary edemas[2].

Pneumonectomies result in the heart's entire cardiac output being directed into the remaining lung, which is believed to increase pressure and shear stresses within the remaining pulmonary vasculature. Changes in blood flow are sensed by the endothelial glycocalyx, a protective mechanotransduction layer on the endothelial cell layer of the blood vessels. The glycocalyx is a gel-like layer that ranges in thickness from 0.1–1 μm throughout the vasculature[3].

While the direct relationship between pneumonectomies and glycocalyx damage is not understood, there is a potential link between the blood flow changes created by pneumonectomies and the health of the glycocalyx. The increase in shear stress in the remaining lung's vasculature following a pneumonectomy is speculated to cause damage to the glycocalyx at a faster rate than naturally repairable, which could contribute to postoperative complications and risks to the patient's health[4].

This project attempted to model post pneumonectomy pulmonary vasculature in a 3D virtual model created in SOLIDWORKS. Fluid simulations on this model were run in COMSOL Multiphysics FE to determine regions of particular interest, which were then selected for an in vitro model. The in vitro model used a fluidic chamber design to simulate multiple sections of vasculature with normal and pneumonectomy flow conditions. Human lung microvascular endothelial cells (HLMVECs) were seeded onto custom fibronectin-coated polydimethylsiloxane (PDMS) pieces and microvascular endothelial cell culture media was run through the system using a peristaltic pump. Lastly, the cells and glycocalyx were fixed, stained, and fluorescently imaged using a Keyence BZ-X microscope to assess the state of the cells and glycocalyx following exposure to the fluid flow.

2. Literature Review

To start this project, it was important to understand the general physiology and function of the lungs in the human body, as well as the cardiovascular system, to produce more informed results. Our research began with an understanding of the importance of the functions that the lung provides to gain a cognizance of just how important this study and its implications could be. Our main focus in this study was the endothelial glycocalyx, but we needed to first understand the general vascular system and then more specifically the pulmonary vasculature. Afterwards, we studied the pneumonectomy procedure and its related pathologies. Finally, we looked at previous literature to see where we could advance existing methods to produce results specifically regarding the endothelial glycocalyx following a pneumonectomy.

2.1 Physiology and Function of the Lungs

The pulmonary-vascular system is the means by which blood is oxygenated and travels through the body to spread energy and nutrients[5]. The lungs and heart work in tandem to keep the body's cells oxygenated and to remove waste[6]. As a breath is taken, air travels through the larynx and down the trachea (also known as the windpipe) which divides into the two bronchi before passing into the lungs. Within the lungs, the air travels from the bronchi into the bronchioles, which are smaller air passages in the lungs, and then finally into the alveoli (Fig. 2.1). Alveoli are small air sacs covered with capillaries where oxygen enters the bloodstream and carbon dioxide exits deoxygenated blood to be expelled. A healthy person has about 300 million alveoli in order to maximize surface area for gas exchange to occur efficiently[5]. Each alveolus consists of a thin endothelial layer, allowing for gas exchange with the capillaries, as can be seen in Fig. 2.2.

The lungs themselves are divided into lobes covered with the inner visceral pleura. The visceral pleura sits adjacent to the parietal pleura. These two pleura are serous membranes that sit next to each other with a small space in between, called the pleural cavity. This cavity contains a few milliliters of pleural fluid. As the lungs inflate and deflate, the two pleura slide against each other[7]. The right lung consists of three lobes, the superior, middle, and inferior, and the left has two, the superior and inferior. The left lung is smaller to allow room for the heart[5].
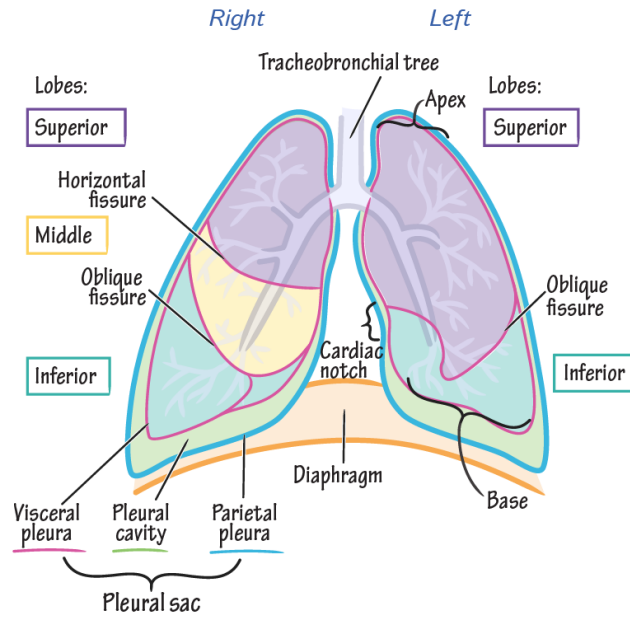
Figure 2.1: Basic lung anatomy. The right lung contains the superior, middle, and inferior lobe while the left lung contains the superior and inferior lobe. The parietal and visceral pleura can be seen with the pleural cavity on the bottom left [8]
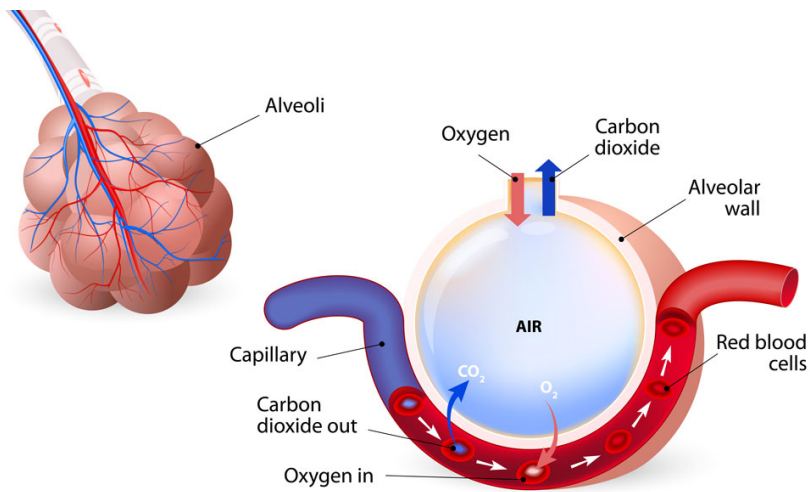
Figure 2.2: Alveoli gas exchange. The left side of the image depicts the alveoli (pink) with capillaries (red and blue). The right depicts a closer view of the alveoli and capillaries, with the gas exchange across the alveoli-capillary membrane shown on the underside of the alveoli[9].

2.2 The Pulmonary-Vascular System

The vascular system has three main functions: distributing oxygen and nutrients, thermoregulation, and removing waste matter[10]. The circulatory system consists of three main blood vessels: arteries, veins, and capillaries, each with their own specific function. In the pulmonary vasculature, the arteries carry deoxygenated blood from the heart to the lungs. Pulmonary veins carry oxygenated blood from the lungs back to the heart before being circulated to the body[11]. In the rest of the body, arteries transport oxygenated blood from the heart and veins carry deoxygenated blood back to the heart. The smallest blood vessels are capillaries, where gas exchange occurs in the body. In the lungs, oxygenated blood travels from the capillaries of the pulmonary veins to the left atrium of the heart. From there, the blood enters the left ventricle before being pumped into the body[12]. Throughout the body, capillaries allow for the oxygenated blood to be extracted by cells. This allows the cells to produce adenosine triphosphate (ATP), an important energy source for cells[5]. Carbon dioxide is returned to the bloodstream as a cellular product. Veins carry the deoxygenated blood back to the heart which pumps the deoxygenated blood to the lungs and ultimately into the pulmonary capillaries to be oxygenated once again at the alveoli[13].

In addition to distributing oxygenated blood, the vascular system also distributes nutrients. As blood flows through the intestinal capillaries, it picks up glucose, vitamins, and minerals that are deposited in the tissue beds within the body[11]. Waste material is taken into the bloodstream, to be filtered by the kidneys prior to removal from the body through the urinary system [10]. The other main function of the vascular system is to control the body's temperature through its innate function of regulating blood flow throughout the body. When the body breaks down nutrients being delivered through the capillaries, heat is produced. This heat is then circulated throughout the body using the blood flow[11].

Finding the exact measurements for the morphology of the pulmonary arteries was challenging, as research showed that arterial measurements, bifurcations, and branching patterns all differ between people[14]. Measurements of the main pulmonary artery (MPA) in literature vary, but average out to roughly 29.5 mm in diameter among human males[14]. This splits into the right pulmonary artery (RPA) and left pulmonary artery (LPA), which average about 19.8 mm and 22.1 mm in diameter, respectively[14]. The RPA and LPA then divide into basal branches. The right lung often has four basal segments (anterior, medial, posterior, and lateral), whereas the left

lung often has three basal segments (anteromedial, posterior, and lateral) per lobe[15]. These branch sizes are not easily found in the literature, nor are specific measurements of the even smaller pulmonary arterioles and pulmonary capillary vessels.

2.3 The Glycocalyx

Though the endothelial glycocalyx (eGCX) is a physiologically small component of the cardiovascular system, it plays an important role in circulatory regulation. The glycocalyx has been visualized for over 40 years, only recently has more research focused on its role and function in the body. The glycocalyx is a gel-like layer that sits upon the endothelial layer of the blood vessel wall, forming a barrier between the interior blood vessel wall and the blood itself[16]. The glycocalyx, or GCX, is a mechanotransducer that is able to send signals to regulate adjacent cell properties in response to changes in shear and tensile stresses. The network of the GCX is made up of a dense layer of sugars (mainly mannose and galactose), proteins, and lipids[16]. These sugars form together into glycans, which can either be free-floating through the blood or bound to proteins or lipids, creating proteoglycans, glycoproteins, or glycolipids, respectively[16]. Proteoglycans consist of glycosaminoglycan (GAG) chains that attach to the cell membrane via plasma proteins or receptors. GAGs consist of heparan sulfate (HS), hyaluronic acid (HA), chondroitin sulfate (CS), dermatan sulfate, and keratan sulfate (primarily HA, HS, and CS)[17]. HS is the most abundant and accounts for around 50–59% of the total GAGs present in the eGCX. These side chains can bind with embedded P-glycoprotein 1 (PG protein) or core proteins, which consist of glypicans (glycosylphosphatidylinositol anchor) and syndecans (membrane-spanning domain), as well as CD44, a surface adhesion receptor. These bound complexes serve a major role in controlling growth factors, anti-inflammatory responses, mediating vessel dilation, and vascular permeability[16]. Figure 2.3 depicts the composition of the glycocalyx.

The GCX varies in thickness through different vessels and in different segments of the vasculature. In thinner vessels such as capillaries, the GCX tends to be around a few hundred nanometers thick, while in vessels such as arteries, it can be as thick as a few micrometers[18].
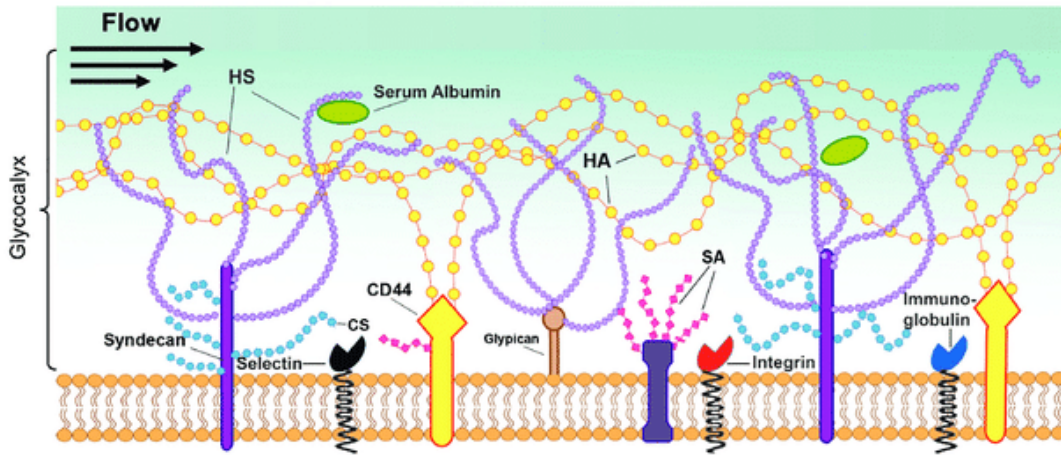
Figure 2.3: A drawn model depicting the glycocalyx, a gel-like sticky layer consisting of proteins and sugars. It is situated on the outermost level of the cellular membrane of cells [19].

The forces of shear stress from the blood flow determine endothelial cells' physiology and responses. One of the main functions of GCX is to regulate blood flow by instructing vessels to dilate and contract in response to increased or decreased stresses, but it also helps regulate leukocyte levels and vessel perfusion[20]. Therefore, damage to the GCX affects many basic functions of the body. GCX exposure to an abnormal increase in shear stress induced by a surgery such as a pneumonectomy may cause lasting damage to the glycocalyx, which could potentially be attributed to several post-surgery complications[21].

2.4 Pneumonectomy

A pneumonectomy is a lifesaving procedure for patients who require a lung removal. The most common reason for a pneumonectomy is lung cancer. Other complications such as pulmonary tuberculosis, bronchiectasis, traumatic lung injury, and fungal infections can necessitate a lung being removed[1]. In many cases, pneumonectomies are the only option. Despite possibly severe and life-threatening complications, many pneumonectomy patients have an active life after recovery[2]. Lung cancer is the second-most common cancer across both sexes after skin cancer and is primarily found in people older than 65. Lung cancer is one of the leading cancer-related deaths killing an estimated 130,180 people in 2022 alone [21]. Furthering research surrounding the lungs and pulmonary arterial conditions will contribute to preventative

measures, hopefully decrease the risks associated with pneumonectomies, and make lung treatment procedures safer and more effective.

2.4.1 Pneumonectomy Procedure

Before a pneumonectomy is conducted, pulmonary function tests are conducted and cardiac risk is assessed to determine if the patient is healthy enough to undergo the surgery. For some patients with conditions such as valvular disease (valves within their heart exhibit damage or are diseased), additional precautions are taken to assess risk[2].

A pneumonectomy is an open-chest procedure that is sometimes performed as a video-assisted thoracoscopic surgery (known as a VATS procedure). Through this method, there is a reduction in exposure and it is less invasive. Physicians use thoracotomy instruments such as rib spreaders, contractors, specific thoracic tissue forceps, and scissors. A bronchial blocker is placed inside the bronchus to isolate the "bad" lung from the bronchus[2].

The procedure itself starts with the physician making a posterolateral thoracotomy incision on the same side as the target lung. The ribs may be spread completely or partially removed, as seen in Figure 2.4 below.
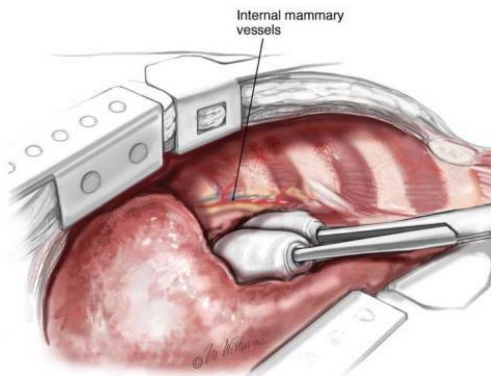
Figure 2.4: Chest retractors placed between the lung and ribs to spread and expose the area[22].

The surgeons will clamp and cut the bronchus and blood vessels to collapse the lung.
In order for the lung to be removed, the surgeon must cut the lung from the pleural space. The visceral pleura is cut away from the parietal at any adhesions, and any remaining connective

tissue attaching the lung to the diaphragm or surrounding tissue is removed. After the lung is removed, the bronchus and arteries are cauterized to prevent any leaking before then sealing the incision[2].

2.4.2 Pneumonectomy Complications

Postoperative care decreases the likelihood of complications and provides oxygen supplementation as needed, along with invasive monitoring. Despite this, 25-60% of patients suffer from some form of complication[2]. Postoperative complications can be grouped into two categories: early and late complications, based on when these complications typically occur relative to the date of the surgery. Early complications such as cardiac arrhythmias, cardiac herniation, pulmonary edema, pneumonia, and bronchopleural fistulas can all occur jointly or separately[23]. Cardiac arrhythmias are the most common complication–the patient's heart will beat at an abnormal rate which can typically last for the first three days after surgery[2]. Cardiac herniation typically occurs within the first day after surgery, when the patient experiences a sudden drop in blood pressure that can lead to hemodynamic instability with symptoms ranging from chest pain to inadequate blood flow[2]. Pulmonary edemas, in which the lungs are filled up with too much fluid, often result from improper hypotension management[4]. Pneumonia typically occurs in older patients who have habitually smoked in the past, but may also relate to the depth of the incision during surgery[24].

While some of the complications are extremely rare, most are very dangerous. For example, postpneumonectomy pulmonary edema affects less than 5% of patients but has a mortality rate of 80–100%. It is shown to be more common after a right pneumonectomy since the right lung carries a larger amount of blood (55%). Research has shown that while the causal mechanism is unknown, it is speculated that changes to capillary permeability and increased hydrostatic pressure play a significant role [4].

2.5 Prior Art

To guide this project, the work completed by the MQP team in the previous year was consulted. Additionally, a literature review was performed to find existing research and data on relevant topics. This section covers four different experiments that investigated the effects of the increase in arterial pressure on the eGCX post pneumonectomy.

2.5.1 A Parallel-Plate Flow Chamber to Investigate Endothelial Glycocalyx Remodeling after Pneumonectomy

In a study conducted by a former MQP team at WPI, the students sought to explore the effects on the eGCX due to shear stress changes within blood flow resulting from a pneumonectomy. To model these effects, they designed a parallel plate flow chamber with interchangeable left and right pneumonectomy designs. By seeding the control and pneumonectomy models with HLMVECs and running media through the chamber (see Fig. 2.5), the group was able to examine the aftermath of the damage using a confocal microscope. Aided with this information and fluid flow simulations conducted in SOLIDWORKS on their models, they were able to determine that in the simulated effects of post pneumonectomy conditions, the glycocalyx experienced an average increase of 278.58% in shear stress. The study demonstrated that the effects of shear stress do greatly increase on the endothelial cells post-surgery, which could damage the glycocalyx[25].
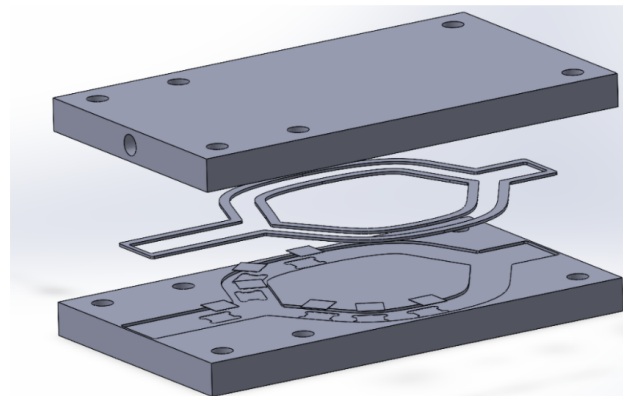
Figure 2.5: Previous MQP team's parallel plate flow chamber, shown in SOLIDWORKS exploded view. The inner gasket was interchangeable to create the pneumonectomy shape. The non-pneumonectomy, or control, shape is shown. The small squares in the bottom plate were glass slides onto which the HLMVECs were seeded[25].

2.5.2 Blood Flow and Pulmonary Vascular Pressure

In one study performed on adult male rats, the rats were evenly split up into two groups: an experimental group and a control group. The experimental group received a right

pneumonectomy, while the control group received a thoracotomy with no pulmonary resectioning. The study found that pulmonary arterial pressure increased on all postoperative days (3, 7, and 28 days). The pneumonectomy group had a 29 mmHg pressure on day 3, which then increased to 33 mmHg and 35 mmHg on days 7 and 28, respectively (seen in Fig. 2.5) below).
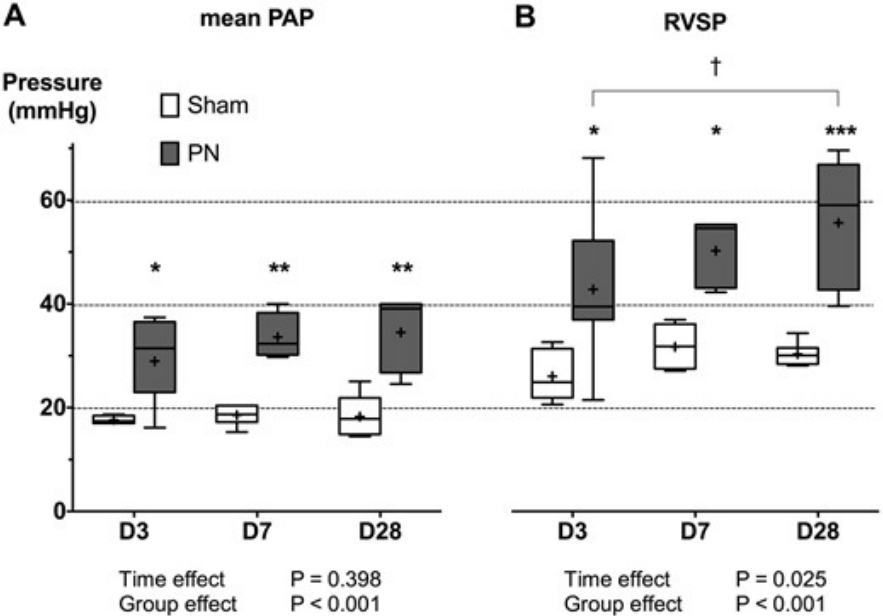
Figure 2.6: The mean pulmonary arterial pressure (PAP) and right ventricle systolic pressure (RVSP) that were measured by the catheterization of the right heart in the control (sham) and test (PN) group for the three postoperative days[26].

Meanwhile, the control group experienced no significant changes in pulmonary arterial pressure over the 28 days. The proportion of muscularized distal pulmonary arteries increased from 67% to 83%, and the wall thickness of the muscularized arteries increased as well. Overall, the model observed moderate but sustained pulmonary hypertension, which was related to the high muscularized rate of the distal pulmonary arteries and a significant increase in wall thickness[26].

2.5.3 Long Term Effects of Pulmonary Resection on Cardiopulmonary Function

In another study, eight patients with lung cancer underwent pulmonary resectioning, with pulmonary function and hemodynamic tests conducted before and after the operation. The pulmonary arterial pressure was shown to increase within six months while the patient was

exercising. The study found that the procedure decreased ventilatory capacity, exercise tolerance, and quality of life. The detrimental impacts shown by postoperative testing showed that cardiopulmonary function worsened faster within six months and continued to decline gradually through 40 months of observation. Interestingly, the study showed that the alveolar capillary membrane area increased after initial deterioration in the first six months[27].

2.5.4 Structural and Functional Properties of the Endothelial Glycocalyx, Capillaries, and Veins

Ying Zheng and his team created an in vitro model to study the structural and functional properties of the eGCX, capillaries, and veins. Human umbilical vein endothelial cells (HUVECs) were cultured in PDMS on a "multi-height microfluidic platform" that would expose the cell monolayer to shear stress forces that would "recapitulate the physical environment in arterial, capillary, and venous regions of the vasculature." After exposing the endothelial cell monolayer to shear stress, the experiment demonstrated that shear stress at different locations in the vasculature influenced cell morphology. They used fluorescently labeled actin filaments to assess the elongation of the cells over time. The results showed that cells lengthened significantly in response to extended exposure to shear stress when observed at predetermined time points. This study illustrated that the cells continued to respond to shear stress over time and that the increased shear stress negatively affected the morphology of the endothelial cells[28].

3. Project Strategy

This chapter covers the goals the team set out to achieve and the methods utilized to work toward these goals.

3.1 Initial Client Statement

The initial client statement was to design a device that assesses the impacts of a pneumonectomy on the eGCX in a 3-dimensional model. The purpose of this project was to determine how the glycocalyx changes due to increased vascular flow and shear stress post pneumonectomy while meeting the client statement requirements.

3.2 Design Requirements

To guide the project, objectives, constraints, and specifications were identified and modified as needed through the duration of the design process.

3.2.1 Objectives

In order to meet the goals of the client statement, this project needed to:

1. Determine Vascular Areas of Interest. A 3D model of the pulmonary vasculature tree was designed and run through computer fluid simulations to determine where the greatest impact of the increased shear stress occurred in the lung vasculature.
2. Design and Create an In Vitro Model. An Organ-on-a-Chip (OoC) design was implemented to model the areas of interest and control models in vitro.
3. Test the In Vitro Model. The chip was seeded with HLMVECs which were exposed to various flow rates with a mechanical pump.
4. Stain and Image the Results of the In Vitro Model. Viewed confluency, damage, and the overall state of the glycocalyx and endothelial cells under different shear stress conditions.

3.2.2. Constraints

The primary constraints on this project were the design specifications, budget, and time. The team's budget to meet the client's need statement was 1,000 USD. Digitally simulating the 3D model saved some budget and utilizing the past team's materials was beneficial. Other cell

culture techniques would have been an option if not for the time and budget constraints. The team also had only one academic school year (about 8 months) to complete the project.

General biocompatibility, ease of construction, ease of reproducibility, ease of seeding, physiological accuracy (such as 3D modeling a relatively accurate pulmonary arterial tree), and ease of imaging were some of the design specifications that guided the project's development. When designing the 3D model, the team struggled to find consistent measurements and morphology for the pulmonary arterial tree. The team also failed to find a readily available and functional 3D model for flow simulations. Creating the SOLIDWORKS 3D pulmonary vasculature model from scratch took about eight weeks in total and continued to be reworked during the COMSOL simulation process over the next six months. Ultimately, creating elaborate and more realistic models with smaller vasculature was abandoned due to the lack of time. The team had no prior knowledge of the COMSOL software, which delayed quantitative data collection from the flow simulations for multiple months.

As discussed later in Chapter 4, the 3D model was limited to the sparse literature found on the morphology supplemented with FIJI data collection. This technique to determine the morphology of the 3D model was lacking and had significant room for error. An additional limitation was the attempt to replicate cylindrical vasculature, which provided a challenge when creating the in vitro model. Molding cylindrical vasculature in a biocompatible material suitable for cell seeding–rather than rectangular vasculature–made creating a substrate piece more complex. As our in vitro model morphology was dependent on the digital model, and that model had vasculature that was not microfluidic, we were limited to creating a chamber that could accommodate non-microfluidic vasculature. This forced us to switch from a collagen-based model to a PDMS model. This switch created imaging challenges later in the project due to the thickness of the PDMS and its optical properties.

3.2.3 Product Specifications

To view the impacts of shear stress on the glycocalyx, pneumonectomy conditions had to be compared to non-pneumonectomy conditions. This meant that a control model had to be designed. These models needed to replicate the geometric shape and features of pulmonary arteries while including an inlet and outlet for the fluid flow. The device had to be watertight to prevent any fluid from leaking and be sterile to prevent contamination of the cells. Additionally,

the device design could not disrupt the flow in a way that was not similar to the fluid flow of real vasculature. Additionally, the flow rate chosen to run through the vessels had to be appropriate for their sizes. The in vitro model had to support living HLMVECs and glycocalyx growth. In the computer flow model, the right and left lung had to be different and able to be compared to the control non-pneumonectomy model.

The general functional components that the project deliverable needed to contain were placed in a table to clearly show their functional and performative aspects, as can be seen in Table 3.1.

Table 3.1: Functional and performance specifications of the in vitro model.

	Function	Performance
Model Type	A model that allows for testing of controlled flow rates over time which is also biocompatible for endothelial cells	- Plexiglass base (DIMENSIONS 75x75x12mm exterior, 50x50x3.4mm well (made it shallower than PDMS height by 0.1mm to try to get the PDMS pieces to press together, inlet/outlet to match tubing size (one plexiglass set for 6.3mm OD tubing (size 16) and one set for 8mm OD tubing (size 25)) - Tubing openings on sides of model to limit gravity based flow and to produce laminar flow - PDMS piece with desired vasculature shape for cell attachment and accurate in vitro flow modeling - Separable structure to allow for fixing, staining, imaging, and deconstruction after tests for reuse

Cell Seeding	A cell type that represents blood vessel structure, forms the glycocalyx, and is can adhere to the test substrate	- HLMVECs
		  - Adhere to treated PDMS and have contact inhibition to limit overcrowding
		  - Seed at ≥1 million cells/mL

Imaging	Use immunofluorescence staining to easily see changes to the glycocalyx layer and cell confluency	- Use a Keyence BZ-X810 fluorescence microscope to image the cells on the PDMS mold without needing glass slides (Depth of 3.5 mm) - Wheat Germ Agglutinin (WGA) and DAPI

		to stain for protein layer and cell presence (nuclei)
Blood Flow	Replicate an accurate cardiac flow rate consistent with physiological conditions for experiment duration	- Achieve a flow rate between 175-210 mL per minute (per our vessel size) (See Section 5.3.1 and Appendix I)
Shear Stress	A pump type that is able to run flow from a reservoir for extended periods of time	- Flow is controlled and can run for experiment duration (approximately 6 hours) - Target shear stress: 10-12 dyn/cm^2 (See Section 5.3.1 and Appendix I)

Bifurcations	Replicate bifurcation locations and angles at points of interest	- Control Normal (same in pneumonectomy)
		  - 92 deg (first bifurcation, bigger vessel)
		  - 146 deg (second bifurcation, smaller vessel)

3.3 Engineering Standards

The primary standard engineering requirement for the organ-on-a-chip model was cytotoxicity. The device was not in contact with human subjects or blood. Cytotoxicity tests were conducted to determine cell death by observing the cell confluence before and after exposure to the test materials. As outlined in ISO 10993-1, the device being tested is required to be sterilized before testing with a justifiable method to avoid microbial contamination of the cell culture without altering the device properties or viability. The various components were sterilized using one or more methods including autoclaving, soaking in 70% ethanol, and UV treatment and aseptic technique was always used[29]. The SOLIDWORKS files meet ISO 19005-2 (PDF/A-2) standards once saved in PDF v. 1.4–1.7[30].

3.4 Need Statement

After determining the objectives, functions, and specifications of the device based on literature, the following revised client statement was created: Develop a 3D fluidic chip that models the morphology of pre and post pneumonectomy morphology and conditions to better

understand that relationship between pneumonectomies and the eGCX. Further understanding of post pneumonectomy complication causes can allow for pre- and post-operative care changes to mitigate morbidity and improve patient lives.

3.5 Management Approach

To ensure proper and timely fulfillment of the team goals for the project, weekly schedule documents and term-long Gantt charts were created to serve as a reference for the team throughout each week and each term. As shown in Fig. 3.1, the Gantt charts consisted of multiple action items with specific time frames for each item, with the expectation being that those tasks were completed by their respective deadlines. The Gantt charts were used to keep the project on track for success and completion.

#	TASK TITLE	START DATE	END DATE	DURATION (days)	COMPLETE?
1	**Project Conception and Initiation**				
1.1	Discuss team dynamics and channels for communication	8/24/22	8/26/22	2	☑
1.2	Outline future delivarables	8/26/22	8/31/22	5	☑
1.3.1	Literature Review	8/26/22	9/14/22	18	☑
1.3.2	Write Background section of paper	8/31/22	10/14/22	44	☑
1.3.3	Evaluate Current Market and Existing Solutions	9/7/22	9/14/22	7	☑
1.3.4	Write Revised Client Statement	9/14/22	9/21/22	7	☑
1.3.5	Design Specifications and Needs Analysis	9/14/22	9/21/22	7	☑
1.4	Initial SolidWorks lung model design	9/28/22	10/14/22	16	☑
1.5	Initial SolidWorks model of in-vitro model	10/2/22	10/12/22	10	☑
2	**Project Definition and Planning**				
2.1.1	Create Material List	10/23/22	10/26/22	3	☑
2.1.2	Order Materials	10/23/22	11/6/22	14	☑
2.2	Refined SolidWorks lung model	10/23/22	11/9/22	17	☑
2.3	Initial COMSOL simulations	11/9/22	11/22/22	13	☑
2.4	PDMS testing	11/13/22	11/30/22	17	☑
2.5	Refined in-vitro model design	11/30/22	12/10/22	10	☑
2.6	Initial COMSOL data collection	12/4/22	12/17/22	13	☑
2.7	Initial fluid flow testing with draft of in-vitro model	12/7/22	12/17/22	10	☑
3	**Project Design and Testing**				
3.1	Initial leak testing	1/11/23	1/13/23	2	☑
3.2	Initial PDMS imaging testing	1/17/23	1/17/23	1	☑
3.3	Cryosectioing & paraffin wax procedure	1/22/23	2/10/23	18	☑
3.4	Initial pump calibration	1/30/23	2/3/23	3	☑
3.5.1	Initial Cell culturing attempts	2/1/23	3/23/23	51	☑
3.5.2	Initial Cell seeding attempts	2/1/23	3/23/23	51	☑
3.5.3	Viewing cells with Nikon TS 100 microscope	2/1/23	3/19/23	47	☑
3.6	Refined fluid flow testing on in-vitro model	2/5/23	2/5/23	0	☑
3.7	Final pump claibration	2/8/23	2/8/23	0	☑
3.8	Initial Finalized budget	2/9/23	2/10/23	1	☑
3.9	Refined Solidworks lung model	2/12/23	2/17/23	5	☑
3.1	Refined in-vitro model design	2/12/23	2/17/23	5	☑
3.11	Refined COMSOL simulations and data collection	2/17/23	3/3/23	14	☑
3.12	Initial Keyence fluoresence testing	2/20/23	3/3/23	11	☑
4	**Finalize Design and Deliverables**				
4.1	Redesigned PDMS Stamp	3/20/23	3/22/23	2	☑
4.2	Finalized flow setup	3/28/23	4/4/23	6	☑
4.3	Initail images with WGA and DAPI stains	3/28/23	3/29/23	1	☑
4.4	Ran dynamic and static sterility tests	4/4/23	4/13/23	9	☑
4.5	Submitted executive summary and ethics statement	4/5/23	4/12/23	7	☑
4.6	Fix & Stain cells	4/13/23	4/20/23	7	☑
4.7	Imaging with Keyence fluorescence microscope	4/13/23	4/20/23	7	☑
4.8	Project Presentation day	4/21/23	4/21/23	0	☑
4.9	Submit paper and eCDRs	4/27/23	4/27/23	0	☑

Figure 3.1 Academic Year-Long Gantt Chart

In A-Term, the team's goals were to define team dynamics, complete the literature review and project strategy portions of the final report, and create a physiologically accurate SOLIDWORKS model of a lung. Towards the end of the term, the team shifted focus towards designing the in vitro model and compiling a materials list. The team acquired more materials and worked to refine the in vitro model, developing a prototype to test the concept more thoroughly. The SOLIDWORKS model was finalized, but upon attempts to perform the fluid flow simulations in SOLIDWORKS and then in COMSOL, extensive issues with the model were

discovered, and it had to be redesigned through many more iterations to achieve a working model for fluid flow simulation in COMSOL. In C-Term, the team performed its most lab-heavy work, culturing the cells for experimentation, testing methods for staining and imaging the cells, and working on achieving the desired flow through the in vitro model. Significant time was also spent improving the flow simulations in COMSOL with the control model as well as the right and left pneumonectomy models. In D-Term, the team concluded its work by finalizing the flow simulations and completing additional simulations using the exact in vitro designs used. The in vitro setup was run for the longest achievable time, and staining and imaging were finalized. This paper and a corresponding presentation were finished and presented for the culmination of the team's MQP.

4. Design Process

This chapter covers the specifications chosen to guide the design of the in vitro model and the process employed to meet these specifications.

4.1 Needs Analysis

The device design was created to meet the client's need for determining the impact of pneumonectomy-induced, elevated shear stress upon the glycocalyx. The design of the SOLIDWORKS model and the in vitro model itself needed to replicate similar vascular morphology and fluid flow conditions. Our goal was to improve upon the previous team's two-dimensional model, which consisted of large, flat vasculature with only one bifurcation to model normal vasculature as well as left and right pneumonectomies[25]. The previous team also attempted a digital 3D model but was unable to complete it. To expand upon their work, we pursued both a digital and in vitro 3D model.

4.1.1 Functional Specifications

Before determining the design itself, we determined our overall needs to meet the client's statement. To determine which design factors were "needs" versus "wants," the desired design aspects were compiled into a Pairwise comparison chart (shown in Table 4.1). The Pairwise chart ranked each need against every other need individually. "1" indicated a superior need, and "0" indicated an inferior need, comparing the item on the vertical axis to the item on the horizontal axis. Total scores for each factor were generated through the summation of each row, showing which needs deserved the highest weight.

Table 4.1 : Pairwise Comparison Chart for the in vitro model, used to determine design factors

Objectives	Realism	Biocompatibility	Ease of Reproducibility	Ease of Imaging	Timeframe	Ease of construction	Cost	Ease of Seeding	Score
Realism	X	0	1	1	1	1	1	1	6
Biocompatibility	1	X	1	1	1	1	1	1	7
Ease of reproducibility	0	0	X	1	0	1	0	0	2
Ease of imaging	0	0	1	X	1	1	1	1	5
Timeframe	0	0	0	0	X	1	1	0	2
Ease of Construction	0	0	1	0	1	X	1	0	3
Cost	0	0	0	0	1	0	X	0	1
Ease of seeding	0	0	1	0	1	1	1	X	4

The Pairwise comparison chart showed that realism and biocompatibility were the most desired specifications, with time frame, cost, and reproducibility taking lower priority. To meet the need for accessible imaging, the desired design would be able to be taken apart in some capacity to allow for imaging. Ideally, the material used would not need to be ruined or heavily processed to allow imaging. A related need was to be able to stain and obtain clear images that allowed for analysis of the cells and glycocalyx following trials.

The vasculature being modeled needed to be realistic. This meant mimicking literature-derived morphology and measured diameter and bifurcation angles of human pulmonary vasculature. This vasculature and design must also be dynamic and experience anatomical shear stresses dictated by literature. In order to observe the impacts of these stresses on the glycocalyx, the glycocalyx needed to be able to grow, adhere, and remain healthy without influence from factors that weren't shear stress. The cells used needed to generate a glycocalyx. The cells also needed to fulfill the realism and imaging needs, as they had to be stained and imaged fluorescently to view the presence of the glycocalyx. The biocompatible need meant that the material selected and its treatment must keep the chosen cells healthy and support adhesion, all with no contamination. While not pictured in the Pairwise chart, another need for the vasculature was being able to replicate multiple morphologies, specifically a control and pneumonectomy model, which would allow for the comparison of locations of interest in both models.

While reproducibility and cost were not as heavily weighted as morphological accuracy, they remained important factors. The ultimate goal was to produce a model that included all of the desired design specifications.

4.1.2 Performance Specifications

The part of the in vitro device that contained the vasculature needed to be wide and long enough to support appropriate vasculature shapes without requiring excessive material. The vessel morphology would be determined by the digital model. The digital model would replicate anatomical pulmonary vasculature, and attempt to model a simplified version of the full pulmonary vasculature, with main and distal pulmonary arteries. The depth of the in vitro device needed to house a well for the chosen vasculature, but an overly deep well would have required excessive material and been counterproductive for imaging. Additionally, the in vitro design had

to survive sterilization and incubation, requiring durability toward some heat, humidity, and use in an autoclave or under UV light. To introduce the dynamic flow and the resulting shear stress, heart-like rhythms could be generated using a peristaltic pump. The tubing selected for the model had to meet both the peristaltic pump size requirements and the in vitro model vasculature size. The complete design had to interact with the peristaltic pump and be able to fit inside an incubator to keep cells alive.

4.2 Alternative Designs

In our initial design brainstorming, four distinct in vitro design options were considered: organ-on-a-chip (OoC), bioprinting, tissue-engineered blood vessels (TEBVs), and an entirely PDMS model. All of the models considered had the capacity to model different vasculature shapes and sizes to varying degrees.

One of the alternative ideas was a full PDMS model, which would have consisted of PDMS molded into the shape of the vasculature. This most closely followed the previous team's recommendations—they suggested 3D printing PVA (polyvinyl alcohol) molds to create seamless PDMS tubes to seed HLMVECs and run fluid through[25]. The challenges of this design would have included cost, structural integrity, and imaging. PVA is water soluble, making the PDMS demolding process much easier, but would render the PVA unusable once dissolved after every trial. The tubular PDMS would have likely required external support or would have been thicker, making for a more challenging molding process and imaging. Imaging could have occurred through cutting the model to stain and image small sections or through the complete removal of cells, leaving the entire model useless afterwards.

Another alternative design was tissue-engineered blood vessels (TEBVs)[31]. TEBVs are created by seeding cells onto a tubular scaffold to form ring-like structures. One of the main issues with this process was that it had only been done on a very small scale and took a long time. One study involving the TEBVs took 28 weeks for a small section of vasculature. One of our project needs was to model a bifurcation and produce multiple iterations of blood vessels in vitro, so the time limitation of the TEBVs design was a deterrent.

The remaining design was an organ-on-a-chip design, as discussed in 2.5.3 [28]. The concept of OoC designs showed promise in terms of cost, resources, and time, and our final design most closely replicates this method with functional alterations.

Our main changes to this model were due to our need for dynamic flow and budget. Initial iterations of this design option involved the planned use of collagen. Our final model resulted in being on a much larger scale than the design that inspired this concept. Due to our increased requirement for a substrate material that could withstand the dynamic flow and the need to replicate different vasculature shapes, we were unable to afford using collagen. We ultimately switched to PDMS as a substrate, which produced some imaging problems (see Chapter 5), but was affordable and easy to mold.

Another alternative design that was considered was the use of a removable silicone membrane lining the PDMS. This would have allowed us to image a very thin sample using a confocal microscope, as the silicone membrane was very thin. However, applying the membrane to the tube-shaped parts of the PDMS molds created a lot of small folds and creases that would have perverted the vasculature's accuracy, cell adhesion, and fluid flow through the model. This was proved when we observed the PDMS with a silicone layer under a brightfield microscope. One option to reduce these folds included the application of heat to the silicone membrane when adding it to the PDMS, but it would have warped the silicone. Heat-treating the silicone to reduce the creasing would have also made it difficult to image, so this option was not pursued.

4.3 Design Process and Final Design Models

Before choosing our final design, we assessed how well design options met our design criteria using a Pugh chart, as seen in Table 4.2. The OoC design was found to be the most feasible out of the other designs, primarily from a cell seeding, biocompatibility, and realism standpoint, which were heavily weighted based on the Pairwise chart (Table 4.1). In general, none of these designs had easy imaging methods, if they had any at all, and the potential for imaging in the OoC design was determined to have the most potential.

Table 4.2: Pugh Chart Analysis, used to determine which designs to pursue

Objectives	Weight	2D baseline	OoC	Bioprinting	TEBVs	PDMS model
Realism	4	0	1(4)	1(4)	1(4)	1(4)
Biocompatibility	5	0	1(5)	1(5)	1(5)	0
Ease of reproducibility	3	0	1	-1(3)	-1(3)	-1
Ease of imaging	4	0	-1(4)	-1(4)	-1(4)	-1(4)
Timeframe	2	0	1(2)	0	-1(2)	1(2)
Ease of Construction	4	0	1	-1(4)	-1(4)	-1(4)
Cost	2	0	0	0	-1(2)	0
Ease of seeding	4	0	1	-1(4)	0	0
Rank Score	-	0	7	-6	-6	-3

The general concept of the in vitro design was informed by the previous team's work and recommendations for modeling pneumonectomy effects on the eGCX, combined with the microfluidic device created by Zheng and his team discussed in Chapter 2[28].

4.3.1 In Vitro Model Concepts

One of the main changes we made early on was changing the vasculature shape. Zheng's model used rectangular vasculature, using a rectangular PDMS stamp[28]. We wanted to replicate the cylindrical nature of blood vessels and produce a physiologically accurate model. Our initial design for this model used collagen as the vasculature shape that the cells would be seeded on. To create the cylindrical shape, we would separately create two mirror-image molds that would be coupled to create the vasculature shape. The plexiglass would have machined wells and inlet ports for collagen injection. Once the collagen set, the plexiglass would be unscrewed, the PDMS stamp would be removed, and one of the two matching halves of collagen would be produced. Once both collagen halves were formed, the plexiglass would be screwed together (with the collagen halves sandwiched together in the middle) to form the completed cylinder of vasculature. This early conceptual design can be seen in Fig. 4.1.
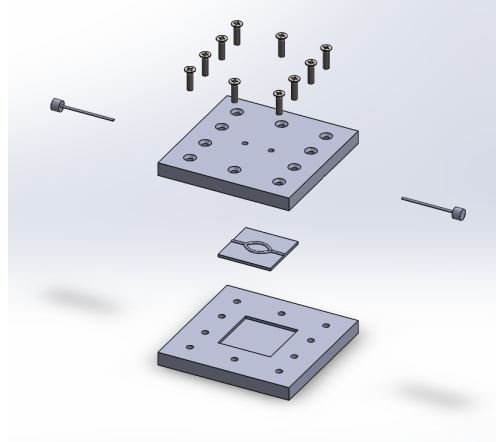
Figure 4.1: Conceptual SOLIDWORKS design on OoC for molding collagen. The large square pieces were the plexiglass and the small square piece between the plexiglass was the PDMS stamp. The cylindrical pieces on the sides were dowels to block the collagen from leaking out the inlet and outlets. The two small holes in the top plexiglass piece were the injection ports for adding collagen once the setup was screwed together.

Early concepts of the OoC model were 25 mm smaller than the final design, closer to the scale of Zheng's design. Originally, the interior of the chip was only 25 mm wide, with the exterior measuring 50 x 50 mm. We made the chip larger to allow for bifurcations, varied vessel diameters, and to have more space to stay true to the physiological angles of vasculature of our digital model.

Early concepts used collagen as the vasculature shape that would be set around a mold made of PDMS. The PDMS mold would have been made by pouring and mixing the base and curing agent (10:1 ratio) in a negative mold (Figs. 4.2 and 4.3). Our early concepts included an aluminum base that would have held the PDMS mold while the collagen was added. There was no gasket in our designs, as Zheng and his team used only the mechanical stress of screws in their model and found that sufficient to prevent leaking between the two collagen mates[28].
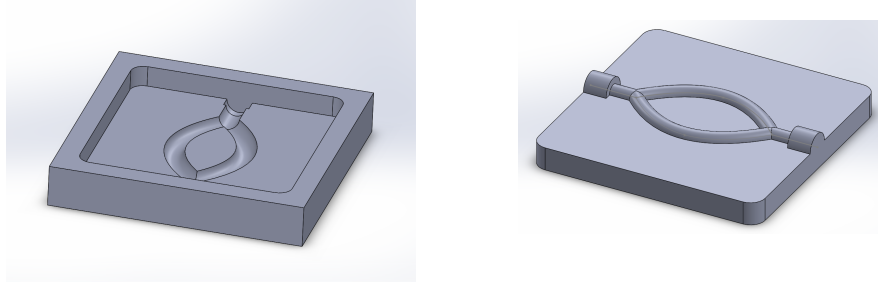
Figure 4.2 and 4.3: Negative PLA mold for PDMS (*left*), and PDMS stamp after setting in PLA negative mold (*right*). The PDMS stamp (*right*) would then have been used to form collagen gel into the desired vasculature shape.

These early concepts were made into minimum viable products. These models, like the one in Fig. 4.4, allowed for a better understanding of the appropriate size and the model's interactions with the tubing and PLA components.

Figure 4.4: Rudimentary cardboard physical model

After these early concept models were formed, we continued on to our 3D SOLIDWORKS model. This would help to inform our in vitro model vasculature morphology.

4.3.2 SOLIDWORKS Model Prototyping and Final Design

The first step in making the OoC model come to life was to determine what vasculature we were going to model. Our initial goal was to create a complex pulmonary vasculature model that would be used for flow simulations in COMSOL in three variations: a control (no pneumonectomy version), and two pneumonectomy models, one per side. We first searched for

existing 3D models online, but did not find any suitable for our needs. This required us to create our own. We wanted this model to replicate anatomical vasculature sizes, but found very limited data for basal branches and smaller vessels.

To determine the desired vasculature's values to complete the COMSOL simulation model, we used a combination of CT scan measurements and literature values. Radiography images of the pulmonary vasculature were used in Fiji, an open-source image processing software, to determine vessel diameters. One source that showed CT scans of large and medium-sized pulmonary vasculature was used to obtain measurements in Fiji[32]. These CT scans are shown in Figs. 4.5 and 4.6.
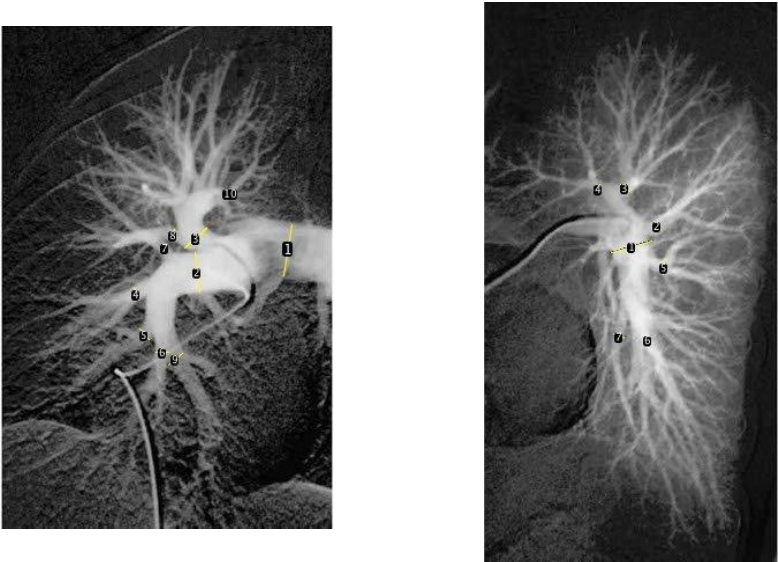
Figure 4.5 (*left*) and 4.6 (*right*): Radiography Images of right (*left)* and left (*right)* pulmonary vasculature, with vessel diameters (yellow) measured in Fiji. Measurement 1 was the scale, based on literature data[14] respectively.

Literature shows that measurements of the main pulmonary artery (MPA) vary, but average around 29.5 mm in diameter in males[14]. The right and left arteries are about 19.8 mm and 22.1 mm in diameter on average[14]. We used these values as the scales for the CT Scans in Fiji.

Table 4.3 : Pulmonary Artery Segment values determined across literature and radiography measurements categorized into vessel diameter ranges for easier modeling

39

Pulmonary Artery Segment	Diameter (mm)
Main Pulmonary Artery (MPA)	29.5
Right Pulmonary Artery (RPA)	19.8
Left Pulmonary Artery (LPA)	22.0
Right Anterior Segment (RUL)	9.0
Secondary Segments	4.0 - 7.0
Tertiary vessels	3.25
Small and Capillary values	0.5 - 1.5

The cumulative values of arteries obtained were categorized into segment types to assist with the SOLIDWORKS model and compiled into Table 4.3. This table was referenced when creating the model. One value not included above was the stump length sizes. Literature shows that pneumonectomy stump lengths are about 5 mm long [33], and that value was used for our SOLIDWORKS model stump lengths.

SOLIDWORKS Concept

The SOLIDWORKS 3D model of a pulmonary arterial tree was initially created with a series of sketches, both in the 2D and 3D planes, with surface sweeps revolving around each sketch to form the structure. The surface loft tool was used to connect tubes of differing diameters. The layout of the model and the diameters of the tubes within the model were all based on the Fiji data referenced in Section 4.3.2.

The model underwent many revisions, mainly revolving around simplifying the structure for the ease of creating flow simulations when it was transferred to COMSOL. As seen in Fig. 4.7, open faces (seen in blue) formed where two sweeps met, making flow simulations impossible. In order to address this issue, all of the tubes that were created with surface sweeps

were turned into solid sweeps to eliminate any open faces or crevices. This change was also made for ease of use in COMSOL to set up parameters for flow simulations.
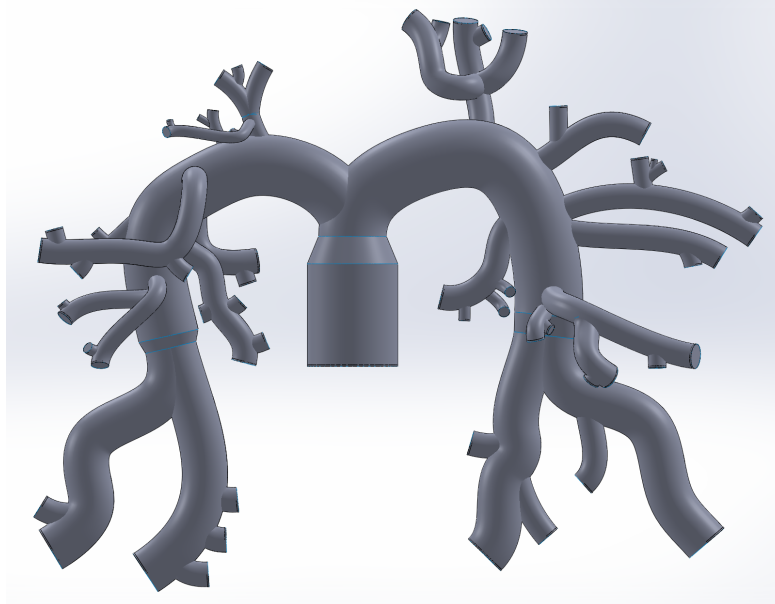
Figure 4.7: Initial SOLIDWORKS Model. Small blue lines can be seen where open faces formed where two sweeps met.

While first attempting initial simulations on the model above (Fig. 4.7), the group ran into many issues with its complex nature. As a result, a number of tubular structures were identified as less significant with the help of Professor Mensah and these structures were removed to simplify the model. After the model was created, it was duplicated twice to cut the left and right sides of the model, generating a left pneumonectomy model and a right pneumonectomy model, respectively. The final control model can be seen in Fig. 4.8 and the pneumonectomy models can be seen in Figs. 4.9 and 4.10. All three models were then transferred over to COMSOL for fluid flow simulations. In addition to prior challenges, replicating organic vascular morphology was a more advanced process and required us to learn new SOLIDWORKS features and scale back on the initial design.
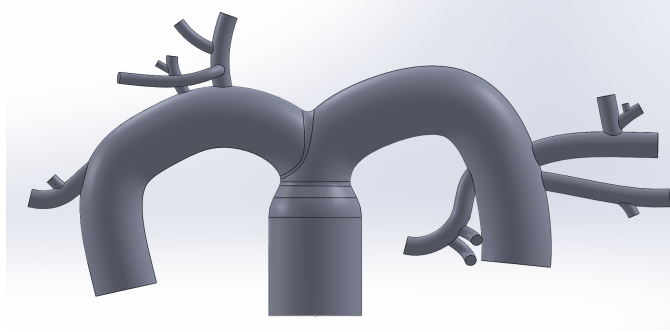
Figure 4.8: Initial simplified control (no pneumonectomy) SOLIDWORKS model.
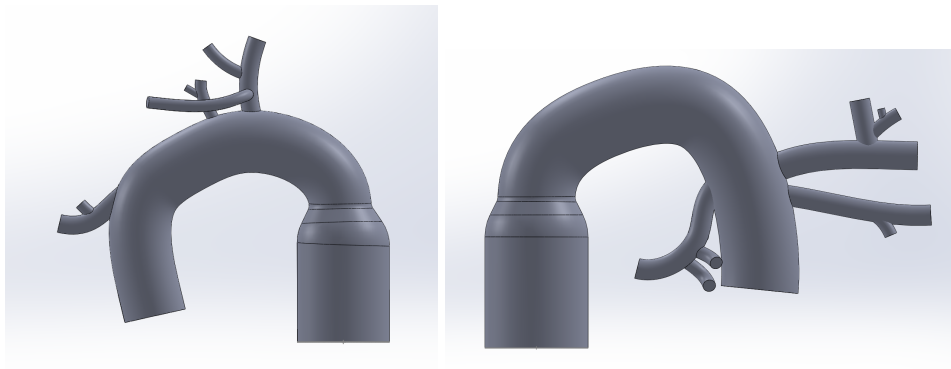
Figures 4.9 (*left*) and 4.10 (*right*): Initial simplified models of left (*left*) and right (*right)* pneumonectomy models.

The above figures (Figs 4.8, 4.9, 4.10) needed to be reverted back to hollow surface sweeps instead of solid sweeps to introduce wall thickness. Additionally, it was noted that for ease of analysis, the model could be transferred from a part file into an assembly file through which each vessel could be isolated and studied. This change would also allow for differing thickness levels along the model based on vessel diameter and their matching wall thicknesses found in literature as opposed to having uniform thickness. With these considerations implemented to further improve the accuracy of our results, we produced the models as seen in Figs. 4.11, 4.12, and 4.13 below.

Figure 4.11: Control model (no pneumonectomy) as an assembly in SOLIDWORKS.

Figures 4.12 (*left*) and 4.13 (*right*): Models of left (*left*) and right (*right*) pneumonectomy assemblies in SOLIDWORKS.

While the models now contained unique thickness levels across the varying vessels and were now converted into assemblies, there were still some issues with the model. The vessels obstructed flow inside of the model since the vessels were designed in a way that the surface sweeps overlapped or jutted into one another as seen in Fig. 4.14 below.
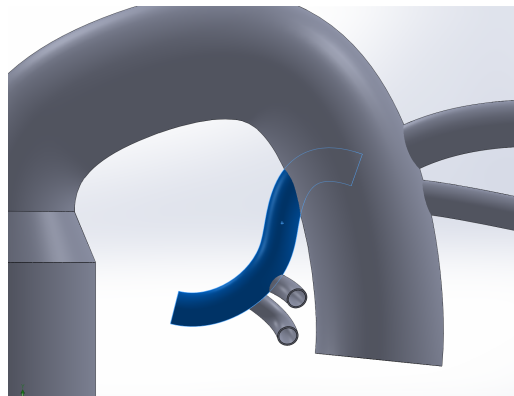
Figure 4.14: Smaller vessel obstructing flow in right artery.

In previous attempts to construct the model in SOLIDWORKS, a tool called surface trim was used to cut a vessel at the point in which it obstructed another to remove all obstructions within the model. Unfortunately, in an assembly file, every vessel was combined with its set thickness and each part could no longer be edited individually, rendering the surface trim tool useless. Additionally, the surface loft and filet tools we had used previously to smooth out the connection between the right, left, and main arteries had the same limitation as the surface trim tool.

Final SOLIDWORKS Model

To resolve the issues mentioned above, we reverted to an original iteration of the models where they were solid parts. The vessels were then hollowed out by using the sweep cut tool. Using the sweep cut and assigning the correct inner wall dimensions made it possible to successfully assign individual wall thicknesses to different vessels as well as avoiding obstructions within the model preventing smooth flow. The greatest difficulty was at the neck of the pulmonary artery where the two main pulmonary arteries branched off from each other. In Fig. 4.15, the visible exterior wall of the model appears to be smoothed out with filets around the lofted section. When hollowing this out, we were unable to replicate the smoothness because the sweep cut tool would not match the geometry produced by the filets. Hence, we have the section view below of this in Fig. 4.15. This affected our COMSOL fluid flow results because in real vasculature, it is smoother.
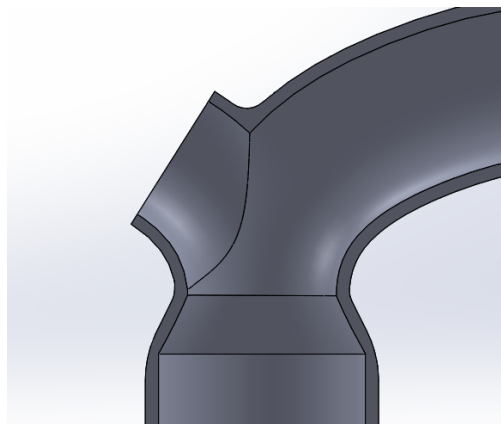
Figure 4.15: Section view along midplane of right pneumonectomy model.

The last refinement to the digital 3D models was including a stump in place of the removed lung for a more accurate representation of pulmonary vasculature physiology post pneumonectomy. To implement this redesign, the spline for the lung being removed was shortened to a length of about 5 mm for each model as seen in Figs. 4.16 and 4.17 below to represent the actual length of stumps based on literature values that were found[33]. The finalized full control model being used to collect our final flow simulation results can also be seen below in Fig. 4.18.
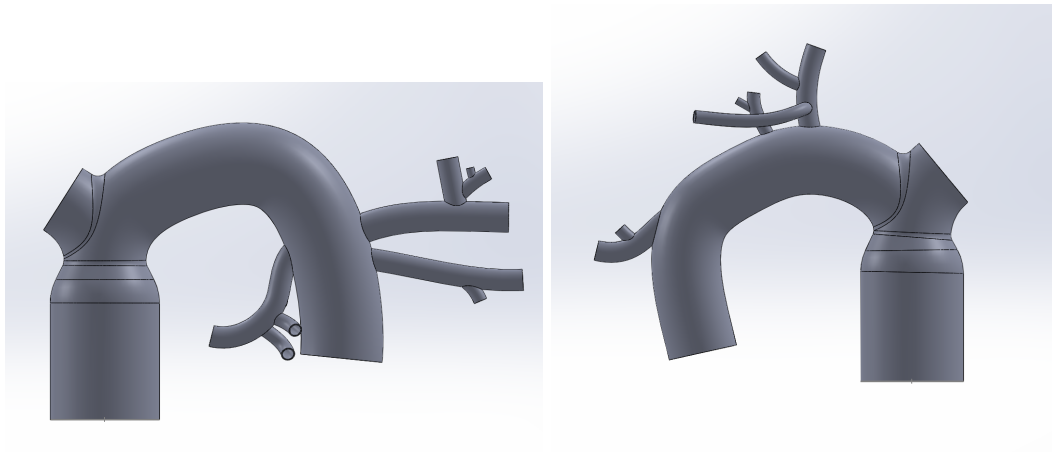
Figure 4.16 and 4.17: Finalized right (*left*) and left (*right*) pneumonectomy models with stump included in SOLIDWORKS.
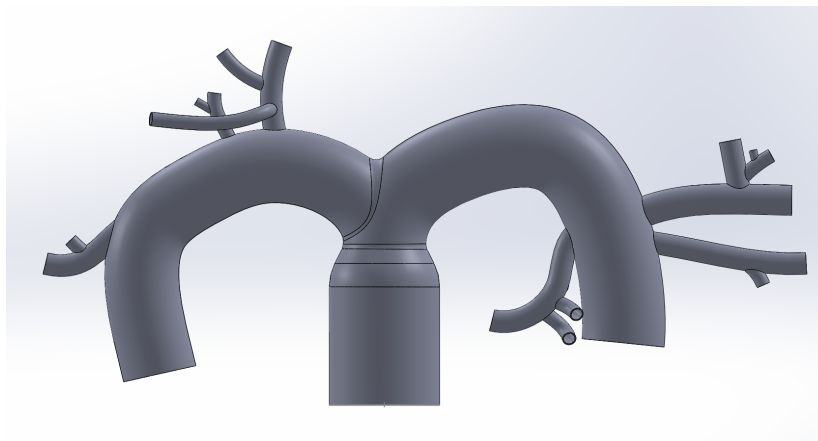
Figure 4.18: Finalized control model (no pneumonectomy) in SOLIDWORKS.

4.3.3 In Vitro Model Process

Only the vasculature shape within the OoC design was based on the COMSOL simulation data, so while the SOLIDWORKS models were developed and COMSOL data were being collected, iterations of the OcC component of the project were also being worked on. The exterior plexiglass structure and mold designs for the PDMS received focus, initially.

Material Characteristics

Materials were determined primarily based on previous literature on an organ-on-a-chip model[34] and are depicted in Table 4.4. Plexiglass, screws, PDMS, and PLA were all chosen based on physical properties, mechanical factors, and cost effectiveness. The plexiglass and PDMS were affordable and adequately sturdy while allowing for ease of surface alteration with chemical treatments and sterilization. Additionally, the plexiglass and PLA were chosen for their compatibility with PDMS. The materials in contact with the PDMS needed to be easily sterilized yet could not impact the surface of the PDMS in a way that would influence the cell seeding and fluid flow.

Table 4.4: List of Materials and specifications for the OoC in vitro model

Materials	Purpose	Reason for Material Choice	Size
Plexiglass	To create the outer boundary of the modeled system and provide structural support	Cheap, machinable and transparent	(Identical top and bottom) Outer: 50mm x 50mm x 5mm Well: 20mm x 20mm x 1mm
Screws	Mechanically hold the device together during testing	Easily removable after testing and are more secure than alternative methods	M3 x 0.5 mm ~ 8mm depth

Dowel stops	Enclose the system when seeding HLMVECs	Easy use and necessary for a horizontal flow vasculature	2x media (OD fits ID of size 16 tubing)
Polylactic Acid (PLA)	3D printing material for the positive PDMS mold	Cheap, easily printed, no deformation upon exposure to gels and moisture	Used available size from WPI Makerspace (0.4 mm filament)
Polydimethylsiloxane (PDMS)	Serve as vasculature model while supporting cell adhesion. Capable of being imaged through	Easily moldable and replicable as well as having an easily modifiable surface structure for treatments	~30 ml of 10:1 PDMS base to curing agent per model
Tubing (Peroxide-Cured Silicone)	Transport fluid from peristaltic pump to model and back, producing laminar flow in model	Clear, biocompatible, compatible with pump, and matches the vessel size	25 ft of size 16, ID: 3.1 mm 25 ft of size 25, ID: 4.8 mm

Initial Mold Modeling

The original concepts consisted of a PLA mold to shape the PDMS stamp, followed by the positive PDMS mold being placed within an aluminum base. The aluminum-PDMS base would be screwed to the top half of the plexiglass, and collagen would be injected through the inlet ports of the plexiglass, which would be made using a CNC machine. These small inlet ports can be seen in the concept design shown in Fig. 4.1.

This concept changed when the choice was made to switch from collagen to PDMS as the vessel model. Ultimately, it was decided that collagen could not be used as the primary substrate. At around 300 USD for 50 mg, the material was too expensive. If we had replicated the concentration of collagen in Zheng's work, we would have used 180 mg of collagen per model,

far exceeding our budget. We decided to change the substrate material from collagen to PDMS and move forward with a plan to apply only a layer of collagen to the PDMS. The new PLA would instead be a positive mold (shown in Fig. 4.19) in order to generate a negative imprint in the PDMS.
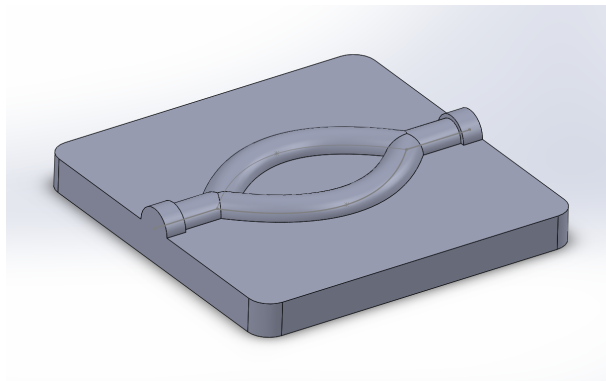
Figure 4.19: Early positive mold to be made of PLA, with tubing accommodation at the inlet and outlet. Shown in SOLIDWORKS.

Early concepts planned to have the peristaltic pump tubing that would deliver fluid into the model where the PDMS met the wall of the plexiglass. After speaking with Ian Anderson, a machine shop specialist at the Goddard Machine Shop at WPI, he recommended that we adjust the design to have the tubing go slightly further into the mold to ensure laminar flow and to prevent leakage. To do this, the inlet and outlet points of the now-positive PLA mold were widened to match the outer diameter of the tubing. Ultimately, size 16 tubing was selected as it was closest to the desired vessel diameter, as determined by the COMSOL data. This tubing had an inner diameter of 3.10 mm and an outer diameter of 6.30 mm. The vessel sizes for this model and for the COMSOL-derived models had a radius of 1.55 mm to match the tubing size for optimal laminar flow. However, Anderson also recommended that we make the radius on the PLA mold smaller than 3.15 mm. By making the space for the tubing slightly smaller, the tube would be lightly squeezed between the PDMS halves once assembled. Therefore, we made the outer radius at the ends of the PLA mold 3 mm. The sealing ability of the tubing with the PDMS and the seal between the two PDMS halves were tested by running water through the setup with the MasterFlex L/S peristaltic pump (see Section 4.3.3 for flow testing details).

The next decision to finalize the mold design was to eliminate the aluminum base due to material cost and time. Instead, the PLA molds for PDMS were expanded to be screwed into the

plexiglass if necessary, as can be seen in the Fig. 4.20 and 4.21 models. Ultimately, the screw holes were removed because PDMS had no issues curing in the PLA with nothing on top.

All of the PLA models were printed using an Ultimaker 3 3D printer, and early controls were tested at various temperatures to cure the PDMS. These preliminary tests showed that the PLA bubbled, warped, and shrank when placed in an oven between 40 and 65°C, even though PLA's glass temperature is generally 50°C or higher[35]. To solve this problem, we tested setting the PDMS in the mold at room temperature. While this did take over 48 hours to cure, it protected the PLA from shrinkage and warping.
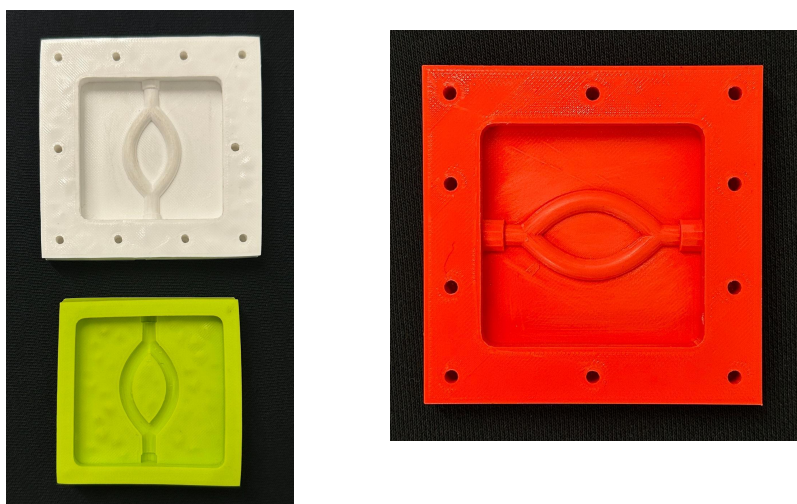
Figure 4.20 (*left*) and 4.21 (*right*): Original PLA molds before (*left)* and after (*right)* switching from oven curing to room temperature curing, with screw holes still used in two of the molds.

Two ratios of base to curing agent were tested for forming PDMS: 5:1 and 10:1. The 5:1 ratio was intended to form harder PDMS, but the difference was observed to be insignificant for the purposes of this project. The 5:1 ratio required more of the curing agent to be used, which was more costly. Therefore, the 10:1 ratio was selected moving forward. To mold the PDMS, 3D (extrusion-style) printing was used. A key concern was ensuring that the PDMS would not stick to the mold while setting to allow for removal without tearing or influencing the shape of the negative channel. It was determined that the PDMS was easily removed from the mold with a thin tool such as a razor blade or scalpel. However, the resolution of the 3D printed PLA was not perfect–the additive nature of 3D printing produces ridges in the surface of the PLA. To combat

this, the team lightly sanded the mold with 400-grit sandpaper, which somewhat smoothed the PLA. However, sanding was ultimately abandoned because it produced fine dust that was extremely difficult to clean from the small ridges and valleys of the molds. This dust ended up in the PDMS and negatively impacted its clarity for imaging.

To adequately evaluate the results of a pneumonectomy and other vasculature shapes on the glycocalyx, we modeled a control. The control (no pneumonectomy) mold (as seen in Fig. 4.22) replicated right and left pulmonary arteries, with one basal branch on each side. Having a basal branch allowed the cells at the multiple bifurcations to be analyzed, as literature showed that that is typically where increased shear stress is found. Only one initial pneumonectomy model was designed, as shown in Fig. 4.23.
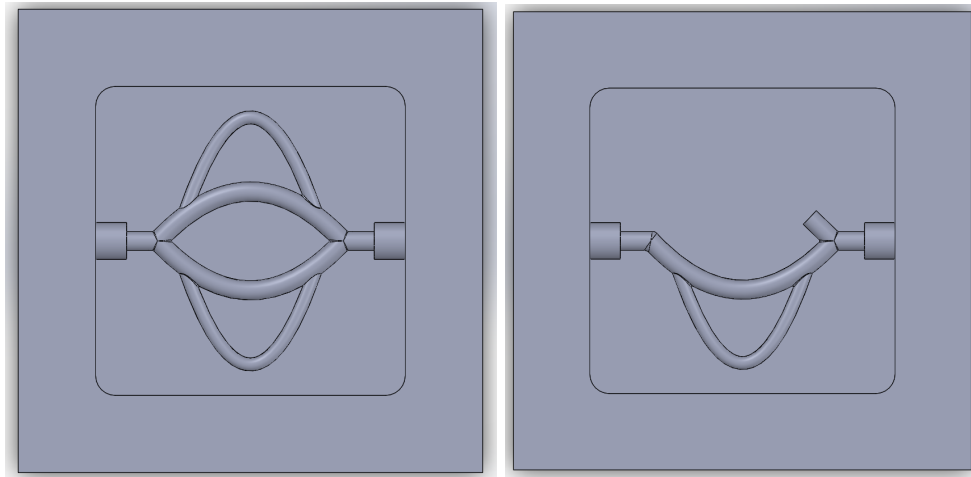
Figure 4.22 (*left*) and 4.23 (*right*): Initial COMSOL-based PLA molds, shown in SOLIDWORKS. Control (*left)* and pneumonectomy control (*right*). The control mold was used for both left and right pneumonectomy fluid flow tests.

COMSOL Points of Interest

After the data from the COMSOL model was collected and analyzed, the COMSOL-based PLA molds were designed. Based on the COMSOL data, we chose points of interest from each side of the model. These locations of interest were determined by qualitatively observing where high shear stress was found in the full model shown in Fig. 4.24 below.
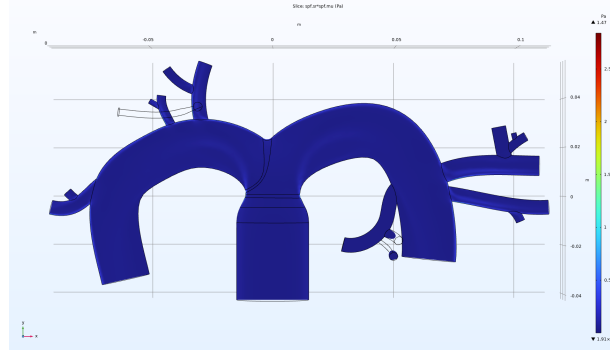
Figure 4.24: Final SOLIDWORKS model, following fluid flow simulations in COMSOL. Warmer colors indicate regions of higher shear stress and cooler colors indicate regions of lower shear stress.

The COMSOL simulations from both the left and right pneumonectomy models showed a clear increase in shear stress, particularly at bifurcations. The first section we chose to model can be seen in Fig. 4.25. On both sides of the model, simple bifurcations were seen to have higher shear stress (see Chapter 5). However, instead of modeling very similar bifurcations, we chose to model a second location of interest that had two bifurcations, making three vessels total (Fig. 4.26). This provided us with data to compare one bifurcation to two bifurcations in a small area and the different impacts on shear stress and the glycocalyx.
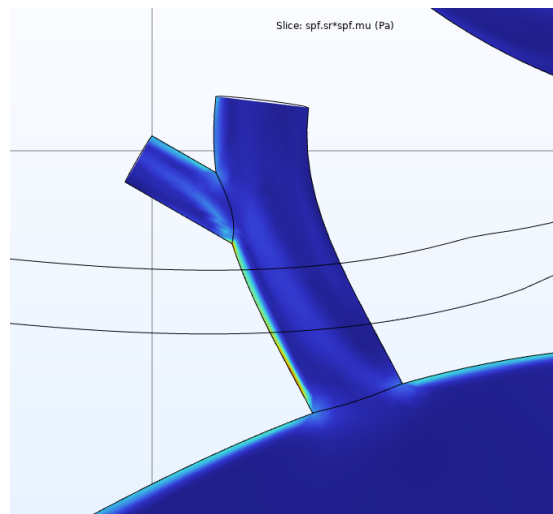
Figure 4.25: Location of Interest #1, with one bifurcation. This was found on the patient right side of our model.
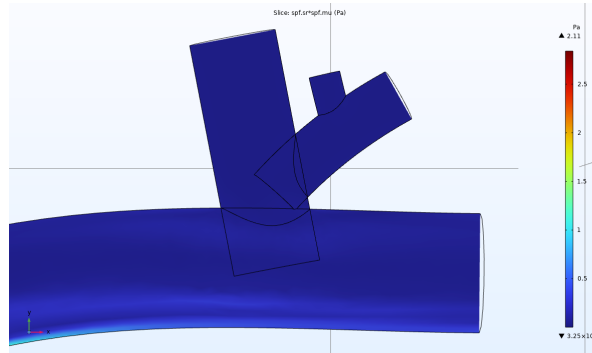
Figure 4.26: Location of Interest #2, with two bifurcations, found on the patient left side of our model.

The measurements of the vessels and bifurcation angles on these points of interest were recorded in Fiji and replicated in SOLIDWORKS to create two molds, as seen in Figs. 4.27 and 4.28. The angles and diameters of the vasculature for these molds were taken from the SOLIDWORKS model at those locations of interest.
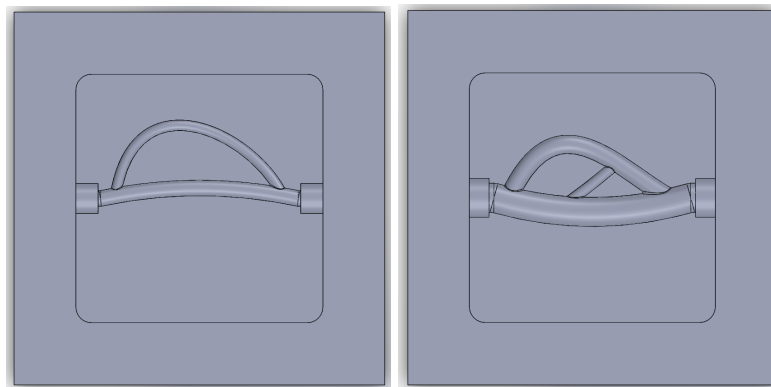
Figure 4.27 (*left*) and 4.28 (*right*): Initial SOLIDWORKS PDMS molds with inlets are on the right side. Single Bif. (*left)* is based on Location of Interest 1, and Double Bif. (*right)* is based on Location of Interest 2.

Plexiglass Machining

The final plexiglass model was sent to Ian Anderson after resizing the inlet and outlet ports to match the finalized tubing sizes (sizes 16 and 25, or outer diameters of 6.3 mm and 8 mm, respectively). Fig. 4.29 depicts the first physical model, which contains the screw holes that were used to bring the two components together and the inlet and outlet holes on the sides for the

tubing. The small inlet and outlet holes were originally meant for collagen. By the time the model was finished, we had decided against using collagen, in exchange for the positive PLA-negative PDMS molding method. The PDMS in the images below is an early prototype, loosely based on literature and not our own simulation results. Figure 4.30 depicts the complete plexiglass chamber enclosure.
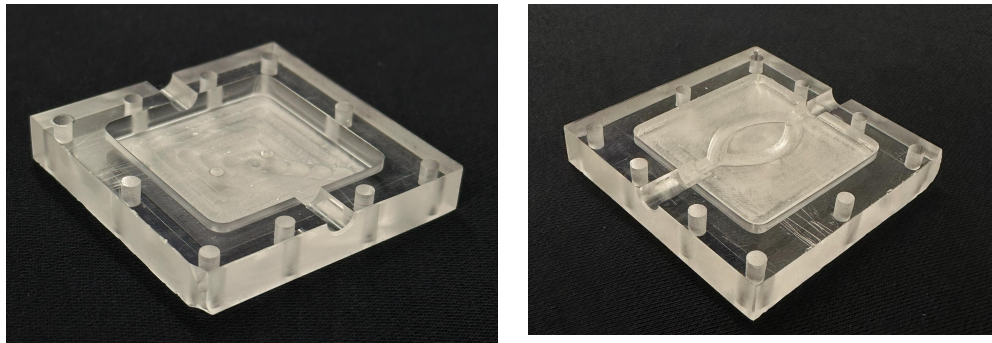
Figure 4.29: First plexiglass model, with (*right*) and without (*left*) PDMS vasculature
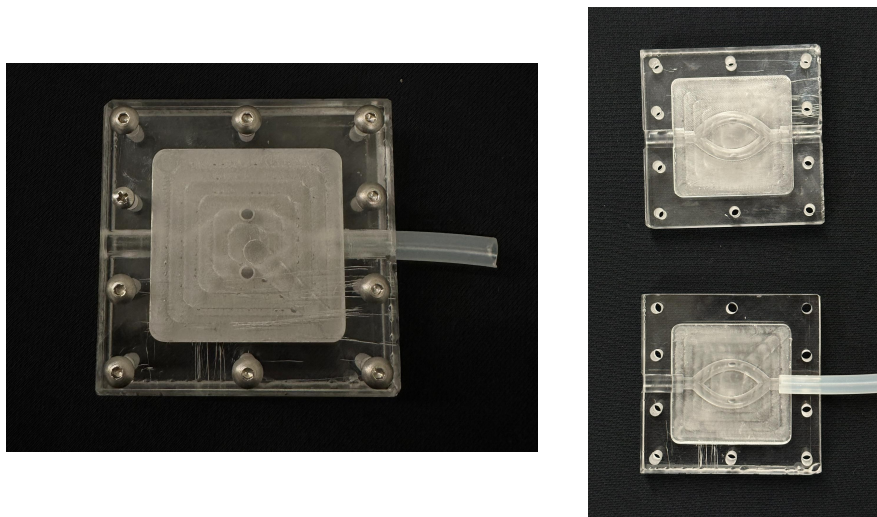
Figure 4.30: Full initial plexiglass model with PDMS, closed (*left*) and open (*right*)

Tubing

The final tubing sizes were chosen to match the COMSOL data and the molds. To match the COMSOL data, size 16 tubing was chosen for the finalized design. Initially, the only mold that used separate tubing was the double bifurcation model, as the vasculature was of a larger

size according to the literature-based SOLIDWORKS model. In order to stay true to that value, we decided to use different tubing for that model. However, the double bifurcation model was ultimately abandoned in exchange for the final redesigns as seen in Fig. 4.28.

Design Assembly

Once our PLA molds had been printed and the PDMS vasculature pieces were formed, we started to assemble our final in vitro design. Figure 4.31 shows how we set up our model for leak and flow testing. Figure 4.32 shows how we would set up the entire model in the incubator for our verification testing and final in vitro tests as discussed in Chapter 5.
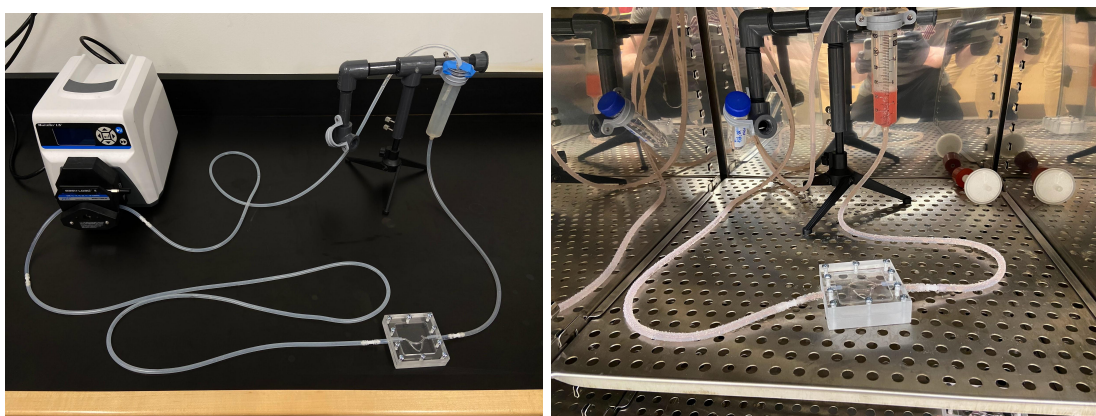
Figures 4.31 (*left*) and 4.32 (*right*): The finalized flow setup assembled on a benchtop (*left*) and in an incubator (*right*). The incubator seen in 4.31 (*left*) is not pictured in 4.32 (*right*), as it is located outside the incubator.

Leak and Flow Testing

Initial flow tests conducted with water showed that there were leaks in the initial chip design and flow setup. To locate leaks accurately, food coloring was added to the water. The interface between the tubing and PDMS at the inlet and outlet of the vasculature were the most problematic, but the interior of the vasculature had almost no issues. Small C-clamps were used to compress the middle of the chip more, but it did not appear to make a significant difference during testing. The mechanical force of the screws was determined to be sufficient for sealing the PDMS halves together.

To better seal the tubing to the PDMS at the inlet and outlet, a silicone gel sealant (Loctite Clear Silicone Waterproof Sealant) was applied to the PDMS before aligning the tubing and closing the plexiglass halves around the tubing as shown in Fig. 4.33.
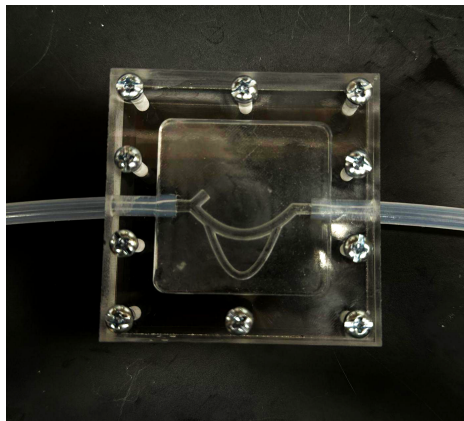
Figure 4.33: Initial fluid flow setup leak testing with size 16 tubing and pneumonectomy vasculature design.

After this change was made, there were little to no signs of leakage from the model, showing great improvement from the original fluid flow testing. However, the process of disassembling the plexiglass model became extremely difficult sometimes. The amount of silicone sealant had to be greatly reduced in order to separate the plexiglass, PDMS, and tubing following testing without damaging the model. Additionally, the silicone would sometimes travel around the edge of the tubing, partially or completely obstructing flow once it set. To mitigate this issue, 3D printed dowels were fabricated to sit inside short pieces of tubing while the silicone sealed the tubing to the PDMS. The tubing pieces were long enough to reach the PDMS while extending out of the plexiglass jigs but were cut shorter than the dowels. The dowels were inserted just enough to extend into the PDMS vasculature to ensure the prevention of silicone blockages, as seen in Fig. 4.34.
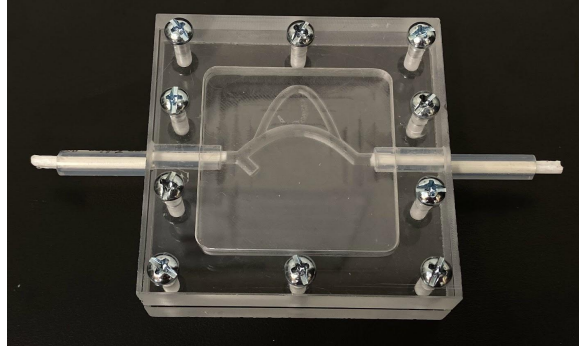
Figure 4.34: 3D Chip after silicone application. The white PLA dowels inserted into short tubing pieces prevented unwanted silicone curing in the tubing or vasculature and blocking flow.

Once the silicone set, the dowels were carefully removed by pulling on the exposed ends with pliers. At this point, the short tubing pieces would be thoroughly sealed to the PDMS vasculature and could be connected to the rest of the flow setup using straight tubing connectors (McMaster-Carr Tight-Seal Moisture-Resistant Plastic Barbed Tube Fittings for Air and Water, Straight Connectors, 1/8" ID). These connectors were easy to use and autoclavable.

With leaks resolved, additional flow testing was conducted with a focus on flow duration. A syringe stand was used to hold two 50 mL syringes as reservoirs for fluid (see Fig. 4.35). It was found that the outflow syringe consistently filled faster than the inflow syringe, resulting in liquid spilling out of the outflow syringe in only a few minutes or less if the pump wasn't stopped. The setup was adjusted, with many different heights tested to see if the syringe overfilling could be prevented using hydrostatic pressure. At its best, the two-syringe reservoir setup lasted about 55 minutes before overflowing (this was with the outflow syringe at a height of around 34.5 cm above the benchtop, which was achieved using a ring stand).
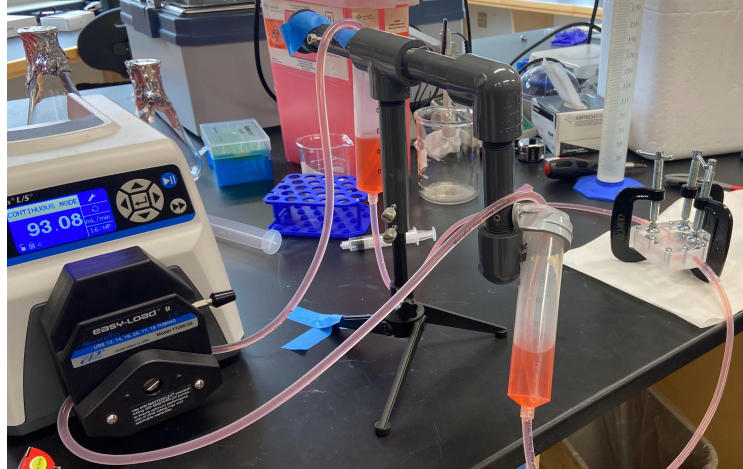
Figure 4.35 : Flow testing using two-syringe reservoir setup. The chip was also compressed using small C-clamps at this time, though these were determined to be unnecessary.

The overflow was finally resolved by removing the inflow syringe reservoir entirely. The outflow syringe height was varied with no overflow, and the setup was eventually run for 48 hours in the sterility testing (see Section 5.3.3 for more details) with no overflow problems.

Throughout the testing for the leaks and overflow issues, flow abnormalities were observed in all of the initial PDMS designs. Figure 4.36 shows that the smaller vessels consistently contained air bubbles and flow rarely ran smoothly through these vessels. It was hypothesized that the angles, flow pressure, and the hydrophobic nature of PDMS could have been responsible for the lack of flow in these vessels.

Figure 4.36 : Air bubbles formed in a smaller vessel in the pneumonectomy vasculature model during fluid flow testing.

COMSOL PDMS Mold Redesign

Our solution to the flow issues was to redesign the control, pneumonectomy, and single bifurcation models. This redesign involved moving the small vessel to the interior in the control and pneumonectomy models and making the single bifurcation model more symmetrical (see Fig. 4.37). The double bifurcation model was abandoned in this redesign due to its similarity to the control and time limitations. These redesigns were then validated with COMSOL simulations as seen in Fig. 4.38 below to ensure that flow would travel correctly through the entire vasculature and to get an idea of where shear stresses should be highest in the models.
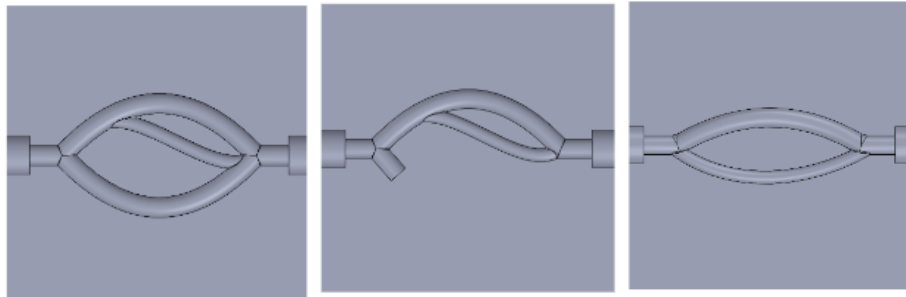
Figure 4.37: Final redesigned control (no pneumonectomy), pneumonectomy, and single bifurcation PDMS models (*labeled left to right*). Flow was run through these from left to right.
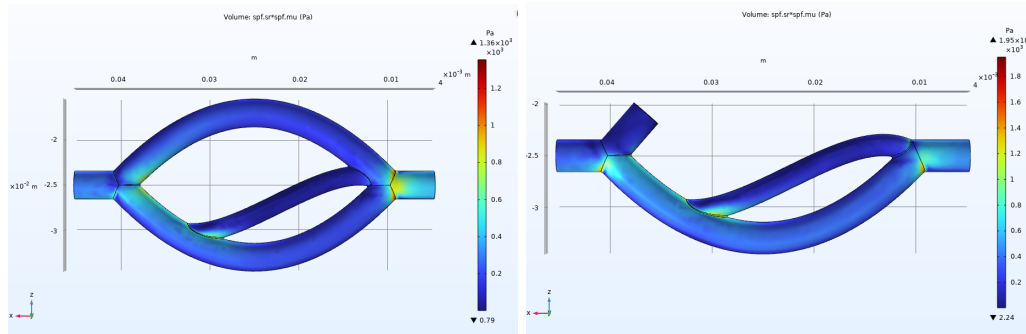
Figures 4.38: Redesigned PDMS control (no pneumonectomy) model (*left*) and pneumonectomy model (*right*) COMSOL simulations of shear stress in the flow through the vasculature.

5. Design Verification

To verify that the design was able to achieve the requirements set for the project, the outcomes of design choices were analyzed to ensure that our final device and results were sufficient. The COMSOL model was checked to ensure that accurate physiological conditions were represented and that data collection was conducted reasonably. The in vitro model was corroborated with the original specifications the team created to ensure that the device was able to produce a closed, contaminant-free system in which cells could be attached and imaged after flow trials.

5.1 COMSOL Model Results

The SOLIDWORKS model (shown in Fig 5.1 below) was moved to COMSOL for the fluid flow simulation and to visualize the results. The data produced by the simulations was exported into Excel spreadsheets and further analyzed using MATLAB.

Before running the stationary laminar fluid flow simulation in COMSOL, we found values in literature we could use for the inlet and outlet conditions, material properties, and the type of flow that would best suit the flow studies. We used values from a study[36] that modeled the fluid-structure interaction in blood vessels using COMSOL. The blood material properties were: density $\varrho = 1060 \ kg/m^3$ and dynamic viscosity $\mu = 0.005 \ Pa·s$[36]. We also used a pressure of 80 mmHg at the inlet and outlets, based on literature systolic pressures[37].

COMSOL uses a free tetrahedral mesh as the mesh that it runs the study through. Therefore, our imported SOLIDWORKS parasolid models with varying vessel wall thicknesses were initially considered the "fluid" in our study. To fix this, we created a meshing sequence by creating a domain within the hollow vessels of the original model that would become the "fluid" in our laminar flow study. Once the mesh was established, we selected the "fluid" mesh and ran the stationary laminar flow study through all three models: the full/no pneumonectomy control model, the right pneumonectomy model, and the left pneumonectomy model.

Shear Stress Simulations

One of the most important reasons the fluid flow simulation was conducted was to study the shear stress changes. Below are the shear stress results, measured in pascals, for the full/no pneumonectomy control model (Figure 5.1), the left pneumonectomy model (Figure 5.2), and the

right pneumonectomy model (Figure 5.3). Because the data we were interested in studying was on the surface or exterior walls of this "fluid" model, we viewed the results in a "volume" visualization.
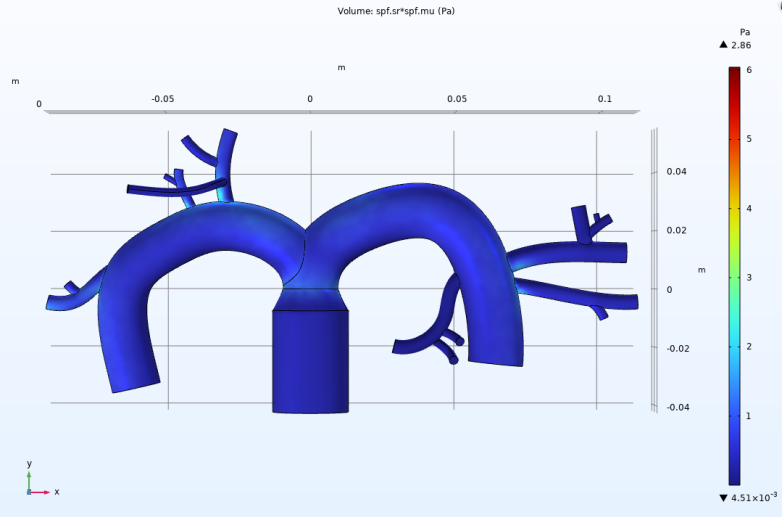
Figure 5.1 : Shear stress volume results for the control full/no pneumonectomy control model.
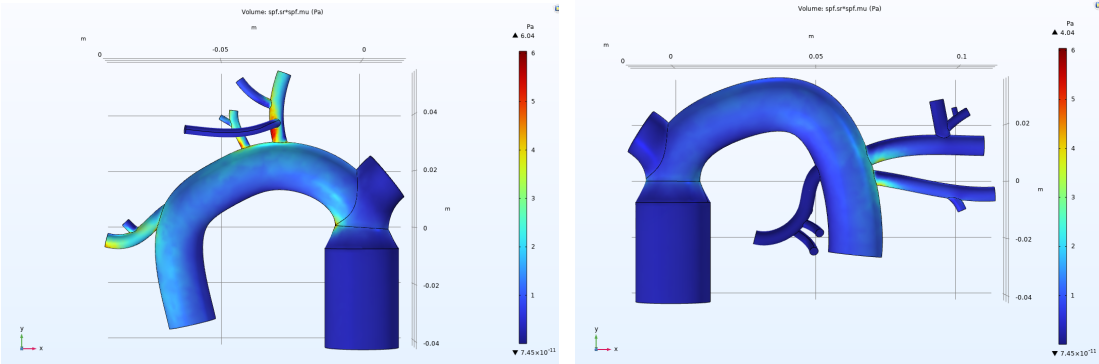
Figure 5.2 (*left*) and 5.3 (*right*) : Shear stress (volume) results for the left pneumonectomy model (*left*) and shear stress (volume) results for the right pneumonectomy model (*right*).

In Figs. 5.1, 5.2, and 5.3, the highest shear stress values were 2.86 Pa, 6.04 Pa, and 4.04 Pa, respectively. In Figs. 5.1, 5.2, and 5.3, the lowest shear stress values were 4.51×10^{-3} Pa, 7.45×10^{-11} Pa, and 7.45×10^{-11} Pa, respectively.

In addition to studying the shear stress volume models as seen in Figs 5.1, 5.2, and 5.3, we wanted to understand what was going on inside the vessels. Below in Figs. 5.4, 5.5, and 5.6,

there are "slices" created on a center midplane (xy plane) that help show the direction of flow within the main pulmonary arteries better than the volume model shows.
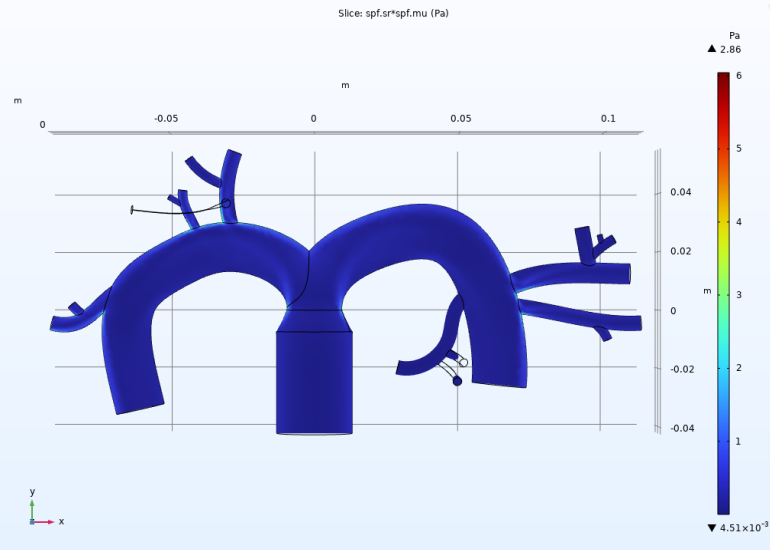
Figure 5.4: Shear stress (slice) results for the full/no pneumonectomy control model.
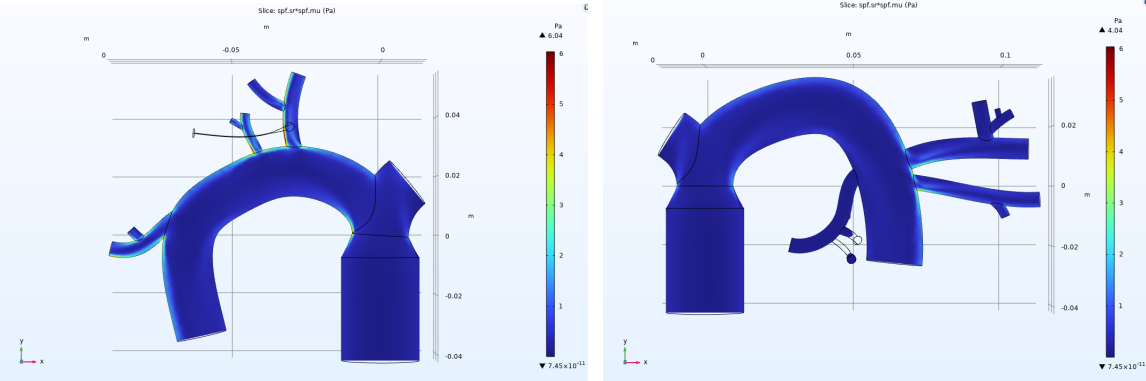
Figure 5.5 (*left*) and 5.6 (*right*): Shear stress (slice) results for the left pneumonectomy model (*left*). Shear stress (slice) results for the right pneumonectomy model (*right*).

The results in the shear stress (volume) better visualized the shear stress at the surfaces/exterior wall of the fluid, which would be along the same location of the inner wall of the blood vessel. The shear stress (slice) results were better for visualizing the shear stress within the vessels along a singular plane–in this case, the midplane along the xy coordinate plane. The shear stress values from COMSOL represented initial expectations that there would be an

61

increase in shear stress in the pneumonectomy models at bifurcations due to the redistribution of flow.

Pressure Simulations

   In addition to visualizing the shear stress results, we also visualized the pressure results. The best method for visualizing the pressure was a slice along a singular plane. In this case, the midplane along the xy coordinate plane. Below are the pressure results, measured in pascals, for the full/no pneumonectomy control model (Fig. 5.7), the left pneumonectomy model (Fig. 5.8), and the right pneumonectomy model (Fig. 5.9).
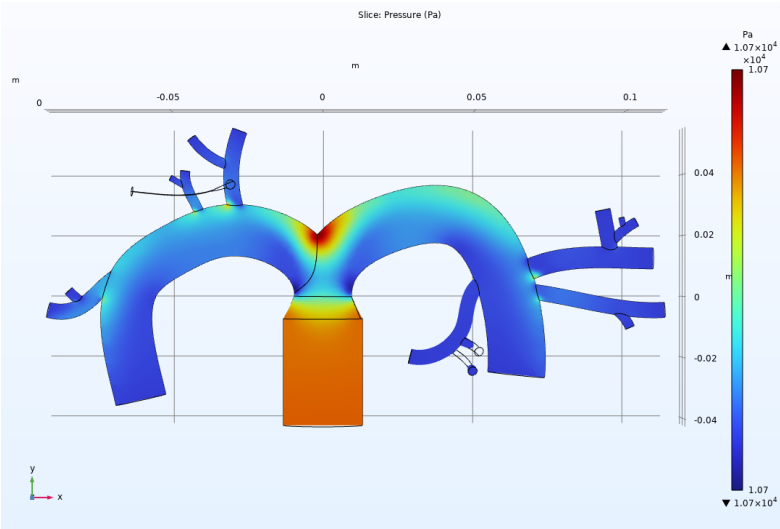
Figure 5.7. Pressure (slice) results for the full/no pneumonectomy control model.
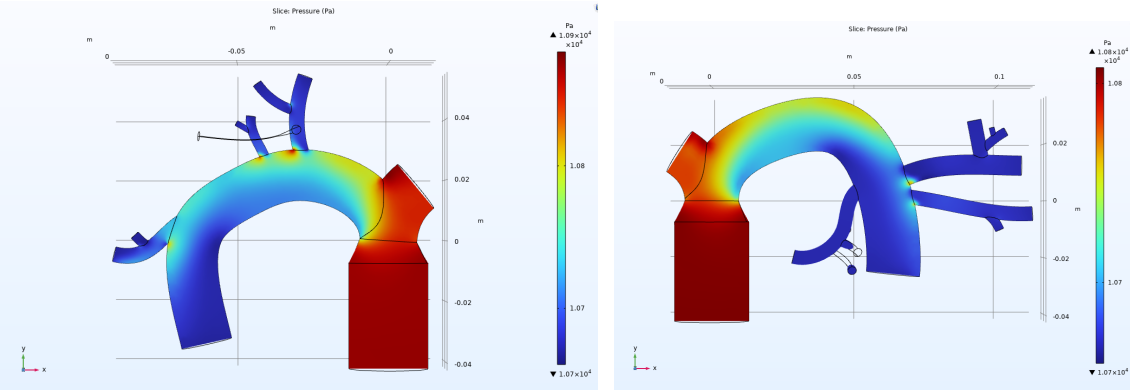
Figure 5.8 (*left*) and 5.9 (*right*) : Pressure (slice) results for the left pneumonectomy model (*left*). Pressure (slice) results for the right pneumonectomy model (*right*).

In Figs. 5.7, 5.8, and 5.9, the highest pressure values were 1.07×10^4 Pa, 1.09×10^4 Pa, and 1.08×10^4 Pa, respectively. All three models (Figs. 5.7, 5.8, and 5.9) shared a low pressure value of 1.07×10^4 Pa.

The pressure (slice) results show that there was an increase in pressure at the inlet and stump area where the two main pulmonary arteries branch off and at bifurcation locations in the pneumonectomy models when compared to the full/no pneumonectomy control model. The pressure values from COMSOL represented initial expectations that there would be an increase in pressure in the pneumonectomy models in specific locations due to the redistribution of flow.

5.2 Cell Culture Testing

The ability to seed HLMVECs in the in vitro model and facilitate normal growth was imperative for the function of the in vitro model. The optimal cell count for seeding was determined through an iterative process.

5.2.1 Cell culture

To source the cells for this project, HLMVECs were subcultured from an existing culture (provided by Professor Mensah's lab) into a T-75 flask. Prior to flow testing, a T-75 flask of HLMVECs was maintained with cell media (Cell Applications, Inc. Microvascular Endothelial Cell Growth Medium), kept in an incubator at 37°C and 5% CO_2. The cells successfully attached to the flask (shown in Fig. 5.10) and proliferated. Since HLMVECs exhibit contact inhibition, they were subcultured upon reaching relatively high confluency. This would prevent over-confluency. After determining the optimal cell count in trials for seeding the PDMS vasculature (deemed to be 500k to 1 million cells per PDMS half or 1-2 million cells total), the cells were subcultured into multiple T-75 flasks to maintain more cells as required for the seeding for the in vitro design. Following this, the HLMVECs were seeded onto the PDMS vasculature as described in Section 5.2.2.
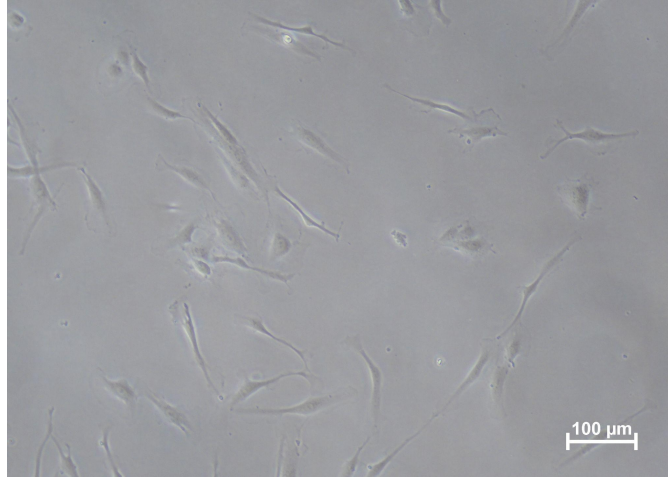
Figure 5.10: 10x image of HLMVECs in T-75 flask (low confluence).

5.2.2 Cell seeding

After testing the silicone membrane as an option for cell seeding as discussed in 4.2, fibronectin coating method was determined to be the best option. Prior to seeding, each half of PDMS was thoroughly sprayed with 70% ethanol and UV treated for at least 15 minutes. These pieces were placed in culture dishes alongside double sided tape pieces which underwent the same sterilization process. Once dry and sterilized, the PDMS pieces were stuck to the dishes with the tape (this was done to avoid the PDMS floating up once media was added, which may have prevented media from remaining in the vasculature with the seeded cells).

For the initial tests, about 100 μL of 194 μg/mL fibronectin was added to each half of the PDMS and spread using a micropipette to pretreat the culture surface (the PDMS vasculature). The fibronectin sat for 30 minutes before the excess liquid was gently aspirated. Following fibronectin coating, about 84k HLMVECs were seeded on each half of the double bifurcation PDMS vasculature pieces. Across all trials, the seeding was done very carefully or with 3D-printed dowels in place at the inlet and outlet of the vasculature to prevent the media from leaking out of the PDMS vasculature and into the dish (presumably taking the cells with it). Media was added in the dish surrounding the PDMS until the level was high enough to cover the PDMS completely.

The cells were imaged 24 hours later using a Nikon TS 100 microscope. Though the cells adhered successfully and appeared healthy, the cell seeding numbers proved to be far too low–the cells in the vasculature were far from confluent (see Fig. 5.11).
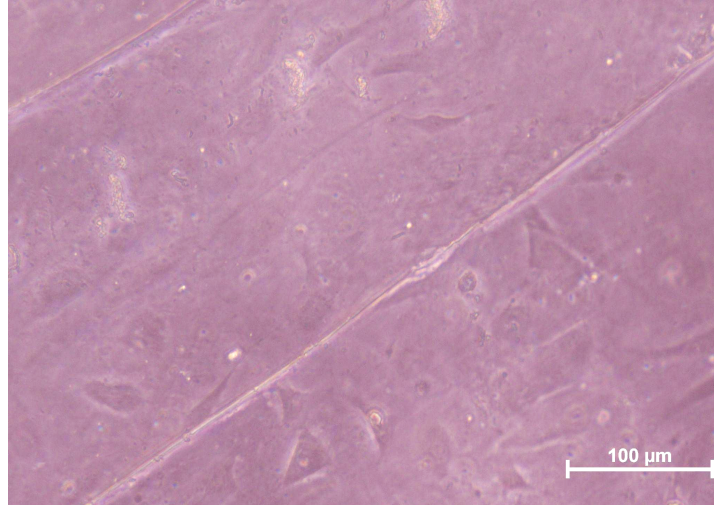
Figure 5.11: 20x image of HLMVECs after adhering to a vessel in double bifurcation PDMS.

Based on the initial seeding attempt, the number of cells seeded was adjusted to 500k per PDMS half. Imaging these cells 24 hours later revealed that they were attached and at least 80% confluent (as shown in Fig. 5.12). The cells were left for another 24 hours and upon viewing them again under the microscope (48 hours total after seeding), many of the cells were not visible. There weren't a lot of dead or detached cells visible in the vasculature or in the dish, but it was decided that 24 hours maximum would be the ideal length of time to wait between seeding the cells and running a flow test. Additionally, for future seeding, media was manually moved from surrounding the PDMS to the vasculature to refresh the media closest to the cells. This was done roughly 6 to 10 hours following seeding.
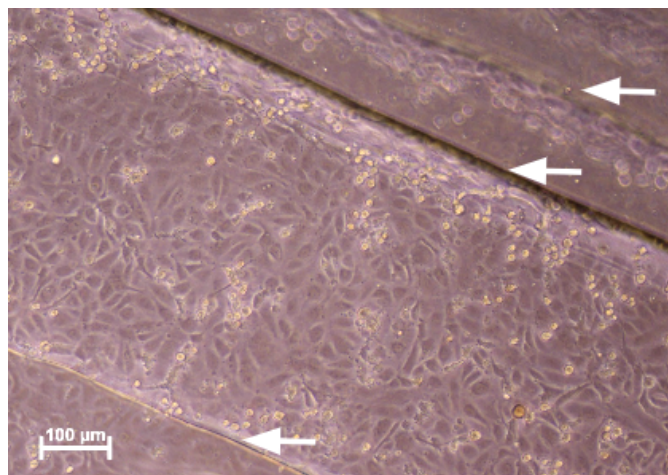
Figure 5.12 : 10x image of HLMVECs on a channel of the double bifurcation PDMS design, prior to fixing and staining with DAPI. This test was static, with media covering the PDMS but not flowing

over it. Arrows mark the steps between the levels of the PDMS–the widest level in the middle is the bottom of the channel.

5.3 Device Assembly Testing

The flow setup consisting of the pump, tubing, reservoir, chip, and connectors had to provide precise control over flow rate to produce the desired shear stresses without any leaks or flow abnormalities. This section covers the process of refining the setup to perform as desired.

5.3.1 Pump calibration

According to literature, blood flows into human lungs at an average rate of around 5 L/min [38]. This generates shear stresses in arterial vessels generally ranging from 10 to 70 dyn/cm^2 [39]. The low end of the shear stress range was targeted for these experiments because smaller vasculature was being modeled. Using this target shear stress, the ideal flow rate for the chip was calculated to be between 175 and 210 mL/min, which would have generated between 10 and 12 dyn/cm^2 of shear stress (see calculations in Appendix I). However, the peristaltic pump used to simulate blood flow through the 3D chip could not exceed 93.08 mL/min for the tubing size used (size 16, or an inner diameter of 3.1 mm). This prevented perfect replication of desired flow rate and corresponding shear stresses, as a flow rate of 93.08 mL/min created shear stresses around 5.312 dyn/cm^2 (see Appendix I).

The pump was primed for about 30 seconds to fill the tubing with water before the outflow cylinder was emptied to prepare for calibration. To calibrate the pump, tubing was run from one 1000 mL graduated cylinder filled with water to an empty 1000 mL graduated cylinder, as shown in Fig. 5.13 below.

Figure 5.13: Pump calibration setup

The tubing size was entered into the pump as well as the flow rate after each trial. The pump was run at its adjusted flow rate following each cycle, with the volume of water collected in the collection cylinder being noted and entered via the pump's interface. The pump was calibrated once the volume produced matched the entered flow rate exactly. This ensured that the flow rate was accurate and consistent for future fluid flow tests.

5.3.2 Sterility Testing

Prior to seeding cells in our in vitro model, we conducted sterility tests on our flow setup to check for the presence of any potential microorganisms that could contaminate our cells, as well as any structural damage to the setup that could occur under the flow. The tests were broken up into two different methods: a static and dynamic sterility test in order to isolate the sources of potential contamination. The static test intended to verify that the silicone gel, PDMS molds and plexiglass jigs were a closed system and that all sterilization techniques performed effectively prevented contamination. The dynamic test was intended to verify that our syringe reservoir was able to release air trapped in the system without allowing any contaminants to enter the system. The dynamic test was also used to detect any effects of extended high flow on the molds and tubing.

Static Sterility Test

        The static sterility test was performed by constructing the chip and filling it with HLMVEC culture media. The ends of the short tubing pieces were secured with two 3D-printed dowels to seal the vasculature with the media inside. The sealed chip is shown below in Fig. 5.14.
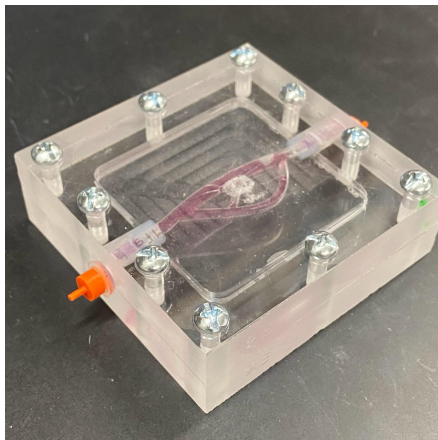
Figure 5.14: Static fluid chip setup with HLMVEC culture media inside and two dowels sealing the ends of the tubing.

        For sterilization, the plexiglass, screws, and dowels were soaked in 70% ethanol for 10 minutes, and then exposed to UV light inside the hood for 15 minutes. The PDMS molds and orange dowels pictured above in Fig. 5.14 were sprayed thoroughly with 70% ethanol and exposed to UV light for the same 15-minute increment. A tube of silicone gel was purchased and opened under the hood after being thoroughly sprayed with 70% ethanol and UV treated. Any silicone gel that was exposed to air between applications and hardened gel was discarded and the tube was resterilized prior to each new application. This tube remained in the hood during all resterilization and applications.

        Once assembled, the device was placed in an incubator at 37°C and 5% CO_2 and left for 24 hours undisturbed. After testing, the device was sprayed with 70% ethanol thoroughly and placed in a hood. Culture media was then extracted and placed onto a 35 mm culture plate to analyze under a Nikon TS 100 microscope for any oddities. Upon visual inspection, it was determined that the media was free of contaminants and any debris as pictured in Fig. 5.15.
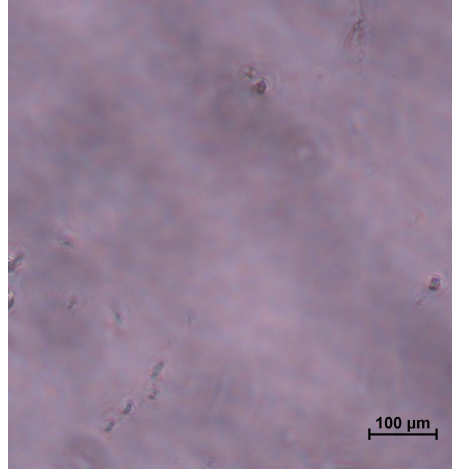
Figure 5.15: HLMVEC culture media on a 35 mm culture plate extracted from a static flow sterility setup after testing for 24 hours.

Dynamic Sterility Test

The dynamic sterility test was designed to determine the sterility of the entire flow setup to ensure that there wouldn't be contamination from the syringe reservoir allowing CO_2 exchange or structural damage to the setup during flow tests. To further limit air-borne contaminants, we introduced a 15 mm plate lid with a hand-drilled ¼" hole. The tubing going into the top of the syringe reservoir passed through the plate lid, then a rubber stopper with two holes, one for the tubing and one to release air. The plexiglass, screws, dowels, and 15 mm plate lid were submerged in 70% ethanol for 10 minutes and then UV treated for 15 minutes. The PDMS and syringe stand were sprayed liberally with 70% ethanol and UV treated for 15 minutes. All tubing segments, connectors, the rubber stopper, and the syringe reservoir were wrapped in tin foil and placed in an autoclave at 121℃ for 50 minutes.

Before flow could be run, the flow setup was assembled in the hood as described in 4.3.1 Silicone was applied to the PDMS halves and left to cure within the constructed in vitro model for two hours under the hood. Once the silicone was cured, warmed media was added to the syringe reservoir so that it ran down through the chip. Upon observing no leaks or issues, the setup was removed from the hood and placed in an incubator (seen in Fig. 5.16 below), which was brought to 37°C and 5% CO_2 in advance. The peristaltic pump was kept outside of the incubator with tubing running through a hole in the back of the incubator that was plugged with paper towels to prevent CO_2 from leaking. The pump was then turned on and ran for a total of 24

hours. At the end of the test, the entire setup was carried to the hood (minus the pump) and sprayed with 70% ethanol. The setup was disassembled by aspirating the media from the syringe before carefully separating the chip. The remaining media was drained and aspirated out of the tubing while the chip was unscrewed and the PDMS halves were split apart, using a razor blade if the silicone gel bound them together in any spots. Media samples were taken from several locations prior to aspiration.
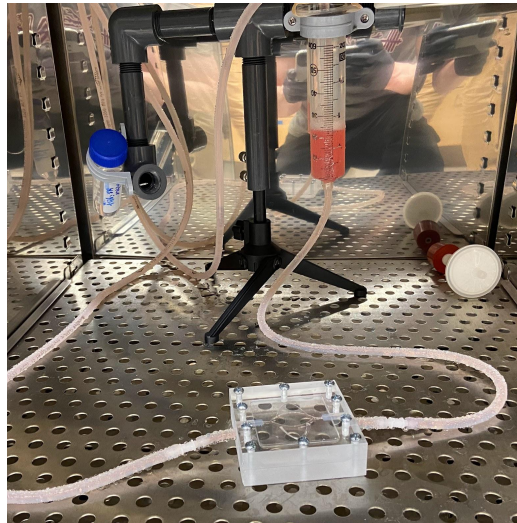
Figure 5.16: Dynamic sterility test setup in the incubator filled with HLMVEC culture media.

The initial dynamic sterility test ran for 48 hours but resulted in a crack forming in the tubing where it ran through the pump–this caused all the media to be pumped out of the system. The cracked tubing is shown in Fig. 5.17 below. To remedy this, a follow-up dynamic sterility test was run for 24 hours and a replaceable section of tubing was created by using connectors on either side of the tubing section running through the peristaltic pump. This section would be discarded after each trial and replaced to avoid any cracks forming due to fatigue.

Figure 5.17: Crack formed in tubing where it ran through the peristaltic pump. This crack formed over the course of a 48 hour flow test.

Another issue was observed from our sterility test after the media was extracted, placed in a 35 mm culture plate, and viewed with the Nikon TS 100 microscope. Many objects (shown in Fig. 5.18 below) were observed floating throughout the media which were believed to be pieces of PDMS that were torn off during the test due to the high flow rate and long run time. To minimize this issue, the run times of the cell-seeded flow tests were reduced to eight hours.
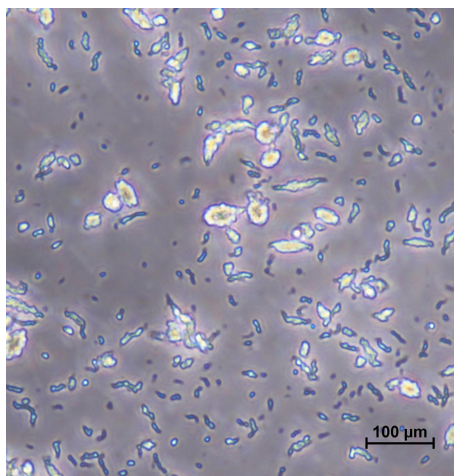
Figure 5.18: Objects believed to be pieces of PDMS floating in a sample of HLMVEC media taken from the syringe reservoir following the 24 hour dynamic sterility test.

5.4 Imaging Testing

In this project, imaging was challenging due to the thickness of the PDMS, the shape of the vasculature, and the scale of the chip. Additionally, pure PDMS has a relatively high refractive index of 1.43, making it even harder to image through[40]. Confocal imaging was ruled out immediately based on the thickness of the samples, so other imaging options were considered and tested.

One alternative was a different microscope, which for this project was a Keyence BZ-X fluorescence microscope. The other options were sectioning-based in order to create samples thin enough to be viewed on the confocal microscope. These options were cryosectioning and paraffin wax embedding. The application of these methods using PDMS was unknown, so both were tested with plain PDMS samples under the guidance of Jyotsna Patel, a histology technician, to determine the most suitable imaging method.

5.4.1 Keyence Fluorescence Microscope

To test the Keyence microscope, dots were marked at different levels and locations on a PMDS sample using a marker. All depths and locations on the PDMS sample were brought into focus successfully, including all levels of the vasculature within the model. An image of the microscope is provided in Fig. 5.19 below. Another benefit of the Keyence BZ-X was its Z-stacking feature. Z-stacking is the method of stitching together multiple vertical layers of images to produce a single combined picture, or stack, that shows all depths in focus simultaneously.

Figure 5.19 : Keyence BZ-X Fluorescence Microscope with a PDMS sample loaded inside.

After testing, the cells were fixed with a 4% PFA (paraformaldehyde) solution and stained with WGA (wheat germ agglutinin) and DAPI (4',6-diamidino-2-phenylindole) for better visualization. The WGA stain is used to highlight the GAGs, which are a prominent molecule within the eGCX. The DAPI stain is used to highlight the nuclei of cells. Examples of these stains imaged on the Keyence BZ-X at 4x and 20x magnification are shown in Figs. 5.20 and 5.21. The WGA stain shows up as green and the DAPI stain shows as blue. The green seen in 5.21 shows GAGs, indicating the presence of the glycocalyx. The blue DAPI shows the nuclei of cells.
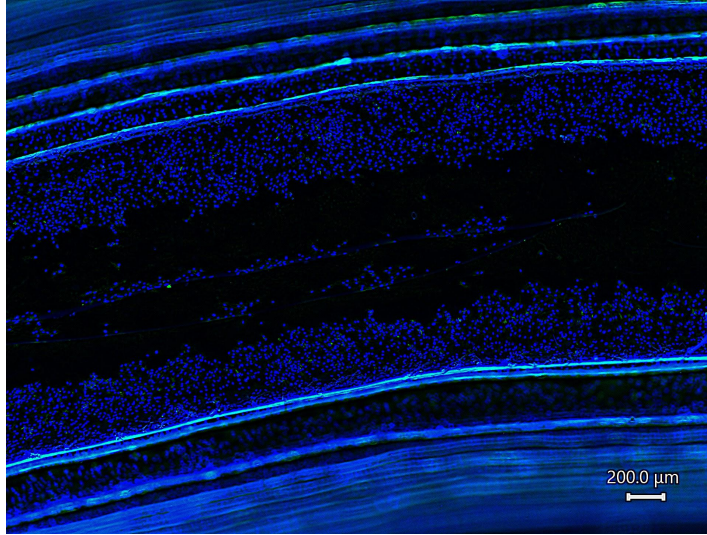
Figure 5.20: 4x image of a vessel within the control PDMS model, stained with DAPI and WGA.
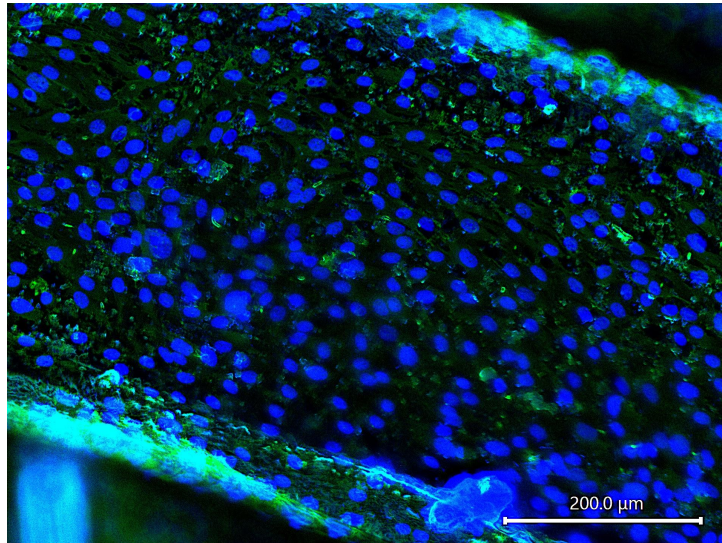
Figure 5.21: 20x image of the bottom of a vessel in the single bifurcation PDMS model, stained with DAPI and WGA.

5.4.2 Alternative Imaging

In addition to the Keyence microscope, other imaging options were pursued, particularly ones that could produced samples able to be viewed using the confocal microscope.

Cryosectioning

To test cryosectioning, a small block of PDMS was immobilized in OCT (optimal cutting temperature) compound and sectioned at different thicknesses to find a section thickness at

which it didn't fall apart. This ideal thickness ended up being anything from 100 to 150 microns. An example section is shown below in Fig. 5.22.
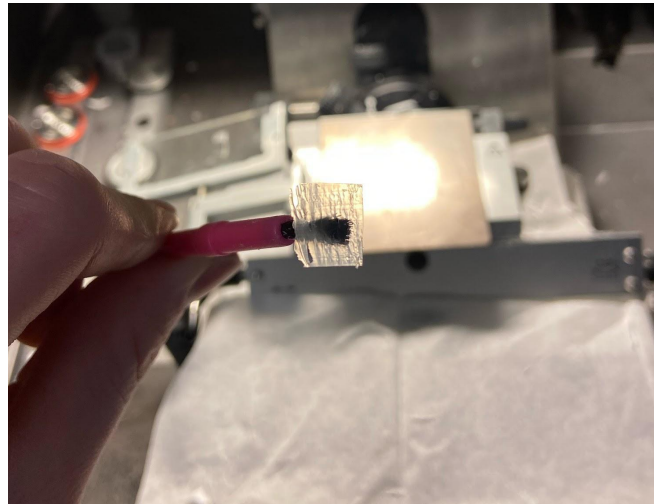
Figure 5.22 : A 100 micron test section of PDMS created using cryosectioning.

PDMS sections were also successfully mounted to a charged glass slide as shown in Fig. 5.23 below.

Figure 5.23: Three slices of PDMS placed on a charged glass slide

With limited histology experience on the team, test sections of PDMS were often wrinkled and inconsistent, likely due at least in part to mishandling or poor technique. Cryosectioning was deemed an unreliable method for these reasons, so it wasn't pursued any further.

Paraffin Wax Embedding

Paraffin wax embedding provided similar challenges to cryosectioning. For the embedding procedure, the PDMS chunks had to be small enough to fit the cassettes available, which would have limited sections to a single cross-sectional view of a PDMS vessel. This would have required the separation of single PDMS pieces into many smaller samples.

For testing, a small piece of plain PDMS was cut and enclosed in a cassette, which was processed in a Tissue-Tek VIP 6AI overnight. The following day, the PDMS was encased in paraffin wax and mounted on a microtome for sectioning. At the recommendation of Jyotsna Patel, the histology technician, the section thickness was set to 6 microns. The PDMS proved to be difficult to section, with many sections scrunching up, tearing, and forming improperly for other reasons. An example of a paraffin wax embedded PDMS section is shown in Fig. 5.24. Eventually, the remainder of the PDMS block broke free of the wax and fell off, which marked the end of the testing. Paraffin wax embedding was not pursued further.

Figure 5.24: Sectioned sample of the PDMS using the microtome

5.5 Final In Vitro Assembly Trials

Once all of the leak and flow testing and design iterations were complete and verified, we moved on to the complete flow trials.

5.5.1 Trial Iterations

The final flow setup was run three times; once with each of the three finalized PDMS vasculature models. The first flow trial was run with the single bifurcation model and suffered a crack in the tubing where it ran through the pump at an unknown time during the trial. The flow was monitored periodically for the first 45 minutes, but the crack was discovered at the eight hour mark. The cells were immediately fixed regardless and their presence was confirmed by imaging using the Nikon microscope (see Fig. 5.25).
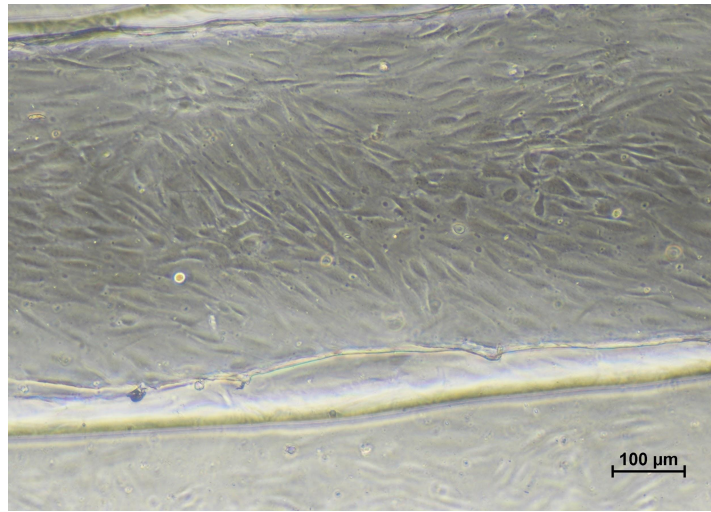
Figure 5.25: HLMVECs imaged at 10x on the Nikon TS 100 following Flow Trial 1. The cells appeared fairly confluent and many had aligned with the direction of flow despite the abbreviated flow caused by a crack in the tubing.

The crack in the tubing was likely due to the reuse of the section used in the pump for the last dynamic sterility test. It was speculated that this weakened the tubing prior to Flow Trial 1. Flow Trials 2 and 3 were run with the control PDMS vasculature model and the pneumonectomy PMDS vasculature model, respectively. New tubing was used to avoid the cracking from Flow Trial 1. These segments showed slight deformation following each trial but did not leak.

The cells for all three trials were fixed with 4% PFA immediately following their conclusions. They were stained with DAPI and WGA, stored in PBS at 4℃, and imaged within 24 to 48 hours of performing the stain to prevent any significant fading of the fluorescence.

5.5.2 Final Trial Procedure

For each trial, the cells were seeded in the PDMS vasculature around 24 hours prior to the start of flow. After about 8 hours, the media was manually refreshed within the vasculature using a micropipette to ensure fresh media reached the seeded cells, rather than relying solely on diffusion through the vasculature and in the thin layer of media covering the top of the PDMS piece.

About 2 hours before the start of flow, the silicone sealant was carefully but quickly applied to the PDMS halves under the hood before the chip was screwed together with the tubing and dowels in place. One dowel was removed and media was injected into the vasculature for the cells, after which the dowel was replaced with a sterile syringe filter to allow for gas exchange. The assembled chip was placed in the incubator for the silicone to dry.

To begin a flow trial, the assembled chip was removed from the incubator, the syringe filter was detached, and the sterilized tubing, connectors, and syringe reservoir were connected in the hood. The system was primed with media using a serological pipette and the 50 mL syringe reservoir was filled a little less than halfway before the rubber stopper was put in place along with the plate lid that served as a secondary barrier to contamination without limiting gas exchange significantly.

Lastly, the entire setup was moved from the hood to the incubator, where the tubing was fed through the back of the incubator to the pump. Once the pump was attached, the flow trial began. Nothing else was kept in the incubator and it was not opened at any point during a flow trial to limit the opportunity for contaminants to enter and to minimize any disturbances that could affect the flow.

5.5.3 In Vitro Results

Quantitative data was not able to be obtained for the in vitro model due to time limitations. The following results are qualitative.

As mentioned in 5.5.2, Flow Trial 1 resulted in a leak, limiting the interpretation of the results. However, cells were present and successfully stained with the DAPI and WGA and imaged on the Keyence BZ-X (seen in Figs. 5.26 and 5.27).
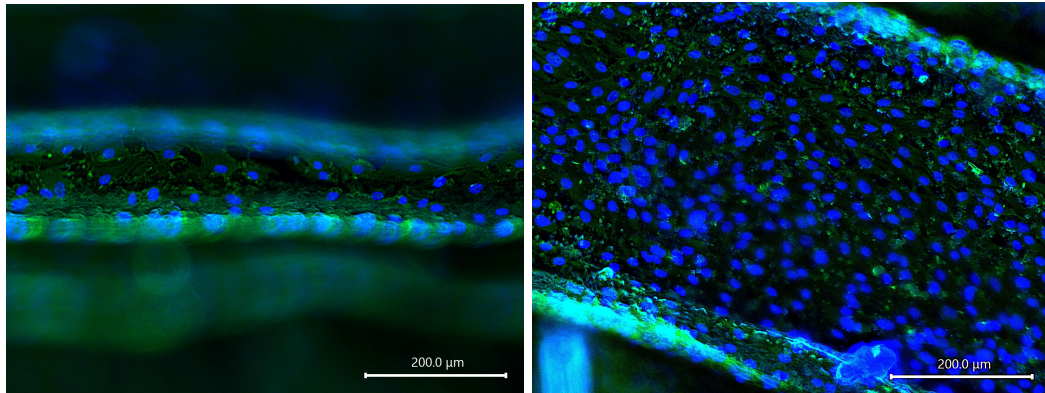
Figure 5.26 (*left*) and 5.27 (*right*): DAPI and WGA stained images taken from Flow Trial 1. Fig. 5.26 was from a single level in the wall of the inlet bifurcation and Fig. 5.27 was from the bottom of the smaller vessel.

Flow Trials 2 and 3 also had many cells present following flow and the DAPI and WGA stains were imaged on the Keyence BZ-X. The WGA stain was challenging to see in these trials, which was addressed with post-processing in the accompanying Keyence analyzer application as well as in ImageJ. Images from corresponding locations in the control PDMS vasculature (Flow Trial 2) and the pneumonectomy PDMS vasculature (Flow Trial 3) are shown in Figs. 5.28 - 5.33.
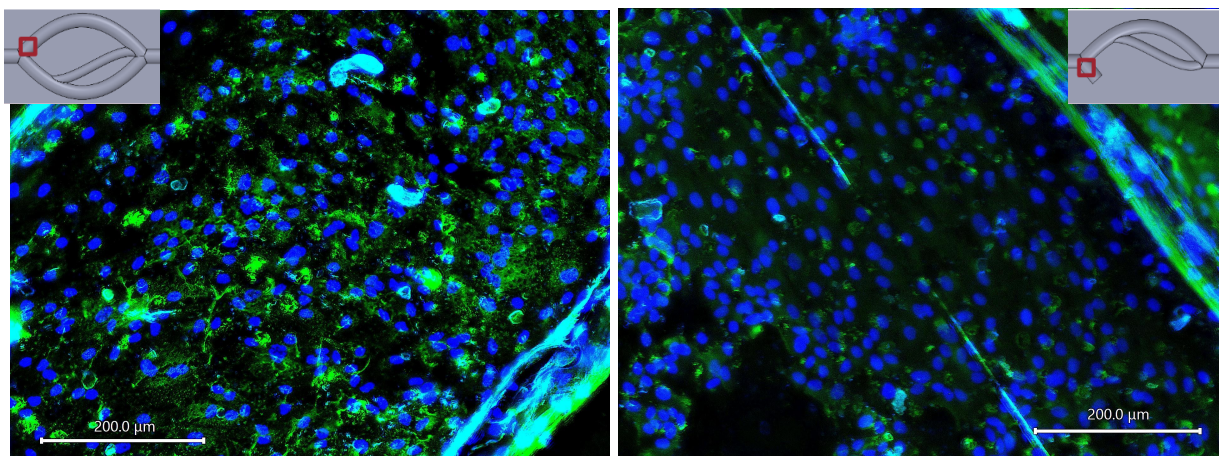
Figure 5.28 (*left*) and 5.29 (*right*): WGA and DAPI stains viewed at 20x in the bottom of the vessel after the inlet bifurcation in the control model/Flow Trial 2 (*left*) and the pneumonectomy model/Flow Trial 3 (*right*). The exact locations are shown in graphics overlaid on the fluorescence images.
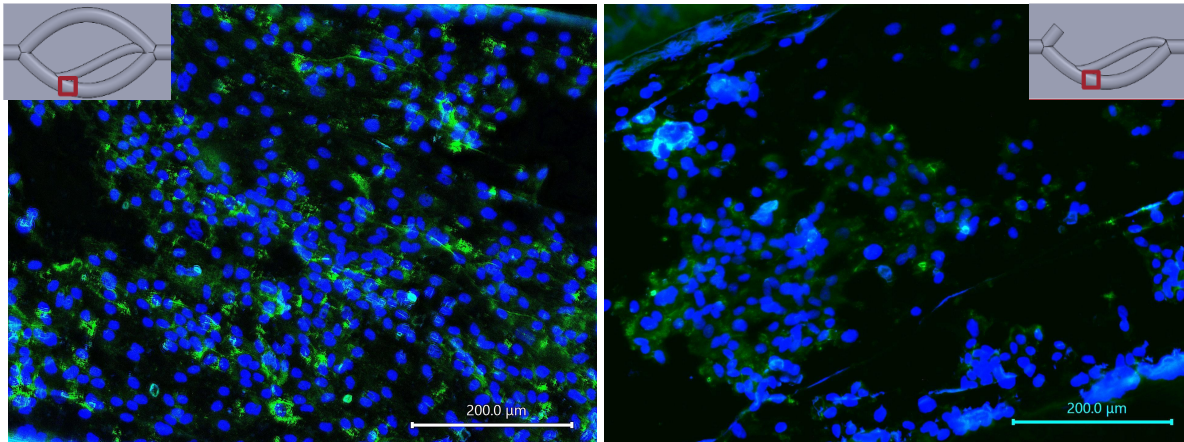
Figure 5.30 (*left*) and 5.31 (*right*): WGA and DAPI stains viewed at 20x in the bottom of the main vessel after the second bifurcation in the control model/Flow Trial 2 (*left*) and the pneumonectomy model/Flow Trial 3 (*right*). The exact locations are shown in graphics overlaid on the fluorescence images.
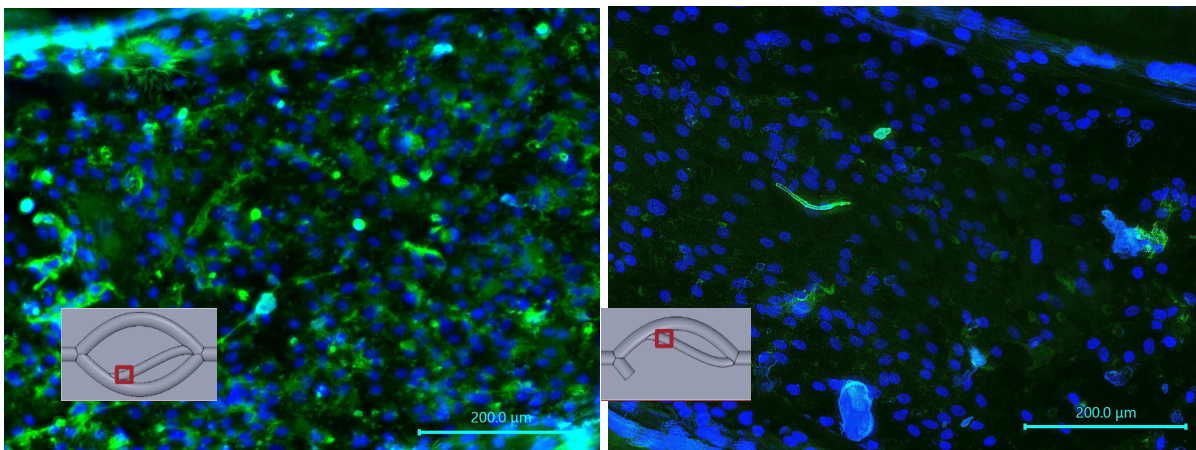
Figures 5.32 (*left)* and 5.33 (*right*): WGA and DAPI stains viewed at 20x in the bottom of the small vessel after the second bifurcation in the control model/Flow Trial 2 (*left*) and the pneumonectomy model/Flow Trial 3 (*right*). The exact locations are shown in graphics overlaid on the fluorescence images.

The above figures (Figs. 5.29 - 5.33) all show less WGA fluorescence in the pneumonectomy model, than in the control.

6. Final Design Validation

6.1 Project Goals

The goals set at the start of this project were completed in one school year. The first goal of the project was to determine specific areas of interest in the pulmonary vasculature that were likely to show higher shear stresses after pneumonectomy. This was achieved through COMSOL fluid flow simulations using a 3D model of pulmonary arteries created in SOLIDWORKS. These simulations were based on measurements taken from available literature and digitally measured images from CT scans of the pulmonary tree. Following the simulations, data was accumulated and analyzed to select three regions of the arterial tree to be modeled in SOLIDWORKS. These regions informed the design of 3D-printed PLA molds for PDMS to create the in vitro model. The team was able to complete the second objective of creating an in vitro fluidic model with machined plexiglass and custom PDMS channels. The chip was assembled after fibronectin was used to coated the PDMS and cultured HLMVECs were seeded in PDMS vasculature.

6.2 COMSOL and MATLAB

After running the fluid flow simulations as discussed in 5.1, we validated our COMSOL results by using Matlab and Excel graphs to compare the COMSOL data and further analyze it. We were able to validate our claim that significant changes to flow do occur after a pneumonectomy by comparing our COMSOL results. Below are the results for the shear stress and the pressure and our data analysis for both.

6.2.1 MATLAB Results and Analysis

The COMSOL volume data for the shear stress results and pressure results were taken from all three models and exported into separate text files. After using the text files in code in Matlab, 6-10 locations along the wall of vessels of interest were selected. The side of the vessel wall that was analyzed was the side that was visually most affected by the direction of flow (it showed the largest magnitude of change in COMSOL). The mean shear stress and pressure values of the points in these locations were calculated in Matlab. Next, the mean data point for each location was recorded in an Excel file. The mean values of the data points in the same locations for the left pneumonectomy model and no pneumonectomy model were compared in a

graph (for shear stress and then for pressure). The mean values of the data points in the same locations for the right pneumonectomy model and no pneumonectomy model were compared in a graph (for shear stress and then for pressure). Using the mean values, the fold change from the no pneumonectomy model to a pneumonectomy model was calculated for each vessel of interest and its shear stress and pressure data. Finally, the p values were found using a t-test in GraphPad Prism to determine the significance of the fold change results.

6.2.2 Region Selection in MATLAB

The text file with exported COMSOL contained all of the data points solved for on the mesh surface in 3D. It contained x, y, z coordinates and a value corresponding to that data point. Our goal was to select a certain number of sections of data points to average out, so we used code to visualize these regions of data points like depicted below in the left pneumonectomy model for shear stress. Using this region in x, y view would also allow the selection around the curvature of the vessel.
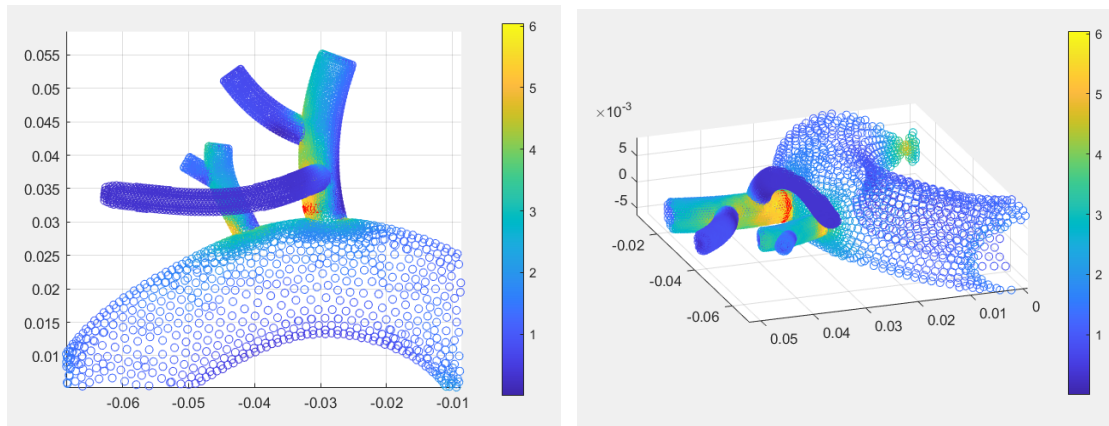
Figure 6.1 (*left*) and 6.2 (*right*) : An example of a MATLAB 3D figure of one of the left pneumonectomy shear stress data ranges viewed from an xy-plane (front) view (*left*) and xyz-plane (isometric) view (*right*).

Using the MATLAB code in Appendix II, we found the mean value of this region of data points along this side of the vessel wall. We then selected 9 more regions to collect a total of 10 data points to use for graphing in Excel. We used this same method in MATLAB to collect the

data points that we used for graphing in Excel for all of the vessels we chose to analyze. All of the code used to find these values for specific regions can be found in Appendix II. The commented out code specifying the desired regions to locate were intended to be uncommented when running the code so the user could look at one region at a time.

6.2.3 Excel Results and Fold Change of Shear Stress and Pressure

First, we compared the shear stress in the left pneumonectomy and the control no pneumonectomy control model. We selected three vessels to analyze. Vessel 1 had 10 data points, Vessel 2 had 6 data points (due to the smaller length of the vessel), and Vessel 3 had 10 data points.

Vessel 1 (Left Pneumonectomy vs No Pneumonectomy Control)

The first vessel of interest was Vessel 1, pictured in red in the figures below. Figs. 6.3 and 6.4 show the qualitative shear stress increase in the pneumonectomy model, and Figs. 6.5 and 6.6 show our data analysis.

Figure 6.3 (*left)* and 6.4 (*right)* : No pneumonectomy control model shear stress COMSOL results (*left*) and left pneumonectomy model (right) both with Vessel 1 highlighted in red.

Figure 6.5 (*left*) and 6.6 (*right*): Excel graph comparing the no pneumonectomy and left pneumonectomy model shear stress mean data points selected along the wall of the vessel (*left*). Excel fold change bar graph showing the fold change values for the no pneumonectomy (NP) model and the left pneumonectomy model (LP) shear stress (*right*).

In Figure 6.6, the value for NP was 1 and the value for LP was 3.235. After conducting a t-test, the p value was found to be less than 0.0001****, which is considered very significant. The greater the number of asterisks, the greater the significance value.

Vessel 2 (Left Pneumonectomy vs No Pneumonectomy Control)

The second vessel of interest was Vessel 2, pictured in red in the figures below. Figs. 6.7 and 6.8 show the qualitative shear stress increase in the pneumonectomy model, and Figs. 6.9 and 6.10 show our data analysis.

Figure 6.7 (*left)* and 6.8 (*right)* : No pneumonectomy control model shear stress COMSOL results (*left*) and left pneumonectomy model (right) both with Vessel 2 highlighted in red.

Figure 6.9 (*left*) and 6.10 (*right*) : Excel graph comparing the no pneumonectomy and left pneumonectomy model shear stress mean data points selected along the wall of Vessel 2 (*left*). Excel fold change bar graph showing the fold change values for the no pneumonectomy (NP) model and the left pneumonectomy model (LP) shear stress (*right*).

In Fig. 6.10, the value for NP was 1 and the value for LP was 3.199. After conducting a t-test, the p value was found to be equal to 0.0001***, which is still considered very significant.

Vessel 3 (Left Pneumonectomy vs No Pneumonectomy Control)

The third vessel of interest was Vessel 3, pictured in red in the figures below. Figs. 6.11 and 6.12 show the qualitative shear stress increase in the pneumonectomy model, and Figs. 6.13 and 6.14 show our data analysis.

Figure 6.11 (*left*) and 6.12 (*right*) : No pneumonectomy control model shear stress COMSOL results (*left*) and left pneumonectomy model (right) both with Vessel 3 highlighted in red.

Figure 6.13 (*left*) and 6.14 (*right*) : Excel graph comparing the no pneumonectomy and left pneumonectomy model shear stress mean data points selected along the wall of Vessel 3 (*left*). Excel fold change bar graph showing the fold change values for the no pneumonectomy (NP) model and the left pneumonectomy model (LP) shear stress (*right*).

In Figure 6.14, the value for NP was 1 and the value for LP was 2.521. After conducting a t-test, the p value was found to be less than 0.0001****, which is considered very significant.

Next, we compared the shear stress in the right pneumonectomy and the no pneumonectomy control model. We selected two vessels to analyze in MATLAB, plot data points in Excel, calculate the fold change for, and find the p values for determining the significance of the fold change data. Vessel 4 had 10 data points and Vessel 5 had 10 data points.

Vessel 4 (Right Pneumonectomy vs No Pneumonectomy Control)

The first vessel of interest in the right pneumonectomy was Vessel 4, pictured in red in the figures below. Figs. 6.15 and 6.16 show the qualitative shear stress increase in the pneumonectomy model, and Figs. 6.17 and 6.18 show our data analysis.

Figure 6.15 (*left)* and 6.16 (*right)* : No pneumonectomy control model shear stress COMSOL results (*left*) and right pneumonectomy model (right) both with Vessel 4 highlighted in red.

Figure 6.17 (*left*) and 6.18 (*right*) : Excel graph comparing the no pneumonectomy and right pneumonectomy model shear stress mean data points selected along the wall of Vessel 4 (*left)*. Excel fold change bar graph showing the fold change values for the no pneumonectomy (NP) model and the right pneumonectomy model (RP) shear stress (*right)*.

In Figure 6.18, the value for NP was 1 and the value for RP was 2.212. After conducting a t-test, the p value was found to be equal to 0.0307*, which is significant.

Vessel 5 (Right Pneumonectomy vs No Pneumonectomy Control)

The second vessel of interest in the right pneumonectomy was Vessel 5, pictured in red in the figures below. Figs. 6.19 and 6.20 show the qualitative shear stress increase in the pneumonectomy model, and Figs. 6.21 and 6.22 show our data analysis.
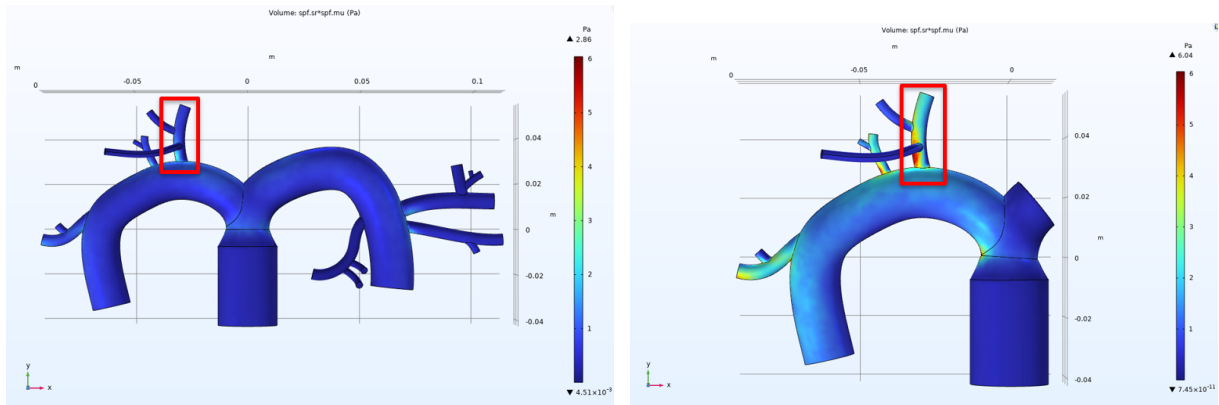
Figure 6.19 (*left)* and 6.20 (*right)* : No pneumonectomy control model shear stress COMSOL results (*left*) and right pneumonectomy model (right) both with Vessel 5 highlighted in red.
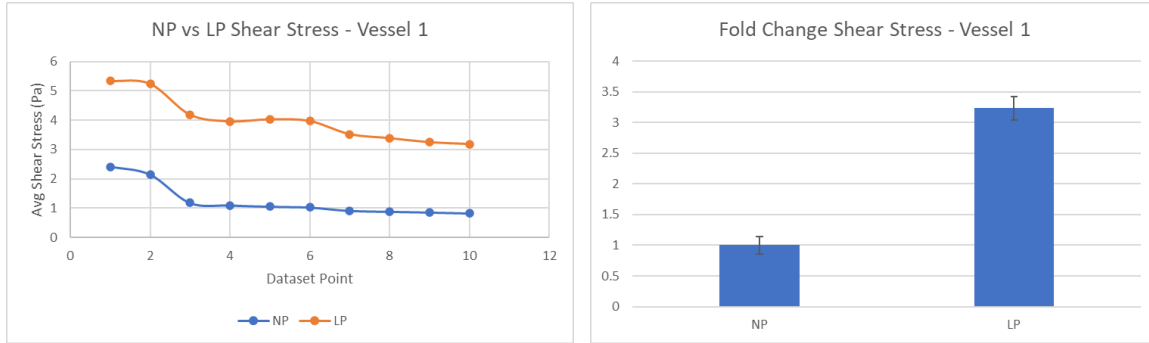

Figure 6.21 (*left*) and 6.22 (*right*) : Excel graph comparing the no pneumonectomy and right pneumonectomy model shear stress mean data points selected along the wall of Vessel 5 (*left)*. Excel fold change bar graph showing the fold change values for the no pneumonectomy (NP) model and the right pneumonectomy model (RP) shear stress (*right)*.

In Figure 6.22, the value for NP was 1 and the value for RP was 2.695. After conducting a t-test, the p value was found to be equal to 0.0061**, which is significant.

Overall, the increase in shear stress was found to be much more significant in the left pneumonectomy model than the right pneumonectomy model when being compared to the no pneumonectomy model. In addition to analyzing the shear stress, we also analyzed the pressure using the same methods.

Vessel 1 (Left Pneumonectomy vs No Pneumonectomy Control)

The first vessel of interest was Vessel 1, pictured in red in the figures below. Figs. 6.23 and 6.24 show the qualitative pressure increase in the pneumonectomy model, and Figs. 6.25 and 6.26 show our data analysis.
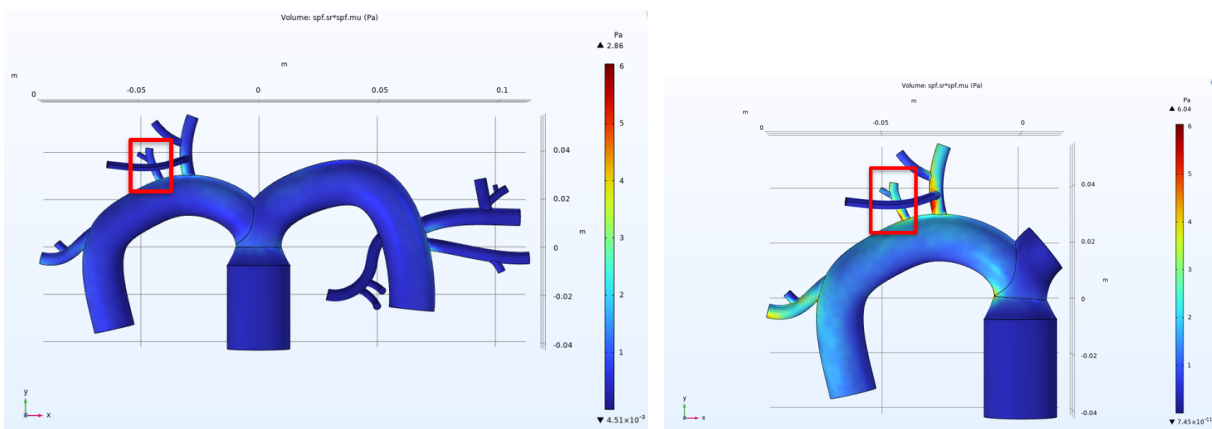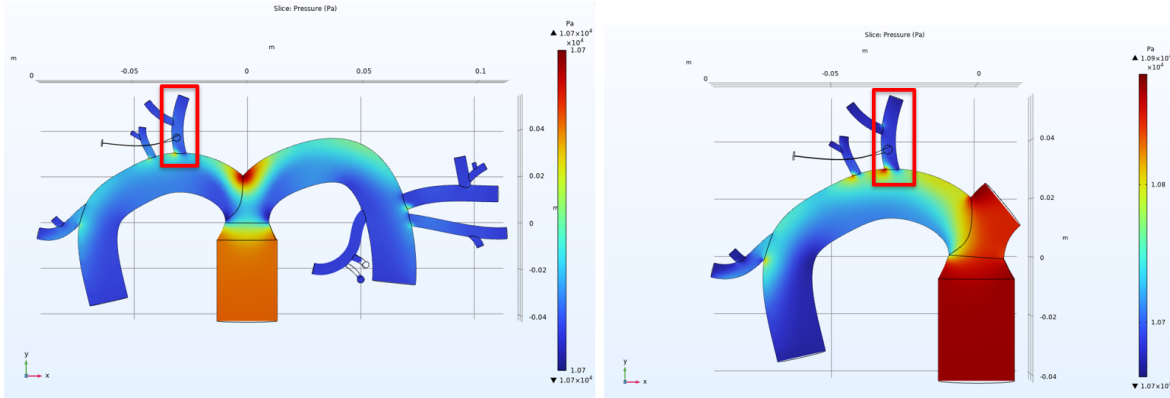

Figure 6.23 *(left)* and 6.24 *(right)* : No pneumonectomy control model pressure COMSOL results *(left)* and left pneumonectomy model (right) both with Vessel 1 highlighted in red.
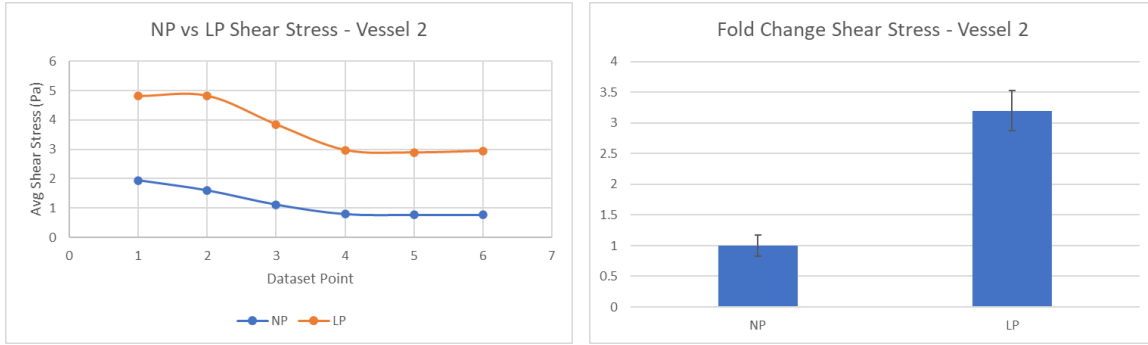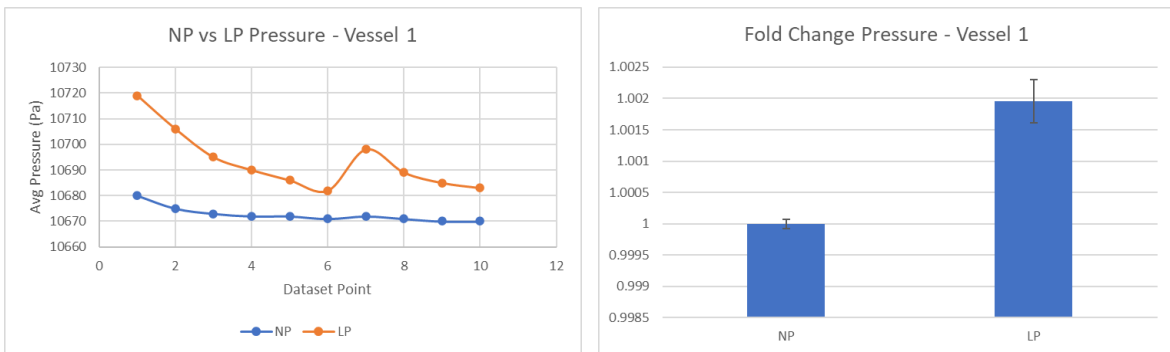

Figure 6.25 *(left)* and 6.26 *(right)* : Excel graph comparing the no pneumonectomy and left pneumonectomy model pressure mean data points selected along the wall of Vessel 1 *(left)*. Excel fold change bar graph showing the fold change values for the no pneumonectomy (NP) model and the left pneumonectomy model (LP) pressure *(pressure)*.

In Figure 6.26, the value for NP was 1 and the value for LP was 1.002. After conducting a t-test, the p value was found to be less than 0.0001****, which is considered to be very significant.

Vessel 2 (Left Pneumonectomy vs No Pneumonectomy Control)

The second vessel of interest was Vessel 2, pictured in red in the figures below. Figs. 6.27 and 6.28 show the qualitative pressure increase in the pneumonectomy model, and Figs. 6.29 and 6.30 show our data analysis.
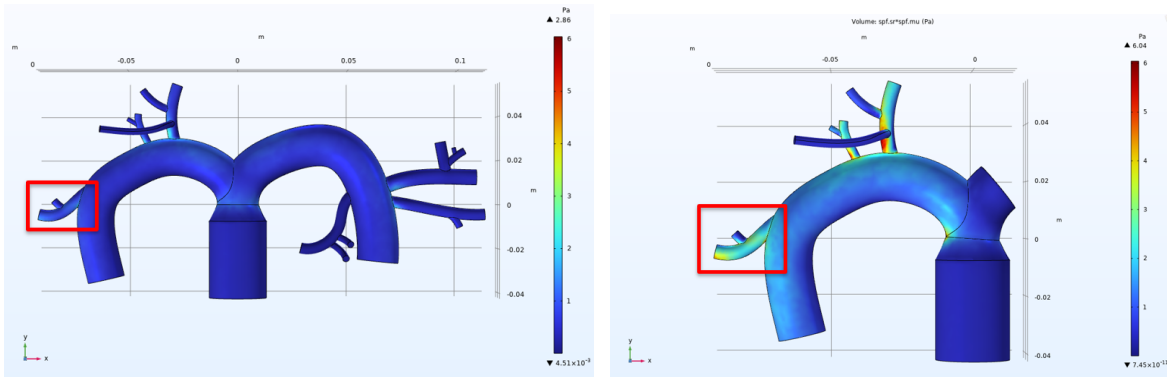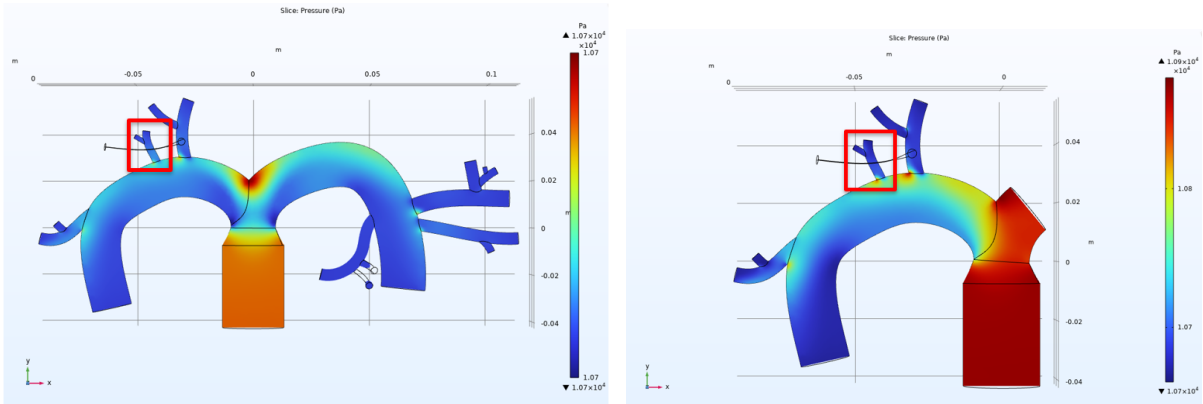

Figure 6.27 *(left)* and 6.28 *(right)* : No pneumonectomy control model pressure COMSOL results *(left)* and left pneumonectomy model (right) both with Vessel 2 highlighted in red.
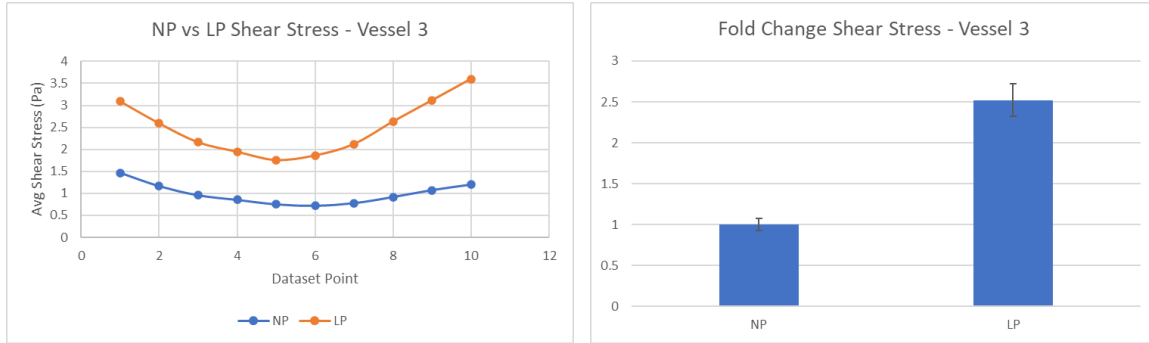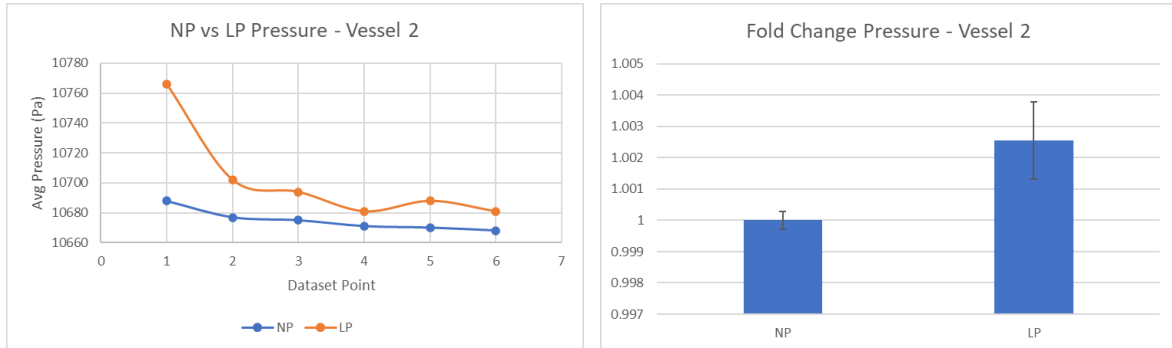

Figure 6.29 *(left)* and 6.30 *(right)* : Excel graph comparing the no pneumonectomy and left pneumonectomy model pressure mean data points selected along the wall of Vessel 2 *(left)*. Excel fold change bar graph showing the fold change values for the no pneumonectomy (NP) model and the left pneumonectomy model (LP) pressure *(pressure)*.

In Figure 6.30, the value for NP was 1 and the value for LP was 1.003. After conducting a t-test, the p value was found to be 0.0726, which is considered to be insignificant.

Vessel 3 (Left Pneumonectomy vs No Pneumonectomy Control)

The third vessel of interest was Vessel 3, pictured in red in the figures below. Figs. 6.31 and 6.32 show the qualitative pressure increase in the pneumonectomy model, and Figs. 6.33 and 6.34 show our data analysis.
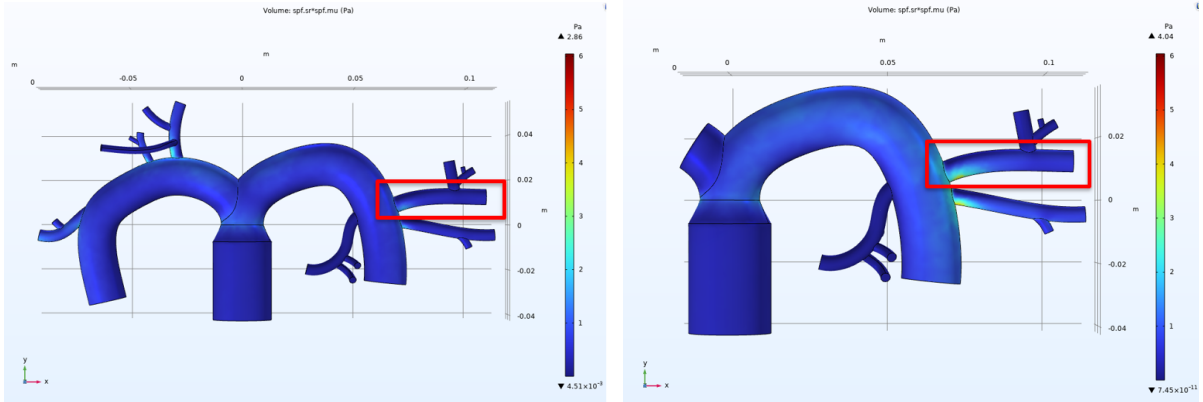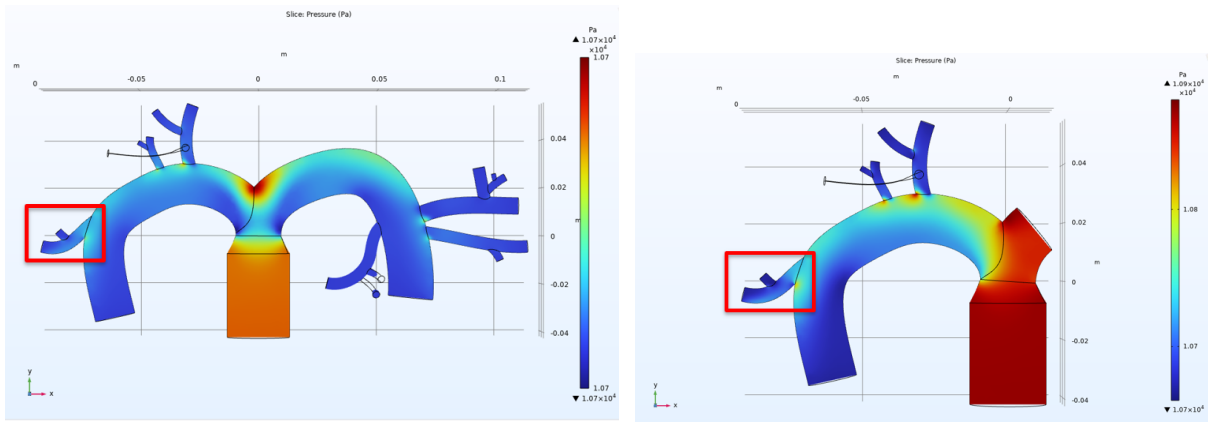

Figure 6.31 *(left)* and 6.32 *(right)* : No pneumonectomy control model pressure COMSOL results *(left)* and left pneumonectomy model (right) both with Vessel 3 highlighted in red.
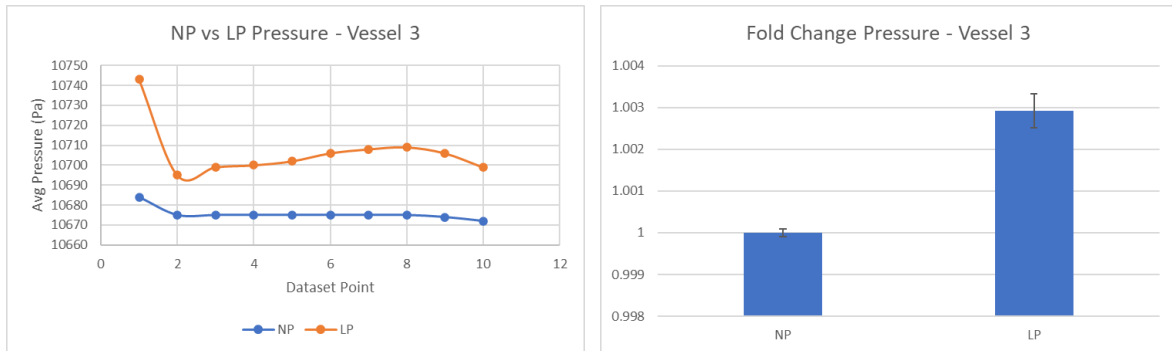
Figure 6.33 *(left)* and 6.34 *(right)*: Excel graph comparing the no pneumonectomy and left pneumonectomy model pressure mean data points selected along the wall of Vessel 3 *(left)*. Excel fold change bar graph showing the fold change values for the no pneumonectomy (NP) model and the left pneumonectomy model (LP) pressure *(pressure)*.

In Figure 6.34, the value for NP was 1 and the value for LP was 1.003. After conducting a t-test, the p value was found to be less than 0.0001****, which is considered to be very significant.

Next, we compared the pressure in the right pneumonectomy and the no pneumonectomy control model. We selected two vessels to analyze in MATLAB, plot data points in Excel, calculate the fold change for, and find the p values for determining the significance of the fold change data. Vessel 4 had 10 data points and Vessel 5 had 10 data points.

Vessel 4 (Right Pneumonectomy vs No Pneumonectomy Control)

The first vessel of interest was Vessel 4, pictured in red in the figures below. Figs. 6.35 and 6.36 show the qualitative pressure increase in the pneumonectomy model, and Figs. 6.37 and 6.38 show our data analysis.
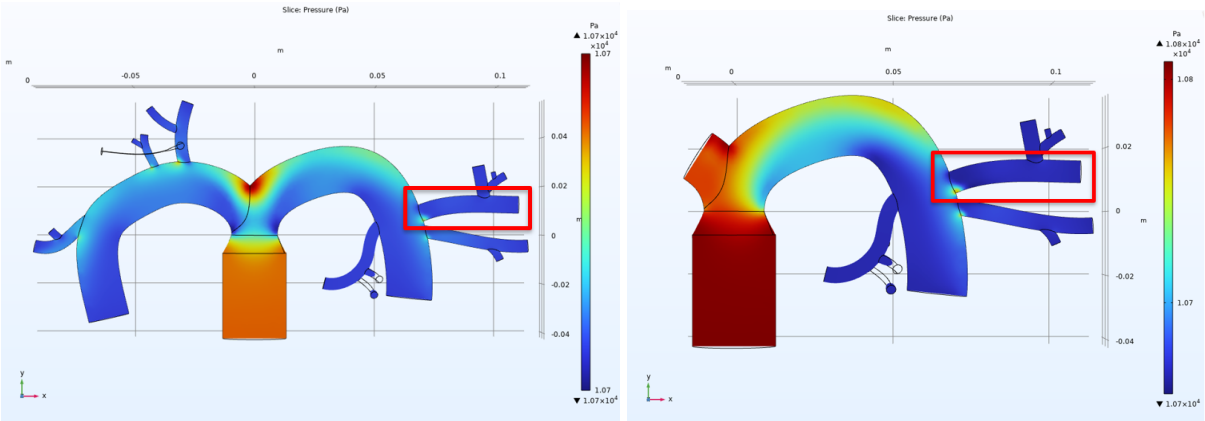
Figure 6.35 *(left)* and 6.36 *(right)* : No pneumonectomy control model pressure COMSOL results *(left)* and right pneumonectomy model (right) both with Vessel 4 highlighted in red.
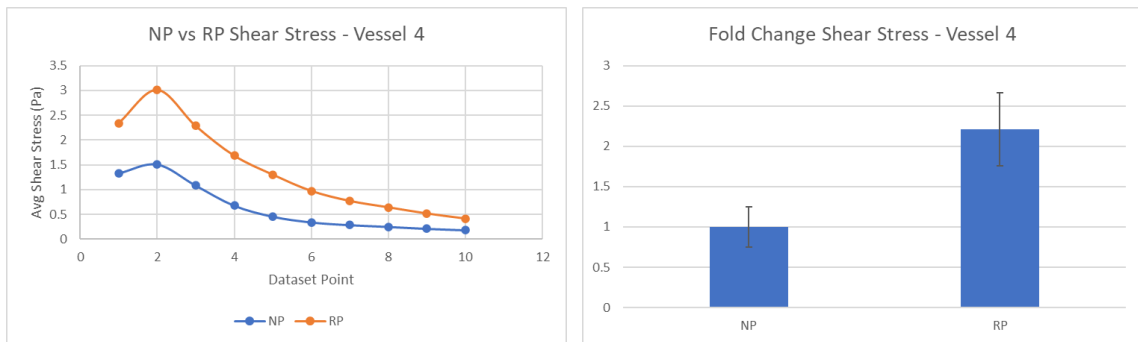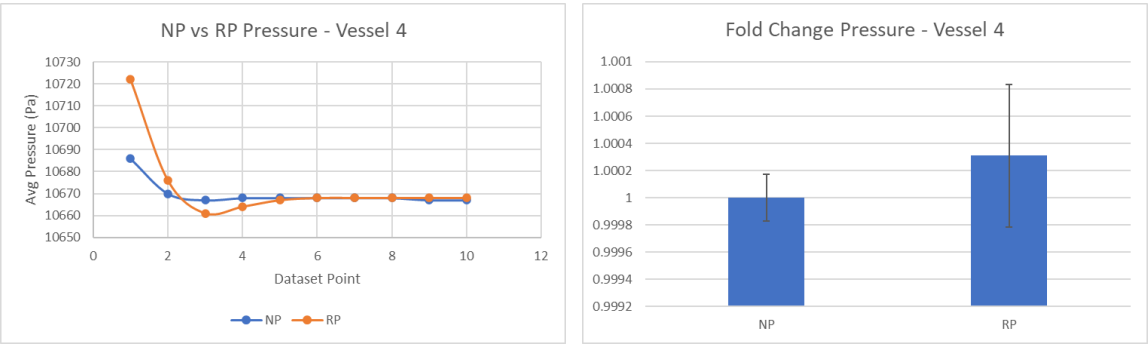

Figure 6.37 *(left)* and 6.38 *(right)*: Excel graph comparing the no pneumonectomy and right pneumonectomy model pressure mean data points selected along the wall of Vessel 4 *(left)*. Excel fold change bar graph showing the fold change values for the no pneumonectomy (NP) model and the right pneumonectomy model (RP) pressure *(pressure)*.

In Figure 6.38, the value for NP was 1 and the value for RP was 1.0003. After conducting a t-test, the p value was found to be 0.5807, which is considered to be insignificant.

Vessel 5 (Right Pneumonectomy vs No Pneumonectomy Control)

The second vessel of interest was Vessel 5, pictured in red in the figures below. Figs. 6.39 and 6.40 show the qualitative pressure increase in the pneumonectomy model, and Figs. 6.41 and 6.42 show our data analysis.
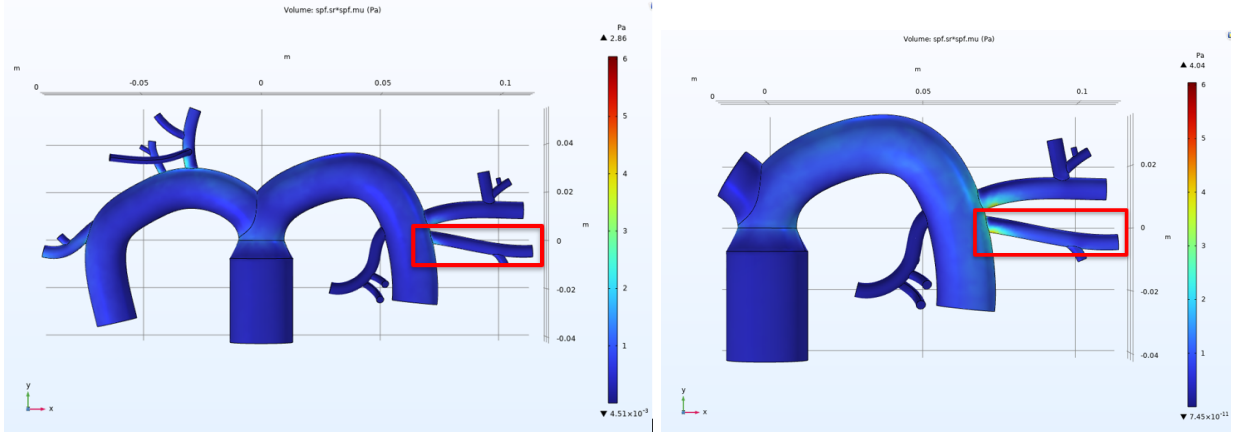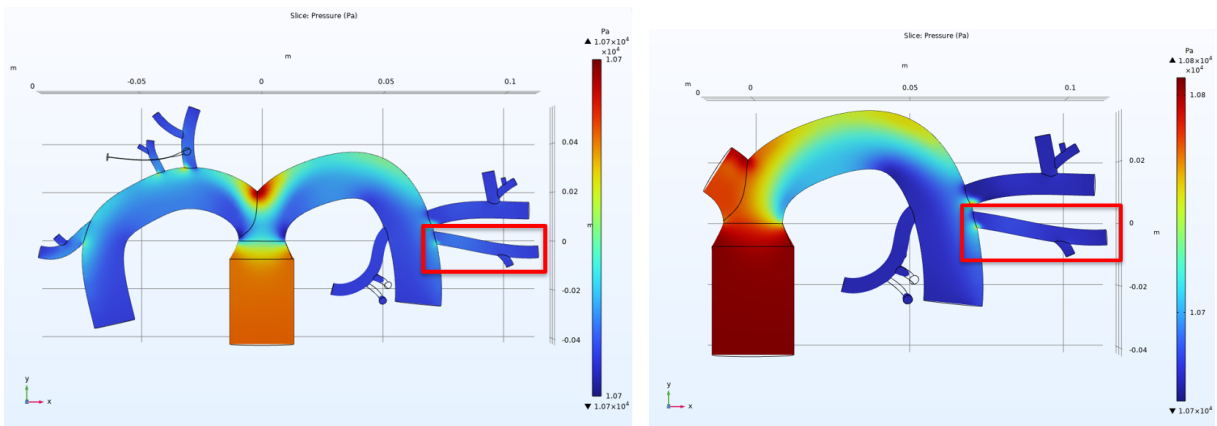

Figure 6.39 *(left)* and 6.40 *(right)*: No pneumonectomy control model pressure COMSOL results *(left)* and right pneumonectomy model (right) both with Vessel 5 highlighted in red.
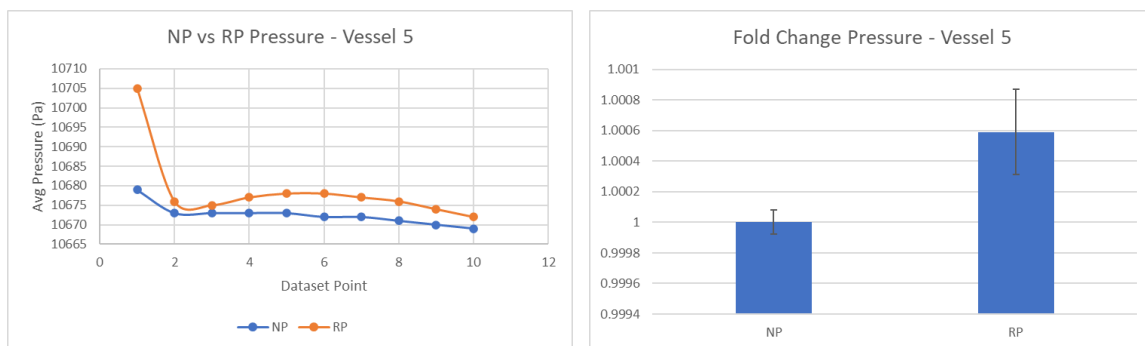
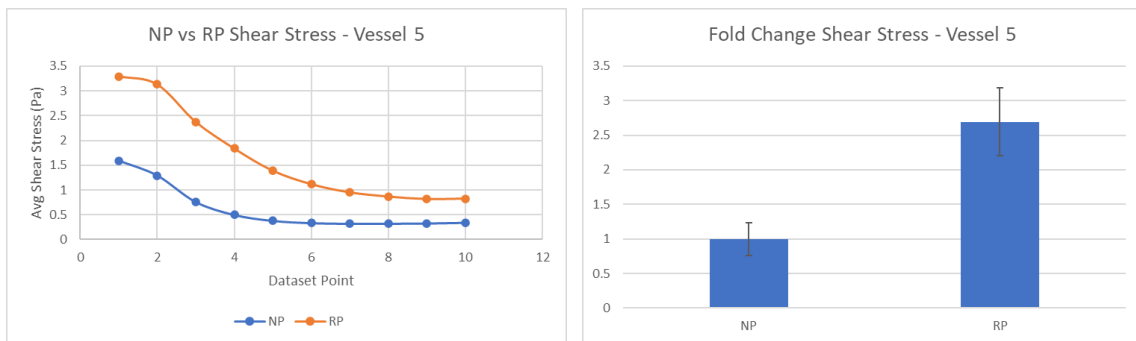Figure 6.41 *(left)* and 6.42 *(right)* : Excel graph comparing the no pneumonectomy and right pneumonectomy model pressure mean data points selected along the wall of Vessel 5 *(left)*. Excel fold change bar graph showing the fold change values for the no pneumonectomy (NP) model and the right pneumonectomy model (RP) pressure *(pressure)*.

In Figure 6.42, the value for NP was 1 and the value for RP was 1.0006. After conducting a t-test, the p value was found to be 0.0563, which is considered to be insignificant.

Overall, the increase in pressure was found to be much more significant in the left pneumonectomy model than the right pneumonectomy model when being compared to the no pneumonectomy model.

6.3 General Ethical Concerns and Mitigation

Our project did not involve any citizen interviews, surveys, or collection of personal information. Additionally, no animal testing was conducted. Results of this research could contribute to future data showing that pneumonectomies damage the glycocalyx and could potentially influence physician recommendations for pneumonectomy patients. Future research may involve in vivo experimentation, animal testing, and clinical studies. These all have ethical concerns beyond those of this project. Patient and animal safety and treatment should be considered seriously and optimized to prevent cruel and unnecessary procedures. In vitro testing should be conducted extensively before moving to animal and in vivo testing to move forward with as much knowledge about the impacts as possible.

6.4 Economic Impact

Our in vitro device does not have a direct paywall, it was constructed using a budget, and materials were provided at discounts and for free in some cases. There is an economic barrier to acquiring the same materials for citizens without a network and student discounts to construct the same experiment.

Whilst not having a direct impact on the public population's finances, these physical and digital models are very replicable and can be used to further research of the eGCX. Current costs associated with complications following pneumonectomies cost patients tens of thousands of dollars. It is estimated that a single complication, often occurring from issues relating to the eGCX, can cost upwards of $11,693 (as high as $18,957)[41]. Future pneumonectomy complication mitigations that are based on this future research could save patient spending by reducing post-pneumonectomy complications. The issue of family burden in which spouses or other family members are missing work to take care of their loved ones can also be addressed by

reducing these complications. Additionally, pneumonectomy recommendations could decrease for patients who are at high risk of complications, such as those with unhealthy vasculature pre-pneumonectomy.

6.5 Environmental Impact

Our proposed device should not have a significant impact on the environment as much of the setup is designed to be reusable and the molds can be easily printed and used for customization. The plexiglass frame and the tubing can be reused and would only require machining and purchasing a single time. The PDMS used to create channels can be recycled and will degrade in the soil. The PDMS can be discarded and destroyed at specified locations and should not have any impact on other natural elements[42]. No pathogens or environmentally dangerous components are used to construct or utilize our models.

6.6 Societal Impact

The design of this fluidic device, while not novel, is capable of being utilized in other similar facets of research. The design of this microchip differs from many other microfluidic devices in that the scalability and process can be used for a wider variety of applications. Additionally, this design is capable of aiding in the explanation of pneumonectomy risks for people who may be required to receive an operation. The SOLIDWORKS and COMSOL simulations and models that have been created can be further elaborated on and used as a baseline for more in-depth simulations to benefit from the knowledge available about pulmonary arterial values.

Our model does not consider varying health levels of pulmonary vasculature, such as heart disease pulmonary vasculature. The in vitro model has limitations in terms of simulating the complete state of a pneumonectomy, and future research should be conducted with more anatomically accurate in vitro vasculature, and in vitro testing should be conducted before changing recommendations for potential pneumonectomy patients.

One ethical concern is that the sourcing of all components of the in vitro model is unknown. Whether the HLMVECs that were sourced from Cell Applications, Inc. were properly maintained and followed all regulations is unknown to us.

6.7 Global Impact

On a global scale, our research may not be applicable in totality since the majority of literature that was found is nationally based. Measurements of the pulmonary tree that were found were based on trials conducted in the United States. This means that the data collected is skewed to the environment and biological characteristics of Americans and does not include global physiology and environments. Expanding our project, in its current state, to a global level would not be possible since the literature and physiological measurements that we found do not account for differences in environment and lifestyle on a global scale. Additionally, an expansion to the global level would fail to consider healthcare disparities on a global scale. The pneumonectomy surgery itself is not widely accessible due to the cost and surgery resources required for the procedure and post-operative care. Inpatient pneumonectomies without complications cost on average $45,080 ± $38,239[2]. This cost is inaccessible for many citizens of the United States as is, and countries with limited medical resources and lower average incomes likely have even less access to pneumonectomies.

6.8 Health and Safety Concerns

The findings from our research can influence the decision-making of individuals after undergoing a pneumonectomy and the professionals guiding pneumonectomy patients in avoiding complications. Our findings and any future projects based on our computer model and design could improve outcomes for surgeons, hospitals, and medical manufacturers associated with equipment used for pneumonectomies.

6.9 Manufacturability

The manufacturability of our design is quite favorable. The plexiglass is fairly easily machined and could potentially be replaced by a cheaper or easier-to-manufacture material. 3D printing using PLA for the PDMS molds is very cheap aside from the cost of the equipment, as well as being scalable. The PDMS itself is more costly but is a common material in the medical industry, making it relatively easy to access. The molding process is simple, though accelerating the setting process in PLA using heat while avoiding deformation of the mold was a challenge in this project. Potentially the biggest expense and barrier to manufacturability of this design is the coating of PDMS. The fibronectin we used was expensive relative to many other materials, and

the application of the coating as well as the manipulations related to the staining and imaging of the cells were more painstaking and delicate. It does seem possible, though, that our design as a whole could be improved, optimized for efficiency, and end up yielding higher-quality results with a bigger budget and more resources.

7. Discussion

This section looks at the results of our simulations and in vitro work and reflects on their significance, accuracy, and more.

7.1 SOLIDWORKS Model and COMSOL Flow Simulations

Literature on shear stress changes due to pneumonectomies is inconclusive and limited. By creating a digital simulation as part of our project, we were able to observe how severe the shear stress change is. Our initial qualitative analysis of the COMSOL model simulations showed increased shear stress at the bifurcations branching from the main right and left pulmonary vasculature. This ultimately showed that bifurcations are where damage to the glycocalyx is most likely to occur, and that the shear stress changes resulting from pneumonectomies are significant.

For the COMSOL pressure results from Vessels 2, 4 and 5, the p values showed that there was an insignificant change from the no pneumonectomy model to the right pneumonectomy model. This was most likely due to the design of the vasculature and the location of the vessels of interest relative to the inlet. There could be overall less of a pressure change the further the location is from the inlet, however, this is hypothesized based on the qualitative and quantitative analysis of the COMSOL results from our models.

Our results also showed that there was a more significant increase in shear stress in the left pneumonectomy model than the right pneumonectomy model when compared to the no pneumonectomy model. This is the opposite to what we would expect to see in an in vivo model. Because the left lung is smaller than the right, right pneumonectomies would result in a larger change, as there is a higher change in blood volume traveling through the left lung as opposed to the right after a left pneumonectomy[14]. This data change is likely due to the fact that we did not create our SOLIDWORKS model to be sufficiently physiologically accurate. This limitation of our model could have been mitigated by measuring the right and left vessel volumes, and by keeping the left vasculature smaller than the right.

Every vessel of interest we analyzed had statistically significant results for shear stress. Simulating the significant shear stress increases showed that the shear stress change is noteworthy and a potential mechanism for some pneumonectomy complications. As damage to the glycocalyx has been shown to increase vascular permeability, coagulation, and inflammation,

complications triggered by such events would be catalyzed by the pneumonectomy itself. Our simulation was limited by the lack of a glycocalyx component that would have simulated glycocalyx properties.

One of the major limitations of our digital design was our lack of experience when creating the SOLIDWORKS model and when running flow simulations. Our initial goal had been to create the model and finish the simulations by the end of B Term, but we did not finish the COMSOL simulations until D Term. Technical skill limitations were one of the reasons that the SOLIDWORKS models were not as elaborate or anatomically accurate as we desired.

7.2 Staining and Imaging

Upon imaging our results, it was clear that this methodology successfully served as a proof of concept for further research testing. Both the DAPI and WGA were fairly clear and visible through much of the mold. However, exposure levels of the WGA and DAPI were often set to 3 - 4.5 seconds per image to pick up on the stains. It seems likely that the lower levels of fluorescence were due to the design or staining. We hypothesize that the creation of the PDMS molds using PLA molds created optical abnormalities between each step up the side of a vessel. The layer height, or increment from each level of the print to the next, was limited to a minimum of 0.1 mm by the machine. Instead of a smooth curve, the sides of the vessels had a subtle but stepped morphology. The seeded HLMVECs appeared to have clustered near the steps and densified in regions near to these lines rather than forming a uniform layer over the PDMS vasculature, as desired. The unwanted result of this was larger quantities of stainable regions near the PDMS steps and increased fluorescence contrast between these "fluorescence highs" and the "fluorescence lows" closer to the middle of the vessel levels. This led to further difficulties in creating balanced images due to the difficulty in scale the vibrance of the stain to adequately show both the WGA and DAPI without washing out the darker colors (shown in Fig. 7.1).
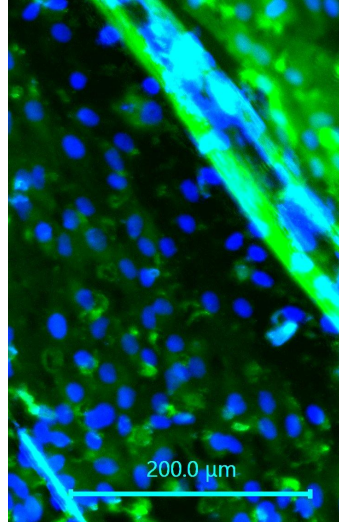
Figure 7.1: 20x image taken near the bifurcation of the control model. Despite Z-stacking, many of the layers had issues with exposure and focus after post-processing.

Despite the physical limitations of the molds, imaging served as a proof of concept and could be used to draw qualitative conclusions. By using the Keyence microscope's ability to Z-stack layers of images and stitch X and Y coordinates together, clear images of large areas were produced, as seen in Fig. 7.2.
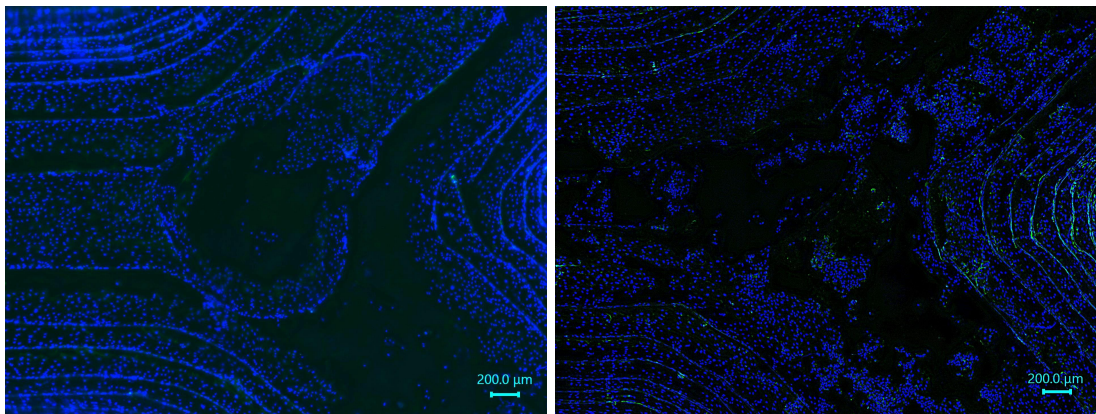
Figure 7.2: 4x magnification images of the inlet bifurcation in the pneumonectomy/Flow Trial 3 (*right*) and control/Flow Trial 2 (*left*) molds after testing and staining with DAPI and WGA.

All of the fluorescence images allowed for comparisons of cell clustering and confluency throughout the vessels and bifurcations. By comparing these images in matching sections of vasculature between the pneumonectomy trials and the control trials, we could make qualitative

assertions about the state of the glycocalyx post pneumonectomy. As depicted in Chapter 5.5.3, the glycocalyx vibrance (green) substantially decreased when viewed under similar imaging settings between the two flow tests. However, due to the delays caused by technical limitations, quantitative analysis was not able to be performed to further validate the results and assumptions taken from initial viewing. It was confirmed that cells were able to remain attached after flow trials and that they were able to be seen in all levels of the channel. However, there were apparent sections occurring most commonly near bifurcations and areas of high pressure where some cells were not visible. This could have been due to detachment that occurred during flow trials thanks to prolonged exposure to high flow rates. Another factor could have been incomplete attachment to the PDMS surface in the first place. It is possible that the fibronectin coating did not allow for complete attachment due to a lack of absorbance into the PDMS. A related explanation for this is the hydrophobic nature of PDMS, which was not modified in any way other than with the fibronectin coating before seeding. These circumstances could have resulted in cells appearing attached under microscope while lacking the same strength of attachment as expected from previous experimentation. To better verify these cases, a control trial of seeded cells should have been run similar to the static sterility test to determine whether the assembly of the device could have contributed to these alterations in cell attachment rather than the flow rate and pressures which occurred during the flow trials.

8. Conclusions and Recommendations

The goal of our project was to better understand the potential relationship between a pneumonectomy surgery and damage to the eGCX. We aimed to model this damage in a 3D fluidic chamber to better understand this relationship. The qualitative results from our in vitro study showed that glycocalyx coverage decreased under the pneumonectomy conditions we created.

The MATLAB results show that there is significant increase in shear stress along bifurcated vessel walls with fold change values between 2 and 3. The COMSOL model simulation shows that bifurcations are where the glycocalyx may experience the most increased degradation. Combined, these results show that the areas of most interest in post pneumonectomy vasculature are along the vessel walls near bifurcations. More research is required to determine if certain vessel sizes experience disproportionately high shear stresses.

Results from this study could be used in tandem with digital modeling of the damage that occurs in the distal branches to locate where exactly the most damage occurs and how much damage occurs to the glycocalyx. This research furthers the limited research done on how a pneumonectomy impacts the glycocalyx. Understanding the state of the glycocalyx as a result of a pneumonectomy can contribute to future studies of glycocalyx recovery and regeneration. This model can serve as a starting point for future glycocalyx regeneration post pneumonectomy, where therapeutics can be introduced into the media (or whatever fluid is used), and their impact on the glycocalyx can be observed.

8.1 Future Simulation Recommendations

For future iterations of this project or research based upon it, we recommend a more complex SOLIDWORKS lung model with significantly more anatomical accuracy. We had difficulty finding distal vessel measurements within the lung, so future efforts should be made to more accurately model the pulmonary vasculature with a focus on small vessels. The largest vessels we modeled were 2.1 mm. Models with realistic morphology and material properties would result in more significant results that could show exactly how shear stress affects vessels. Additionally, the eGCX layer that exists within vessels could be modeled in the lung model to simulate any potential damage that occurs along those sections.

In COMSOL, we set the flow within our system to be laminar, which is not entirely accurate given the changes in flow that we were modeling postpneumonectomy. This was largely due to the fact that we were previously unfamiliar with the software, so we used the most basic flow type available to start off with. In future iterations, introducing a more turbulent and abrupt flow in postpneumonectomy models–similar to what occurs directly after the actual surgery–could generate more accurate results.

8.2 Future In Vitro Recommendations

For future efforts to create an in vitro model, we recommend a focus on the ease of imaging. For instance, redesigning our fluidic chamber to be a microfluidic chip or opting for resin-printed molds for the PDMS could greatly improve the image quality and reduce the effort, time, and equipment required to produce images. With a microfluidic chip, the model would have a lower refractive index compared to our 3.5-mm-thick PDMS molds. Additionally, a microfluidic chip could potentially eliminate some of the risk of leaks, allowing for longer run times which will lead to improved results. A microfluidic chip would be most conducive for modeling microvasculature as well.

With resin printing, the vasculature could be modeled with greater accuracy and fewer abnormalities, creating smoother cylindrical vessels. In our PDMS molds, we encountered manufacturing challenges due to the steps along the walls of our vasculature created based on the 3D printer's layer height (we used an Ultimaker 3 through WPI's Makerspace), which we believe may have impacted on our results. If resin printing is pursued, we recommend also attempting cryosectioning to image the results with a confocal microscope. In addition to it being a cheaper method, cryosectioning can offer a cross-sectional view of the vessels as opposed to a top-down view which may make it easier to visualize any damage and degradation that occurs to the glycocalyx in postpneumonectomy conditions.

References

[1] "Pneumonectomy," *Johns Hopkins Medicine*.
    https://www.hopkinsmedicine.org/health/treatment-tests-and-therapies/pneumonectomy

[2] Beshara, Michael, and Vaibhav Bora. "Pneumonectomy," *PubMed*, 2023.
    https://www.ncbi.nlm.nih.gov/books/NBK555969

[3] Alphonsus, C. S., and R. N. Rodseth. "The Endothelial Glycocalyx: A Review of the
    Vascular Barrier." *Anaesthesia*, vol. 69, no. 7, (2014): 777–784., 10.1111/anae.12661

[4] Dietz, Niki M. "Pathophysiology of Postpneumonectomy Pulmonary Edema." *Seminars in
    Cardiothoracic and Vascular Anesthesia*, vol. 4, no. 1, (2000): 31–35.,
    10.1177/108925320000400105

[5] Brinkham, Joshua E., and Sandeep Sharma. "Physiology, Pulmonary," *PubMed*, 2022.
    https://pubmed.ncbi.nlm.nih.gov/29494033/

[6] Khan, Yusuf, and David Lynch. "Histology, Lung," *PubMed*, 2023.
    https://www.ncbi.nlm.nih.gov/books/NBK534789/

[7] Charalampidis, Charalampos *et al.* "Pleura Space Anatomy," *Journal of Thoracic Disease*,
    vol. 7, no. 1, (2015): 27-32, doi: 10.3978%2Fj.issn.2072-1439.2015.01.48

[8] *Gross Anatomy Glossary: Lungs & Pleura*. Draw It to Know It.
    https://drawittoknowit.com/course/gross-anatomy/respiratory-system/upper-lower-respira
    tory-tracts/965/lungs

[9] Schochet, Peter. *Alveolus Gas Exchange*. 7 Dec, 2015. Presbyterian Hospital Plano, Texas.
    https://www.pedilung.com/pediatric-lung-diseases-disorders/anatomy-of-a-childs-lung/al
    veolus-gas-exchange-pulmonary-alveolus/

[10] Satish, Mohan, and Prasanna Tadi. "Physiology, Vascular," *PubMed*, 2022.
    https://www.ncbi.nlm.nih.gov/books/NBK542252/

[11] "Overview of the Vascular System," *Johns Hopkins Medicine*.
    https://www.hopkinsmedicine.org/health/conditions-and-diseases/overview-of-the-vascul
    ar-system

[12] Chaudhry, Raheel, and Bruno Bordoni. "Anatomy, Thorax, Lungs," *PubMed*, 2022.
    https://pubmed.ncbi.nlm.nih.gov/29262068/

[13] Haddad, Moshe, Sandeep Sharma. "Physiology, Lung," *PubMed*, 2022.
    https://pubmed.ncbi.nlm.nih.gov/31424761/

[14] U. Bozlar *et al*. "Pulmonary artery diameters measured by multidetector-row computed tomography in healthy adults," *Acta Radiologica*, vol. 48, no. 10, (2017): 1086–1091, doi: 10.1080/02841850701545755.

[15] Kandathil, Asha, and Murthy Chamarthy. "Pulmonary vascular anatomy & anatomical variants," *Cardiovascular Diagnosis and Therapy*, vol. 8, no. 3, (2018): 201–207, doi: 10.21037/cdt.2018.01.04

[16] Möckl, Leonhard. "The Emerging Role of the Mammalian Glycocalyx in Functional Membrane Organization and Immune System Regulation," *Frontiers in Cell and Developmental Biology*, vol. 8, (2020) doi: 10.3389/fcell.2020.00253

[17] Harding, Ian C. *et al*. "Endothelial barrier reinforcement relies on flow-regulated glycocalyx, a potential therapeutic target," *Biorheology*, vol. 56, no. 2–3, (2019): 131–149, doi: 10.3233/BIR-180205

[18] Dogné, Sophie, Bruno Flamion, and Nathalie Caron, "Endothelial Glycocalyx as a Shield Against Diabetic Vascular Complications," *Arteriosclerosis, Thrombosis, and Vascular Biology*, vol. 38, no. 7, (2018): 1427–1439, doi: 10.1161/atvbaha.118.310839

[19] Nian, Keqing *et al*. "Blood-Brain Barrier Damage in Ischemic Stroke and Its Regulation by Endothelial Mechanotransduction," *Frontiers in Physiology*, vol. 11, 2020, doi: 10.3389/fphys.2020.605398

[20] Haroon, Mohammad *et al.*, "Fluid shear stress-induced mechanotransduction in myoblasts: Does it depend on the glycocalyx?," *Experimental Cell Research*, vol. 417, no. 1, (2022) doi: 10.1016/j.yexcr.2022.113204

[21] Pedrosa, Guillermo Sánchez *et al*. "Role of surgical manipulation in lung inflammatory response in a model of lung resection surgery," *Oxford Academic*, Vol. 27, no. 6, (2018): 870-877, doi: 10.1093/icvts/ivy198

[21] "Key Statistics for Lung Cancer," *American Cancer Society*, 2021. https://www.cancer.org/cancer/lung-cancer/about/key-statistics.html

[22] Williams, Marcia. "Pneumonectomy," *Baylor Medicine*. https://www.bcm.edu/healthcare/specialties/the-lung-institute/thoracic-surgery/pneumonectomy

[23] Sahn, S.A., and J. T. Heidecker. "Trauma, Chest | Bronchopleural Fistulas," *Encyclopedia of Respiratory Medicine*, pp 288-295, (2006) doi: 10.1016/B0-12-370879-6/00399-9

[24] Liu, Gan-Wei *et al*. "Identifying Patients at Higher Risk of Pneumonia after Lung Resection," *PubMed*, vol. 9, no. 5, (2017): 1289-1294, doi: 10.21037/jtd.2017.04.42

[25] Raskind, Samantha, Natasha Cruz-Calderon, Gillian Miller, Lydia Masse, and Taylor Paradis. 2022. *A Parallel Plate Flow Chamber to Investigate Endothelial Glycocalyx Remodeling After Pneumonectomy.* : Worcester Polytechnic Institute. (2022).

[26] Sentenac, Pierre *et al*. "Pulmonary hypertension after pneumonectomy: a preclinical model in rats and human pulmonary endothelial cells," *European Journal of Cardio-Thoracic Surgery*, vol. 59, no. 1, (2022): 147–154, doi: 10.1093/ejcts/ezaa277

[27] Miyazawa, Masahisa *et al*. "Longterm effects of pulmonary resection on cardiopulmonary function.," *Journal of the American College of Surgeons*, vol. 189, no. 1, (1999): 26–33, doi: 10.1016/S1072-7515(99)00071-X.

[28] Zheng, Ying *et al.*, "In vitro microvessels for the study of angiogenesis and thrombosis," *Proceedings of the National Academy of Sciences*, vol. 109, no. 24 (2012): 9342–9347, doi: 10.1073/pnas.1201240109.

[29] "Use of ISO 10993-1, Biological evaluation of medical devices - Part 1," *U.S. Food and Drug Administration*, 2019. https://www.fda.gov/regulatory-information/search-fda-guidance-documents/use-internati onal-standard-iso-10993-1-biological-evaluation-medical-devices-part-1-evaluation-and

[30] Wyatt, P. "ISO 19005 (PDF/A)," 2005. https://www.pdfa.org/resource/iso-19005-pdfa/.

[31] Rolle, Marsha *et al*. 2011. Methods of generating small-diameter tissue engineered blood vessels, issued February 10, 2011.

[32] Valji, Karim. "Pulmonary and Bronchial Arteries," *Radiology Key*, 2016. https://radiologykey.com/pulmonary-and-bronchial-arteries/

[33] Pikin, Oleg, *et al*. "Bronchial Stump Re-Resection for Lung Cancer Recurrence after Left Pneumonectomy." *Indian Journal of Thoracic and Cardiovascular Surgery*, vol. 37, no. 1, (2020): 105–107. doi: 10.1007/s12055-020-01030-y

[34] Siren, Erika M. J. *et al.*, "An improved in vitro model for studying the structural and functional properties of the Endothelial Glycocalyx in arteries, capillaries and veins," *The FASEB Journal*, vol. 35, no. 6, (2021) doi: 10.1096/fj.201802376RRRR.

[35] Orellana-Barrasa, Jaime. "Effects of Accelerating the Ageing of 1D PLA Filaments after Fused Filament Fabrication," *MDPI*, vol. 15, no. 1, (2022): 69, doi: 10.3390/polym15010069

[36] Marczewski, A., T. Bednarek, and W. Sosnowski. "Modeling of Fluid and Structure Interaction in Blood Vessels," *Institute of Fundamental Technological Research*, https://www.ippt.pan.pl/repository/open/o144.pdf

[37] Seladi-Schulman, Jill and Jennifer Larson. "About Isolated Systolic Hypertension (High Systolic Blood Pressure)," *Healthline*, 2023. https://www.healthline.com/health/heart-disease/high-systolic-blood-pressure.

[38] Ivanov, K. P. "New Data on the Process of Circulation and Blood Oxygenation in the Lungs under Physiological Conditions," *Bull Exp Biol Med*, vol. 154, no. 4, (2013): 411-414, doi: 10.1007/s10517-013-1963-1

[39] Chiu, Jeng-Jiann, Shu Chien. "Effects of Disturbed Flow on Vascular Endothelium: Pathophysiological Basis and Clinical Perspectives," *American Physiological Society*, vol. 91, no. 1, (2011): 327-387, doi: 10.1152/physrev.00047.2009

[40] Raman, Karthick, T. R Srinivasa Murthy, and G. M. Hegde. "Fabrication of Refractive Index Tunable Polydimethylsiloxane Photonic Crystal for Biosensor Application." *Science Direct*, vol. 19, no. 1, (2011): 146-151., https://www.sciencedirect.com/science/article/pii/S187538921100472X/pdf

[41] Medbery, Rachel L. *et al.*, "Costs Associated With Lobectomy for Lung Cancer: An Analysis Merging STS and Medicare Data," *The Annals of Thoracic Surgery*, vol. 111, no. 6, (2021): 1781–1790, doi: 10.1016/j.athoracsur.2020.08.073

[42] Fendinger, N. J. *et al.* "Environmental Occurrence of Polydimethylsiloxane," *Environmental Science & Technology*, vol. 31, no. 5, (1997): 1555–1563, doi: 10.1021/es9608712

Appendices

Appendix I: Flow Rate and Shear Stress Calculations

Q = volumetric flow rate (mL/min)

D = vessel diameter = 3.1 mm

Δp = change in pressure

μ = viscosity (used viscosity of water at 20°C) = 1.0016×10^{-2})

ℓ = length of vessel

Flow in a pipe: $Q = \pi D4 \Delta p / 128 \mu \ell$

Pressure difference (assuming laminar flow): $\Delta p = 4 \ell \tau w / D$

Combined: $Q = (\pi D44 \ell \tau w / D) / 128 \mu \ell$

Simplified: $Q = 4 \pi D3 \tau w / 128 \mu$

Calculated flow rate based on a minimum physiological shear stress of 10 dyn/cm2, our vessel diameter of 3.1 mm, and the viscosity of water

Used the maximum available flow rate of 93.08 mL/min (generates 5.312 dyn/cm2)

Appendix II: No Pneumonectomy Shear Stress Matlab Code

```matlab
t = readtable('Full_Model_Shear_Stress_Volume_Data.txt');
data = table2array(t(:,1:4));
indx = find((data(:,1)>-0.3)&(data(:,2)>-0.04)&(data(:,1)<0.45));
figure;
scatter3(data(indx,1),data(indx,2),data(indx,3),30,data(indx,4))
axis equal;

%first vessel of interest

%ax = [-0.0328   -0.0302    0.0316    0.0325]; %location 1
%ax = [-0.0332   -0.0306    0.0329    0.0338]; %location 2
%ax = [-0.0334   -0.0308    0.0382    0.0391]; %location 3
%ax = [-0.0336   -0.0310    0.0393    0.0402]; %location 4
%ax = [-0.0336   -0.0310    0.0403    0.0412]; %location 5
%ax = [-0.0335   -0.0309    0.0413    0.0421]; %location 6
%ax = [-0.0324   -0.0304    0.0450    0.0459]; %location 7
%ax = [-0.0322   -0.0302    0.0460    0.0469]; %location 8
%ax = [-0.0320   -0.0301    0.0470    0.0479]; %location 9
%ax = [-0.0318   -0.0301    0.0480    0.0489]; %location 10

%second vessel of interest

%ax = [-0.0432   -0.0423    0.0276    0.0290]; %location 1
%ax = [-0.0438   -0.0426    0.0291    0.0301]; %location 2
%ax = [-0.0444   -0.0432    0.0302    0.0314]; %location 3
%ax = [-0.0464   -0.0455    0.0347    0.0358]; %location 4
%ax = [-0.0471   -0.0461    0.0378    0.0390]; %location 5
%ax = [-0.0471   -0.0460    0.0391    0.0401]; %location 6

%third vessel of interest

%ax = [-0.0736   -0.0721   -0.0011    0.0014]; %location 1
%ax = [-0.0750   -0.0737   -0.0022    0.0004]; %location 2
%ax = [-0.0763   -0.0751   -0.0037   -0.0010]; %location 3
%ax = [-0.0776   -0.0764   -0.0048   -0.0019]; %location 4
%ax = [-0.0794   -0.0775   -0.0053   -0.0039]; %location 5
%ax = [-0.0811   -0.0795   -0.0067   -0.0048]; %location 6
%ax = [-0.0830   -0.0812   -0.0078   -0.0057]; %location 7
%ax = [-0.0850   -0.0831   -0.0078   -0.0061]; %location 8
%ax = [-0.0870   -0.0851   -0.0078   -0.0064]; %location 9
%ax = [-0.0890   -0.0871   -0.0078   -0.0063]; %location 10

%fourth vessel of interest

%ax = [0.0691    0.0712    0.0058    0.0087]; %location 1
%ax = [0.0713    0.0743    0.0065    0.0088]; %location 2
%ax = [0.0744    0.0771    0.0074    0.0092]; %location 3
%ax = [0.0772    0.0797    0.0082    0.0099]; %location 4
%ax = [0.0798    0.0827    0.0086    0.0101]; %location 5
%ax = [0.0828    0.0859    0.0083    0.0104]; %location 6
%ax = [0.0860    0.0888    0.0092    0.0103]; %location 7
%ax = [0.0889    0.0918    0.0092    0.0103]; %location 8
%ax = [0.0919    0.0948    0.0092    0.0105]; %location 9
%ax = [0.0949    0.0980    0.0092    0.0105]; %location 10
```

```matlab
%fifth vessel of interest

%ax = [0.0710    0.0730    -0.0016    0.0001]; %location 1
%ax = [0.0731    0.0750    -0.0020    -0.0005]; %location 2
%ax = [0.0751    0.0770    -0.0024    -0.0006]; %location 3
%ax = [0.0771    0.0793    -0.0028    -0.0014]; %location 4
%ax = [0.0793    0.0813    -0.0032    -0.0017]; %location 5
%ax = [0.0814    0.0836    -0.0035    -0.0021]; %location 6
%ax = [0.0837    0.0859    -0.0041    -0.0028]; %location 7
%ax = [0.0860    0.0888    -0.0046    -0.0034]; %location 8
%ax = [0.0889    0.0918    -0.0053    -0.0041]; %location 9
%ax = [0.0919    0.0947    -0.0062    -0.0047]; %location 10


I = find(data(:,1)>ax(1) & (data(:,1)<ax(2)) & data(:,2)>ax(3) & data(:,2)<ax(4));

hold on;
plot3(data(I,1), data(I,2), data(I,3), 'ro')

help axis
data(I, 4)
size(I)
mean(data(I,4))
```

Appendix III: Left Pneumonectomy Shear Stress Matlab Code

```matlab
t2 = readtable('Left_Pneum_Stump_Shear_Stress_Volume_Data.txt');
data2 = table2array(t2(:,1:4));
indx2 = find((data2(:,1)>-0.3)&(data2(:,2)>-0.04)&(data2(:,1)<0.45));
figure;
scatter3(data2(indx2,1),data2(indx2,2),data2(indx2,3),30,data2(indx2,4))
axis equal;

%first vessel of interest

%ax2 = [-0.0328   -0.0302    0.0316    0.0325]; %location 1
%ax2 = [-0.0332   -0.0306    0.0329    0.0338]; %location 2
%ax2 = [-0.0334   -0.0308    0.0382    0.0391]; %location 3
%ax2 = [-0.0336   -0.0310    0.0393    0.0402]; %location 4
%ax2 = [-0.0336   -0.0310    0.0403    0.0412]; %location 5
%ax2 = [-0.0335   -0.0309    0.0413    0.0421]; %location 6
%ax2 = [-0.0324   -0.0304    0.0450    0.0459]; %location 7
%ax2 = [-0.0322   -0.0302    0.0460    0.0469]; %location 8
%ax2 = [-0.0320   -0.0301    0.0470    0.0479]; %location 9
%ax2 = [-0.0318   -0.0301    0.0480    0.0489]; %location 10

%second vessel of interest

%ax2 = [-0.0432   -0.0423    0.0276    0.0290]; %location 1
%ax2 = [-0.0438   -0.0426    0.0291    0.0301]; %location 2
%ax2 = [-0.0444   -0.0432    0.0302    0.0314]; %location 3
%ax2 = [-0.0464   -0.0455    0.0347    0.0358]; %location 4
%ax2 = [-0.0471   -0.0461    0.0378    0.0390]; %location 5
%ax2 = [-0.0471   -0.0460    0.0391    0.0401]; %location 6


%third vessel of interest

%ax2 = [-0.0736   -0.0721   -0.0011    0.0014]; %location 1
%ax2 = [-0.0750   -0.0737   -0.0022    0.0004]; %location 2
%ax2 = [-0.0763   -0.0751   -0.0037   -0.0010]; %location 3
%ax2 = [-0.0776   -0.0764   -0.0048   -0.0019]; %location 4
%ax2 = [-0.0794   -0.0775   -0.0053   -0.0039]; %location 5
%ax2 = [-0.0811   -0.0795   -0.0067   -0.0048]; %location 6
%ax2 = [-0.0830   -0.0812   -0.0078   -0.0057]; %location 7
%ax2 = [-0.0850   -0.0831   -0.0078   -0.0061]; %location 8
%ax2 = [-0.0870   -0.0851   -0.0078   -0.0064]; %location 9
%ax2 = [-0.0890   -0.0871   -0.0078   -0.0063]; %location 10

I2 = find(data2(:,1)>ax2(1) & (data2(:,1)<ax2(2)) & data2(:,2)>ax2(3) & data2(:,2)<ax2(4));

hold on;
plot3(data2(I2,1), data2(I2,2), data2(I2,3), 'ro')

help axis
data(I2, 4)
size(I2)
mean(data2(I2,4))
```

Appendix IV: Right Pneumonectomy Shear Stress Matlab Code

```matlab
t7 = readtable('Right_Pneum_Stump_Shear_Stress_Volume_Data.txt');
data7 = table2array(t7(:,1:4));
indx7 = find((data7(:,1)>-0.3)&(data7(:,2)>-0.04)&(data7(:,1)<0.45));
figure;
scatter3(data7(indx7,1),data7(indx7,2),data7(indx7,3),30,data7(indx7,4))
axis equal;

%fourth vessel of interest

%ax7 = [0.0691   0.0712   0.0058   0.0087]; %location 1
%ax7 = [0.0713   0.0743   0.0065   0.0088]; %location 2
%ax7 = [0.0744   0.0771   0.0074   0.0092]; %location 3
%ax7 = [0.0772   0.0797   0.0082   0.0099]; %location 4
%ax7 = [0.0798   0.0827   0.0086   0.0101]; %location 5
%ax7 = [0.0828   0.0859   0.0083   0.0104]; %location 6
%ax7 = [0.0860   0.0888   0.0092   0.0103]; %location 7
%ax7 = [0.0889   0.0918   0.0092   0.0103]; %location 8
%ax7 = [0.0919   0.0948   0.0092   0.0105]; %location 9
%ax7 = [0.0949   0.0980   0.0092   0.0105]; %location 10

%fifth vessel of interest

%ax7 = [0.0710   0.0730   -0.0016   0.0001]; %location 1
%ax7 = [0.0731   0.0750   -0.0020   -0.0005]; %location 2
%ax7 = [0.0751   0.0770   -0.0024   -0.0006]; %location 3
%ax7 = [0.0771   0.0793   -0.0028   -0.0014]; %location 4
%ax7 = [0.0793   0.0813   -0.0032   -0.0017]; %location 5
%ax7 = [0.0814   0.0836   -0.0035   -0.0021]; %location 6
%ax7 = [0.0837   0.0859   -0.0041   -0.0028]; %location 7
%ax7 = [0.0860   0.0888   -0.0046   -0.0034]; %location 8
%ax7 = [0.0889   0.0918   -0.0053   -0.0041]; %location 9
%ax7 = [0.0919   0.0947   -0.0062   -0.0047]; %location 10


I7 = find(data7(:,1)>ax7(1) & (data7(:,1)<ax7(2)) & data7(:,2)>ax7(3) & data7(:,2)<ax7(4));

hold on;
plot3(data7(I7,1), data7(I7,2), data7(I7,3), 'ro')

help axis
data7(I7, 4)
size(I7)
mean(data7(I7,4))
```

Appendix V: No Pneumonectomy Pressure Matlab Code

```matlab
t5 = readtable('Full_Model_Pressure_Volume_Data.txt');
data5 = table2array(t5(:,1:4));
indx5 = find((data5(:,1)>-0.3)&(data5(:,2)>-0.04)&(data5(:,1)<0.45));
figure;
scatter3(data5(indx5,1),data5(indx5,2),data5(indx5,3),30,data5(indx5,4))
axis equal;

%first vessel of interest

%ax5 = [-0.0328   -0.0302    0.0316    0.0325]; %location 1
%ax5 = [-0.0332   -0.0306    0.0329    0.0338]; %location 2
%ax5 = [-0.0334   -0.0308    0.0382    0.0391]; %location 3
%ax5 = [-0.0336   -0.0310    0.0393    0.0402]; %location 4
%ax5 = [-0.0336   -0.0310    0.0403    0.0412]; %location 5
%ax5 = [-0.0335   -0.0309    0.0413    0.0421]; %location 6
%ax5 = [-0.0324   -0.0304    0.0450    0.0459]; %location 7
%ax5 = [-0.0322   -0.0302    0.0460    0.0469]; %location 8
%ax5 = [-0.0320   -0.0301    0.0470    0.0479]; %location 9
%ax5 = [-0.0318   -0.0301    0.0480    0.0489]; %location 10

%second vessel of interest

%ax5 = [-0.0432   -0.0423    0.0276    0.0290]; %location 1
%ax5 = [-0.0438   -0.0426    0.0291    0.0301]; %location 2
%ax5 = [-0.0444   -0.0432    0.0302    0.0314]; %location 3
%ax5 = [-0.0464   -0.0455    0.0347    0.0358]; %location 4
%ax5 = [-0.0471   -0.0461    0.0378    0.0390]; %location 5
%ax5 = [-0.0471   -0.0460    0.0391    0.0401]; %location 6


%third vessel of interest

%ax5 = [-0.0736   -0.0721   -0.0011    0.0014]; %location 1
%ax5 = [-0.0750   -0.0737   -0.0022    0.0004]; %location 2
%ax5 = [-0.0763   -0.0751   -0.0037   -0.0010]; %location 3
%ax5 = [-0.0776   -0.0764   -0.0048   -0.0019]; %location 4
%ax5 = [-0.0794   -0.0775   -0.0053   -0.0039]; %location 5
%ax5 = [-0.0811   -0.0795   -0.0067   -0.0048]; %location 6
%ax5 = [-0.0830   -0.0812   -0.0078   -0.0057]; %location 7
%ax5 = [-0.0850   -0.0831   -0.0078   -0.0061]; %location 8
%ax5 = [-0.0870   -0.0851   -0.0078   -0.0064]; %location 9
%ax5 = [-0.0890   -0.0871   -0.0078   -0.0063]; %location 10

%fourth vessel of interest

%ax5 = [0.0691    0.0712    0.0058    0.0087]; %location 1
%ax5 = [0.0713    0.0743    0.0065    0.0088]; %location 2
%ax5 = [0.0744    0.0771    0.0074    0.0092]; %location 3
%ax5 = [0.0772    0.0797    0.0082    0.0099]; %location 4
%ax5 = [0.0798    0.0827    0.0086    0.0101]; %location 5
%ax5 = [0.0828    0.0859    0.0083    0.0104]; %location 6
%ax5 = [0.0860    0.0888    0.0092    0.0103]; %location 7
%ax5 = [0.0889    0.0918    0.0092    0.0103]; %location 8
%ax5 = [0.0919    0.0948    0.0092    0.0105]; %location 9
%ax5 = [0.0949    0.0980    0.0092    0.0105]; %location 10
```

```matlab
%fifth vessel of interest

%ax5 = [0.0710    0.0730    -0.0016    0.0001]; %location 1
%ax5 = [0.0731    0.0750    -0.0020    -0.0005]; %location 2
%ax5 = [0.0751    0.0770    -0.0024    -0.0006]; %location 3
%ax5 = [0.0771    0.0793    -0.0028    -0.0014]; %location 4
%ax5 = [0.0793    0.0813    -0.0032    -0.0017]; %location 5
%ax5 = [0.0814    0.0836    -0.0035    -0.0021]; %location 6
%ax5 = [0.0837    0.0859    -0.0041    -0.0028]; %location 7
%ax5 = [0.0860    0.0888    -0.0046    -0.0034]; %location 8
%ax5 = [0.0889    0.0918    -0.0053    -0.0041]; %location 9
%ax5 = [0.0919    0.0947    -0.0062    -0.0047]; %location 10


I5 = find(data5(:,1)>ax5(1) & (data5(:,1)<ax5(2)) & data5(:,2)>ax5(3) & data5(:,2)<ax5(4));

hold on;
plot3(data5(I5,1), data5(I5,2), data5(I5,3), 'ro')

help axis
data5(I5, 4)
size(I5)
mean(data5(I5,4))
```

Appendix VI: Left Pneumonectomy Pressure Matlab Code

```
t6 = readtable('Left_Pneum_Stump_Pressure_Volume_Data.txt');
data6 = table2array(t6(:,1:4));
indx6 = find((data6(:,1)>-0.3)&(data6(:,2)>-0.04)&(data6(:,1)<0.45));
figure;
scatter3(data6(indx6,1),data6(indx6,2),data6(indx6,3),30,data6(indx6,4))
axis equal;

%first vessel of interest

%ax6 = [-0.0328    -0.0302    0.0316    0.0325]; %location 1
%ax6 = [-0.0332    -0.0306    0.0329    0.0338]; %location 2
%ax6 = [-0.0334    -0.0308    0.0382    0.0391]; %location 3
%ax6 = [-0.0336    -0.0310    0.0393    0.0402]; %location 4
%ax6 = [-0.0336    -0.0310    0.0403    0.0412]; %location 5
%ax6 = [-0.0335    -0.0309    0.0413    0.0421]; %location 6
%ax6 = [-0.0324    -0.0304    0.0450    0.0459]; %location 7
%ax6 = [-0.0322    -0.0302    0.0460    0.0469]; %location 8
%ax6 = [-0.0320    -0.0301    0.0470    0.0479]; %location 9
%ax6 = [-0.0318    -0.0301    0.0480    0.0489]; %location 10

%second vessel of interest

%ax6 = [-0.0432    -0.0423    0.0276    0.0290]; %location 1
%ax6 = [-0.0438    -0.0426    0.0291    0.0301]; %location 2
%ax6 = [-0.0444    -0.0432    0.0302    0.0314]; %location 3
%ax6 = [-0.0464    -0.0455    0.0347    0.0358]; %location 4
%ax6 = [-0.0471    -0.0461    0.0378    0.0390]; %location 5
%ax6 = [-0.0471    -0.0460    0.0391    0.0401]; %location 6

%third vessel of interest

%ax6 = [-0.0736    -0.0721    -0.0011    0.0014]; %location 1
%ax6 = [-0.0750    -0.0737    -0.0022    0.0004]; %location 2
%ax6 = [-0.0763    -0.0751    -0.0037    -0.0010]; %location 3
%ax6 = [-0.0776    -0.0764    -0.0048    -0.0019]; %location 4
%ax6 = [-0.0794    -0.0775    -0.0053    -0.0039]; %location 5
%ax6 = [-0.0811    -0.0795    -0.0067    -0.0048]; %location 6
%ax6 = [-0.0830    -0.0812    -0.0078    -0.0057]; %location 7
%ax6 = [-0.0850    -0.0831    -0.0078    -0.0061]; %location 8
%ax6 = [-0.0870    -0.0851    -0.0078    -0.0064]; %location 9
%ax6 = [-0.0890    -0.0871    -0.0078    -0.0063]; %location 10

I6 = find(data6(:,1)>ax6(1) & (data6(:,1)<ax6(2)) & data6(:,2)>ax6(3) & data6(:,2)<ax6(4));

hold on;
plot3(data6(I6,1), data6(I6,2), data6(I6,3), 'ro')

help axis
data6(I6, 4)
size(I6)
mean(data6(I6,4))
```

Appendix VII: Right Pneumonectomy Pressure Matlab Code

```matlab
t8 = readtable('Right_Pneum_Stump_Pressure_Volume_Data.txt');
data8 = table2array(t8(:,1:4));
indx8 = find((data8(:,1)>-0.3)&(data8(:,2)>-0.04)&(data8(:,1)<0.45));
figure;
scatter3(data8(indx8,1),data8(indx8,2),data8(indx8,3),30,data8(indx8,4))
axis equal;

%fourth vessel of interest

%ax8 = [0.0691   0.0712   0.0058   0.0087]; %location 1
%ax8 = [0.0713   0.0743   0.0065   0.0088]; %location 2
%ax8 = [0.0744   0.0771   0.0074   0.0092]; %location 3
%ax8 = [0.0772   0.0797   0.0082   0.0099]; %location 4
%ax8 = [0.0798   0.0827   0.0086   0.0101]; %location 5
%ax8 = [0.0828   0.0859   0.0083   0.0104]; %location 6
%ax8 = [0.0860   0.0888   0.0092   0.0103]; %location 7
%ax8 = [0.0889   0.0918   0.0092   0.0103]; %location 8
%ax8 = [0.0919   0.0948   0.0092   0.0105]; %location 9
%ax8 = [0.0949   0.0980   0.0092   0.0105]; %location 10


%fifth vessel of interest

%ax8 = [0.0710   0.0730   -0.0016   0.0001]; %location 1
%ax8 = [0.0731   0.0750   -0.0020   -0.0005]; %location 2
%ax8 = [0.0751   0.0770   -0.0024   -0.0006]; %location 3
%ax8 = [0.0771   0.0793   -0.0028   -0.0014]; %location 4
%ax8 = [0.0793   0.0813   -0.0032   -0.0017]; %location 5
%ax8 = [0.0814   0.0836   -0.0035   -0.0021]; %location 6
%ax8 = [0.0837   0.0859   -0.0041   -0.0028]; %location 7
%ax8 = [0.0860   0.0888   -0.0046   -0.0034]; %location 8
%ax8 = [0.0889   0.0918   -0.0053   -0.0041]; %location 9
%ax8 = [0.0919   0.0947   -0.0062   -0.0047]; %location 10



I8 = find(data8(:,1)>ax8(1) & (data8(:,1)<ax8(2)) & data8(:,2)>ax8(3) & data8(:,2)<ax8(4));

hold on;
plot3(data8(I8,1), data8(I8,2), data8(I8,3), 'ro')

help axis
data8(I8, 4)
size(I8)
mean(data8(I8,4))
```